

# Studying Muons with a Modular Detector Setup

M. Boscardin, C. Fuselli, F. Haslbeck, N. Koster, L. Malandris, B. Mattheai, R. Oudheusden, O. A. Ranum, N. Ruijter, A. Sidley, C. van der Stappen, M. Stentella

*NIKHEF, National Institute for Subatomic Physics - Amsterdam, The Netherlands*

November 2, 2021

## Abstract

Eleven muon detectors were built, based on the CosmicWatch desktop muon detectors and combine them with the purpose to measure the angular distribution of cosmic ray muons and to reconstruct and visualize their tracks in 3D. The expectations and restrictions of the detector were simulated using Allpix2. A grid was constructed of possible directions ( $\theta, \phi$ ) and energy values and the simulation was run for each combination of the parameters. The scintillator simulations fall into three main categories: Layered scintillator tests, muon count rate with the lead plates, initial muon energy tests and detector shape configuration tests. The detector shape configuration tests show that the length does not have a large impact on the photons hits, however the thickness does, which is explained by the fact that it is equal to the travelled distance of muons inside the scintillator. The energy simulations show that the number of measured photons are decreasing rapidly with the increasing hitting distance to the center. This was also confirmed by the measurements, see section 4.1. The detectors were calibrated in different ways. The electronic calibration was used to convert the output signal of the detector, ADC, to mV and Sr-90 was used for the energy calibration. We used three detectors, 2 on top of and one below lead blocks to measure the angular distribution and the ADC distribution. The plotted muon count rate over the angular distribution shows that the distribution followed the expected cosine squared trend. The Lead analysis shows that the count rate with increasing lead decreases more than expected with calculated energy loss. This can be partially explained by the distance between detectors. We managed to create a live visualization of the incoming muons.

## Acknowledgements

The Nikhef project student group would like to express gratitude for the people who aided in the process of developing the cosmic muon detector project.

First and foremost, the project would like to thank the institute for subatomic physics, NIKHEF, in Amsterdam, for providing appropriate laboratory and office space to develop the project.

Furthermore, we would like to thank the teaching assistants Marjolein Heidotting, Roberto Russo and Christina Tsolanta for aiding with debugging the electronic systems and providing support throughout the process. Special thanks goes out to our dear detector doctor Gino Hoft and Wim Gotink at the Nikhef institute, who never disappointed in bringing our detectors back to life when we thought they had crossed to the other side. As well, a special thanks to Jean-Paul Fransen at Nikhef who constructed the cables necessary to construct the detector and the NIKHEF electronics lab for their continuous support.

# Contents

<b>Abstract</b>	<b>4</b>
<b>Acknowledgement</b>	<b>4</b>
<b>List of Figures</b>	<b>4</b>
<b>List of Tables</b>	<b>4</b>
<b>1 Introduction</b>	<b>9</b>
1.1 An introduction to muons . . . . .	9
1.2 Cosmic ray muons . . . . .	9
1.2.1 Sources and propagation . . . . .	9
1.2.2 The Cosine Squared Law . . . . .	9
1.3 Muon detection mechanisms . . . . .	10
1.4 Our detector . . . . .	10
<b>2 Geometry and Hardware</b>	<b>11</b>
2.1 Intent of Detector . . . . .	11
2.2 Overview of the CosmicWatch . . . . .	12
2.3 Mechanical design . . . . .	14
2.3.1 Geometry uncertainties . . . . .	16
2.3.2 Geometry uncertainties of our detector . . . . .	17
2.4 Scintillators . . . . .	17
2.5 Coincidence . . . . .	18
2.5.1 Two detectors in coincidence . . . . .	18
2.5.2 Multiple detectors in coincidence . . . . .	20
2.5.3 Control Software (Arduino) . . . . .	21
<b>3 Simulations</b>	<b>25</b>
3.1 Shape simulations . . . . .	27
3.1.1 Energy simulations: . . . . .	29
3.1.2 Final configuration detector simulations: . . . . .	32
3.2 Simulation results . . . . .	36
3.3 Simulation final configuration . . . . .	41
<b>4 Calibration</b>	<b>46</b>
4.1 Radioactive calibration . . . . .	46
4.1.1 Sr-90 energy spectrum calibration . . . . .	46
4.1.2 Spatial properties of the scintillator . . . . .	48
4.2 Electronic calibration . . . . .	52
4.2.1 Generating a Muon Signal . . . . .	52
4.2.2 Injecting Pulses . . . . .	54
4.2.3 Analysing the data . . . . .	54

4.2.4	Voltage analysis . . . . .	54
<b>5</b>	<b>Data Acquisition</b>	<b>60</b>
5.1	Methodology . . . . .	60
5.2	Live plotting . . . . .	61
<b>6</b>	<b>Detector results</b>	<b>64</b>
6.1	Zenith Angular Distribution . . . . .	64
6.1.1	Zenith-angle-dependent ADC and mV distribution . . . . .	64
6.2	Muons passage through lead . . . . .	68
6.2.1	ADC and mV spectrum analysis . . . . .	68
6.3	Time Window . . . . .	69
6.4	Comparison between simulations and data . . . . .	72
6.5	ADC distribution . . . . .	77
<b>7</b>	<b>Conclusion and future prospects and improvements</b>	<b>79</b>
7.1	Conclusion . . . . .	79
7.2	Discussion and outlook . . . . .	80
<b>8</b>	<b>Appendix</b>	<b>83</b>
8.1	Guide to building and soldering the CosmicWatch . . . . .	83
8.2	Troubleshooting . . . . .	86
8.3	Original detector idea . . . . .	94
8.3.1	Detector geometry . . . . .	94
8.3.2	Geometry uncertainties . . . . .	95
8.3.3	Cabling . . . . .	96
8.4	Scintillators . . . . .	99
8.4.1	The role of the scintillator in our detector . . . . .	100
8.4.2	Testing different scintillators . . . . .	100
8.4.3	The final choice . . . . .	101
8.5	Reflections on individual work . . . . .	106

# List of Figures

1	<i>Unpopulated PCBs</i>	12
2	<i>Single CosmicWatch Muon Detector</i>	14
3	<i>BNC, TP1, TP2 and TP3 signals at the oscilloscope</i>	14
4	<i>Possible Detector Grids</i>	15
5	<i>Setup for uncertainty analysis.</i>	17
6	<i>Two detectors in coincidence mode</i>	19
7	<i>Three detectors in coincidence mode</i>	20
8	<i>Signal timing and jack connections</i>	23
9	<i>Signal timing and amplitude</i>	24
10	<i>Example of scintillator shapes</i>	27
11	<i>Non-central simulated muons events</i>	28
12	<i>Muon energy simulations</i>	29
13	<i>Incident positions and direction of simulated muons.</i>	33
14	<i>Final Configuration</i>	34
15	<i>Angular information</i>	34
16	<i>Photons hits with shape changes</i>	36
17	<i>Asymmetric hits</i>	37
18	<i>Photons hits for different energy values.</i>	37
19	<i>Energy cut-off of muons passing lead</i>	38
20	<i>Upper photons hits for energy lead simulation.</i>	38
21	<i>Electrons' photons hits.</i>	39
22	<i>Strontium-90 small scintillator.</i>	39
23	<i>Strontium-90 big scintillator.</i>	40
24	<i>Normalized photons hits for electrons and muons</i>	40
25	<i>Photons hits for <math>(\theta, \phi) = (0, 0)</math>.</i>	41
26	<i>Photons hits for <math>(\theta, \phi) = (22, 0)</math>.</i>	41
27	<i>Photons hits for <math>(\theta, \phi) = (22, 90)</math>.</i>	42
28	<i>Photons hits for <math>(\theta, \phi) = (22, 45)</math>.</i>	42
29	<i>Final configuration with pixels.</i>	43
30	<i>Final configuration scintillators asymmetry hits.</i>	44
31	<i>The energy spectrum of Sr-90/Y-90 [1]</i>	46
32	<i>The setup of the radioactive measurements inside a blackbox.</i>	47
33	<i>ADC distribution measured by the detector over 1 hour with and without the Sr-90 source.</i>	48
34	<i>Background subtracted ADC distribution of Sr-90 source with exponential fit</i>	48
35	<i>ADC distribution zoomed in on endpoint</i>	49
36	<i>Simulation of muons hitting the detector at the center (top) and side (bottom) of the scintillator.</i>	50
37	<i>ADC distribution of long scintillator with the Sr-90 source.</i>	51
38	<i>Muon Signal on Oscilloscope</i>	52
39	<i>Calibration Analysis</i>	53
40	<i>Waveform Generator</i>	53

41	<i>Electronics calibration fits polynomial degree study</i>	56
42	<i>Electronics calibration fits</i>	57
43	<i>Calibration schematics</i>	57
44	<i>I/O plot of Rens's PCB</i>	58
45	<i>I/O plot of Carlo's PCB</i>	59
46	<i>Example of configuration</i>	61
47	<i>Live plotting</i>	63
48	<i>Angular distribution of cosmic ray muons</i>	65
49	<i>Angular distribution setup</i>	66
50	<i>ADC and voltage distributions per detector for different zenith angles.</i>	66
51	<i>Background ADC distribution for zenith angles.</i>	67
52	<i>Set-up of the lead measurements</i>	69
53	<i>Muon count rate versus amount of lead traversed</i>	70
54	<i>ADC distributions per detector for lead measurements.</i>	70
55	<i>ADC background distributions per detector for lead measurements.</i>	71
56	<i>Time difference between events for lead measurements.</i>	71
57	<i>Simulation comparison,lead case rate</i>	72
58	<i>Simulation comparison,lead case pulses</i>	73
59	<i>Simulation comparison,strontium</i>	75
60	<i>Simulation comparison,strontium pulses</i>	75
61	<i>Strontium-90 experimental data</i>	76
62	<i>ADC distribution</i>	78
63	<i>ADC distribution, more detectors</i>	79
64	<i>ESD Mat</i>	83
65	<i>Soldering steps</i>	85
66	<i>Populated main PCB</i>	86
67	<i>OLED screen connector crossed wire</i>	87
68	<i>Wick utilisation</i>	88
69	<i>Measurement +5V Arduino pin</i>	89
70	<i>Measurement VH and GND 6 pin header</i>	90
71	<i>Missing pad: problem and solution</i>	91
72	<i>Broken Arduino: problem and solution</i>	93
73	<i>Desoldering pump</i>	94
74	<i>Sketch of the detector geometry.</i>	95
75	<i>Normalized angular resolution and number of events as function of distance between the scintillator layers</i>	96
76	<i>Manufactured cables</i>	97
77	<i>Setup for the cabling test</i>	98
78	<i>Cabling test results</i>	98
79	<i>Cabling test results</i>	99
80	<i>Different position of the source on the scintillator</i>	102
81	<i>Different position of the source on the scintillator, sketch</i>	103
82	<i>ADC values for glued and one-piece scintillator</i>	104
83	<i>Time difference between 2 counts for the solid and glued scintillator</i>	105

## List of Tables

1	<i>Shape simulation parameters</i>	27
2	<i>Asymmetry simulation parameters</i>	28
3	<i>Energy change simulation</i>	29
4	<i>Strontium-90 Simulations</i>	30
5	<i>Lead simulation</i>	31
6	<i>Final configuration simulation</i>	32
7	<i>Final configuration Monte Carlo simulation</i>	35
8	<i>Monte Carlo simulation results (1hr)</i>	45
9	<i>Adjusted Monte Carlo simulation results (1hr)</i>	45
10	<i>Extreme case Monte Carlo simulation results (1hr)</i>	45
11	<i>Fit parameters</i>	55
12	<i>Monte Carlo comparison</i>	73
13	<i>Adjusted Monte Carlo comparison</i>	74
14	<i>Extreme Monte Carlo comparison</i>	74
15	<i>Angular uncertainties</i>	96

# 1 Introduction

## 1.1 An introduction to muons

The muon was first detected in 1936, by physicists Carl D. Anderson and Seth Neddermeyer at Caltech, by noticing that a negatively charged particle moving at the same velocity as an electron had a smaller curvature than the electron [2]. This is due to its larger mass. The muon makes up one of the three generations of charged leptons in the Standard Model of Physics, coupled to the weak, electromagnetic and gravitational force. It is unstable and has a decay time of  $2.2\mu\text{s}$ , but relativistic effects give cosmic muons a long enough half-life for them to be observed on Earth. Muons are interesting to study because they shed light on a variety of physical phenomena that are difficult to observe directly, such as supernovae. They are also one of the few particles that can be directly detected at hadron colliders, as their decay time is typically longer than that of other particles. They therefore act as a method of indirect observation of a wide variety of particle physics processes in experiments.

## 1.2 Cosmic ray muons

### 1.2.1 Sources and propagation

Cosmic rays are high-energy particles (typically protons or atomic nuclei) that travel through space at almost the speed of light and enter the Earth's atmosphere. They are most commonly produced by supernovae, but can also originate from the sun, due to solar eruptions. Cosmic muons come from the interaction between cosmic rays and atoms in the Earth's upper atmosphere. The incident cosmic ray is known as the primary cosmic ray. Once it interacts with the atmospheric atoms, an air shower occurs. A cascade of particles called the secondary cosmic ray rains down, including charged pions ( $\pi^\pm$ ) and kaons ( $K^\pm$ ), which can then decay into muons, according to Equation 1. These muons travel down to Earth and can then be detected.

$$\pi^\pm \rightarrow \mu + \overset{(-)}{\nu_\mu} \tag{1}$$

$$K^\pm \rightarrow \mu + \overset{(-)}{\nu_\mu} \tag{2}$$

### 1.2.2 The Cosine Squared Law

As a cosmic muon travels through the atmosphere, it loses energy. This energy loss is due mostly to ionization (although high-energy muons also undergo bremsstrahlung and pair production). The larger the distance that a muon travels through the atmosphere, the more of its energy is lost due to ionization, and the higher the probability of it decaying in the air. Muons with a larger zenith angle (angle from the vertical) will traverse a larger distance, and therefore lose more energy on average and decay more often. Muon intensity at sea-level as a function of zenith angle can be modeled by a cosine-squared law [3].

### **1.3 Muon detection mechanisms**

Cosmic muons can be detected using a scintillating material coupled to a light-sensitive device, usually a silicon photomultiplier (SiPM). When a charged particle passes through the scintillator, some of its energy is absorbed and photons are emitted. These photons are then detected by the SiPM, and the signal can be read out by electronics. The mean energy of a cosmic muon at sea-level is 4GeV, and cosmic muons typically deposit a minimum energy of 1-3GeV in a plastic scintillator [4].

### **1.4 Our detector**

Our project aimed to build a muon detector from which positional, angular and energy information can be extracted, and to visualize the data in a live plot. The detector is composed of and based on the CosmicWatch desktop muon detectors [4]. The proceeding sections describe the intent and geometry of the detector, the simulations used, calibration of the detectors using electronics and a radioactive source, data acquisition and the setup and results of measurements taken.

## 2 Geometry and Hardware

### 2.1 Intent of Detector

Recently, muons have received increased interest ranging from hints of possible lepton flavour violation at LHCb [5] or new physics suggested by the anomalous magnetic moment at the  $g - 2$  experiment at Fermilab [6]. Both examples of muon(-related) experiments require very precise measurements and a good understanding of muon properties. High-energy muons have a small interaction cross section and thus can have a penetrative signature. This requires the muon detector to be positioned as the outer layers at any of the large LHC experiments. The penetrative signature separates muons from many other particles and makes them an interesting candidate to study. Along these lines, we found it particularly fascinating and educational to look at the properties of muons produced by cosmic rays interacting with the upper atmosphere. Among the different characteristics of muons that can be studied, the following questions were raised:

- What is the angular muon distribution?
- What is the muon energy deposition in lead?
- Can we recreate the muon path at earth's surface?

The study of cosmic muons can be realized without the need of expensive accelerators, as the natural background is the signal. Moreover, a wealth of data and resources allow the comparison of data and theory. To answer these questions, the final detector will be built by combining multiple smaller units, called Desktop Muon Detectors, which are part of the CosmicWatch Project offered by the Massachusetts Institute of Technology (MIT) and National Center for Nuclear Research (NCBJ). In fact a single CosmicWatch Muon Detector allows us in principle to detect one particular type of particle, namely muons. However, these elementary particles come along with other particles which we will call background particles. These background particles consist of electrons, photons and heavy charged hadrons. By combining multiple CosmicWatch units the background noise can be reduced significantly, allowing the setup to mainly detect muons. This is because muons are the only particles that can travel through multiple detectors without being noticeably deflected nor absorbed as opposed to background particles, moreover in section 2.5. Along these lines, by creating a multiple layered grid of CosmicWatches, it is possible to reconstruct 3D muon tracks by following the path of a single muon through the grid of detectors. By making a tower of CosmicWatches with a layer of lead with an adjustable thickness between the bottom detector and the others, the energy deposition in lead can be measured. Finally, by stacking the CosmicWatches to a tower and taking multiple measurements under an adjustable angle, the angular muon distribution can be measured.

In the following subsections we will start off by describing the way one of these unit works (for an extensive overview of how to build and how troubleshoot a CosmicWatch, see appendices 8.1 and 8.2). Subsequently, we move on by describing the mechanical design of the entire configuration, followed by the different scintillators which were tested for the detector. Then the support structure that holds all detectors is described. Next cables that allow

the scintillator to be separated from the PCB are discussed and finally we review a built-in property of the CosmicWatch called "coincidence mode".

## 2.2 Overview of the CosmicWatch

When purchasing the CosmicWatch, several components are delivered. A complete list of these components, along with a more detailed description of them, can be found in

<https://github.com/spenceraxani/CosmicWatch-Desktop-Muon-Detector-v2>,

`SMT_reference.pdf` (in the `PCB_Files` folder) and `instructions.pdf`, respectively.

Among these elements are three printed circuit boards (PCBs), as shown in figure 1, that are the circuits to which all components have to be attached. This is done through careful soldering. The components consist largely of surface mount devices (SMDs), as for example capacitors and resistors, that, because of their tiny dimensions, can easily be misplaced if not given proper attention. The three different PCBs are: the main PCB, the silicon photomultiplier (SiPM) PCB and the SDCard PCB.

Figure 1: *Unpopulated PCBs*



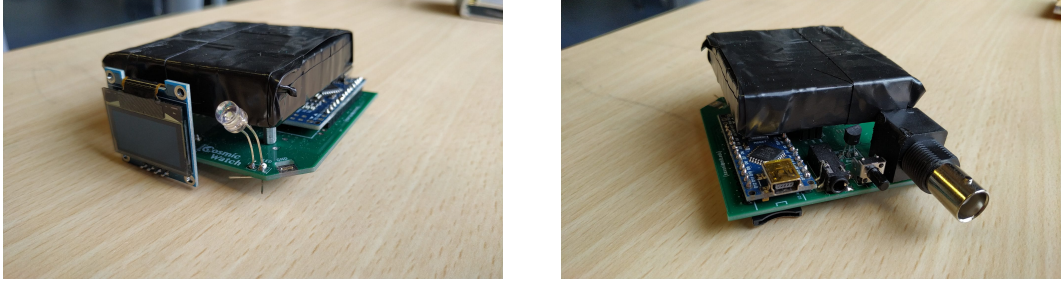
*Three unpopulated PCBs, as delivered on order, still attached to each other through plastic that can be broken. The largest PCB (upper left) is the main PCB, the smallest PCB directly below it (lower left) is the SDCard PCB and the middle sized PCB (lower right) is the SiPM PCB.*

The main PCB serves as the general component that will process the signal. The main PCB holds many capacitors and resistors, the other PCBs, an Arduino Nano, a LED light, a 3.5mm jack, a reset button and an OLED screen. The SDCard PCB can hold a microSDcard, which allows the detector to record data externally. The SiPM PCB consists of a few capacitors and resistors, a 6-pin connector and a SiPM as well as two standoffs allowing it to connect to the main board. The SiPM is in contact with a plastic scintillator, which in turn is wrapped in

aluminium foil. The latter has a hole that is placed on the SiPM while the complete SiPM PCB is wrapped in black electrical tape in order to become light-tight. The detector is powered through a mini-USB cable entering the Arduino, supplying the board with roughly 5V. When a particle enters the scintillator, it will produce photons. These photons will reflect off the aluminium foil, keeping them inside the scintillator until they reach the only exit at the SiPM. A SiPM consists of a microcell grid containing many SPADs (Single Photon Avalanche Diodes). When a single SPAD receives a photon, the latter is absorbed by the silicon photodiode and creates an electron-hole pair. These charges are subsequently accelerated by the electron field of the p-n junction and they will reach the right energy to create other electron-hole pairs. In this way, the process is repeated many times in a mechanism called a "Geiger avalanche", hence a net flow of current is produced and then passed onto the main PCB (the raw (BNC) pulse (see figure 3) gives a signal in the order of 500 ns). It is important to underline that when triggering one SPAD, which is confined to its own cell, the others remain functional and ready to detect any other photons. In this manner multiple photons can be detected at the same time. The single triggered SPAD in fact has a downtime during which no further detection is allowed, due to the recovery process of the photodiode. For a full overview on the functionality of SiPMs we refer to the Introduction to the Silicon Photomultiplier (SiPM) manual [7]. The main PCB comes with three test points, to which an oscilloscope can be attached in order to check the signals. An oscilloscope is an instrument that gives a graphical depiction of a voltage signal as a function of time. The oscilloscope we used offered a plethora of analytic tools to analyse the properties of the signal, such as frequency, amplitude, time rise and time intervals. For a full list of functionalities we refer to its manual [8].

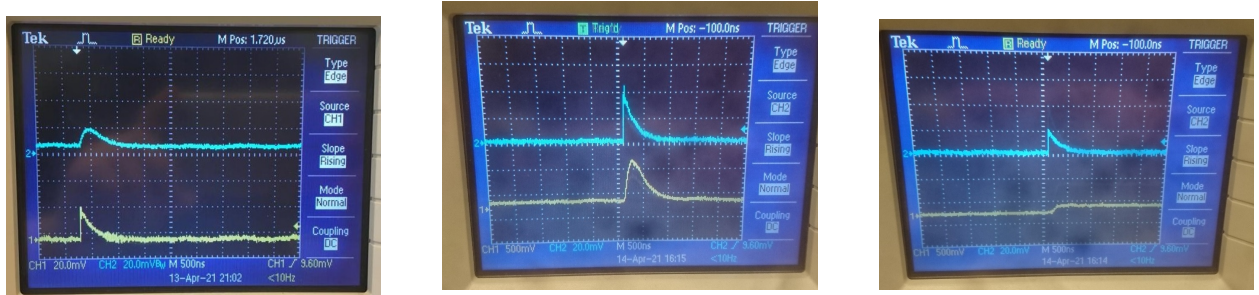
Inside the main PCB, the signal will first flow through a  $1\text{k}\Omega$  resistor named R4 (see figure 3a), then through the amplification circuit, which roughly amplifies the signal by a factor of 25 (see figure 3b) and then into the peak detector. The function of the peak detector is taking the amplified signal and holding this voltage for a longer time (see figure 3c). The signal then slowly decays over a period of a 0.5 ms. This is necessary as the clockspeed of the Arduino Nano is roughly  $5\mu\text{s}$ , which would be too long for it to record the raw signal of an event. After the peak detector, the signal goes into the Arduino Nano, which can then record the event. It will then send out a signal to the LED, which will flash to indicate a detection. The Arduino also controls the OLED screen, which will keep track of the runtime and number of detections made. The 3.5mm jack can be used with a 3.5mm male-to-male cable in order to connect multiple detectors to each other, moreover in 2.5.

Figure 2: Single CosmicWatch Muon Detector



Figures of a CosmicWatch, as seen from the front side (left) and backside (right). On the front the OLED screen and LED are visible, while on the back from left to right, the Arduino, 3.5mm jack, reset button and BNC connector are visible. The black square on top is the scintillator wrapped in aluminium foil (not visible) and taped shut with black electrical tape.

Figure 3: BNC, TP1, TP2 and TP3 signals at the oscilloscope



(a) BNC (yellow) and TP1 (blue) signals. X-axis is adjusted to 500 ns, while the y-axis is 20 mV for both signals.

(b) BNC (blue) and TP2 (yellow) signals. X-axis is adjusted to 500 ns, while the y-axis for blue is 20 mV and 500 mV for yellow.

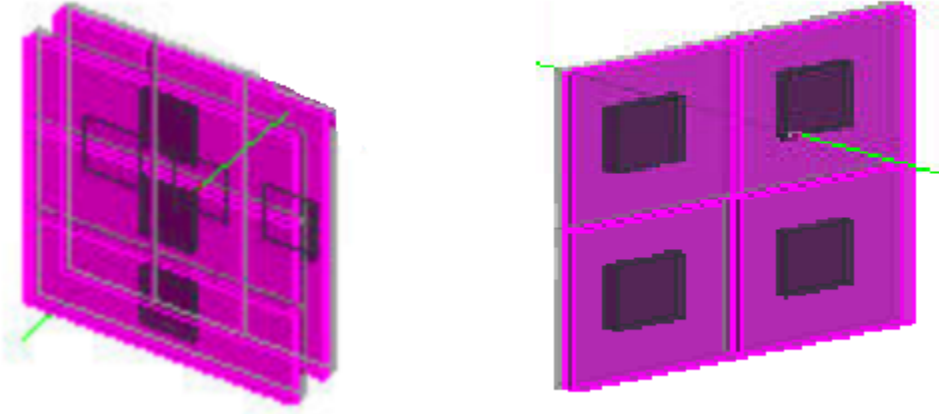
(c) BNC (blue) and TP3 (yellow) signals. X-axis is adjusted to 500 ns, while the y-axis is 20 mV for blue and 500 mV for yellow.

Expected signals of the CosmicWatch testpoints TP1 (a), TP2 (b) and TP3 (c), along with the BNC signal (yellow line (figure a) blue line (figure b and c)).

### 2.3 Mechanical design

Now that we have an extensive overview of the working principles of the single cosmic watches, we can continue to zoom out to review the big picture; the mechanical design of the final detector. For this detector we wanted to use all individual detectors from the Cosmic Watch Project and combine them to make measurements. Since it took several weeks to mount and solder all the PCBs, we decided not to change them or make new and different ones.

Figure 4: Possible Detector Grids



The left panel shows the 3x3 grid and the right panel the 2x2 grid.

This meant that we could only change the scintillators and the idea was to change the squares from the cosmic watch project to strips, so we could make a grid, as can be seen on the left in figure 4. In this design only 6 detectors were needed to form a 3x3 grid. Where 9 were needed if we kept the squares. The number of grids in the detector was dependent on the number of working SiPMs and main PCBs that we had and with a maximum of 13 detectors, we could go as large as 2 grids in total. The 3x3 grid can be seen as a x,y-grid with nine pixels, three scintillators provide the x coordinate and three provide the y coordinate and together they cover the area of 9 squares. The final, 13th, detector would keep its square scintillator and act as a master. So only if this detector measured a signal, the scintillators in the different grids opened a short time window in which they were able to collect a signal.

If, by any reason, we had to work with less than 13 SiPMs we could scale down by replacing one of the layers by a 2x2 grid, that only needs 4 detectors, see the right side of figure 4. In this case we only needed 11 detectors (6 for the 3x3, 4 for the 2x2 and 1 master). It was also possible to drop an entire grid layer, leaving out the 2x2 grid results in only 7 detectors and a 2x2 grid plus master could be achieved with five detectors. This was the lowest number of detectors we needed to reconstruct muon tracks in two dimensions.

In order to avoid scattering inside the grid of scintillators we wanted to put as less PCBs as possible inside the detector and used jumper cables to connect all, relatively small, SiPM PCBs to the main PCBs where the latter could now be placed outside the area where the muons got measured.

The detector configuration of the final experiment consisted of three 5 cm by 5 cm scintillators stacked on top of each other equally spaced 4 cm apart.

### 2.3.1 Geometry uncertainties

In this section we will discuss the uncertainties in the track reconstruction that is introduced purely by the detector geometry and layout. Due to the scintillators having a finite size, we will not be able to know where the muons enters the scintillator. When a muon is measured in the top layer of detectors and the bottom layer, a trajectory can be constructed by drawing a line through the centre of both scintillators. The uncertainty can be computing by considering the extremes of where the muon could have entered the scintillator. This corresponds to the muon entering through the edge of a top layer scintillator and it leaving through the edge of a bottom layer scintillator.

First we will consider a setup where we have one scintillator in the top layer and a grid of 3 by 3 scintillators in the bottom layer. A drawing of this setup can be seen in Figure 5. The uncertainty in the angles  $\theta$  and  $\psi$ , which are defined in Figure 5, is dependent on the scintillator it passes. There are four different scintillators that give different angular uncertainties in  $\phi$  and  $\psi$  labeled I, II, III and IV in Figure 5. By symmetry the other scintillators in the setup will have the same uncertainties as I, II, III or IV. Furthermore, if  $\Delta x$  is equal to  $\Delta y$ , scintillator III gets the same uncertainties as II. By simple trigonometry and algebra, the angular uncertainties in  $\phi$  and  $\psi$  are calculated to be the following:

$$\Delta\phi = 2 \tan^{-1} \left( \frac{0, 5(\ell + \Delta x)}{h} \right) \quad (3)$$

$$\Delta\psi = 2 \tan^{-1} \left( \frac{0, 5(\ell + \Delta y)}{h} \right) \quad (4)$$

$$\Delta\phi = 2 \tan^{-1} \left( \frac{0, 5(\ell + \Delta x)}{h} \right) \quad (5)$$

$$\Delta\psi = \tan^{-1} \left( \frac{0, 5(\ell + 3\Delta y)}{h} \right) - \tan^{-1} \left( \frac{0, 5(\Delta y - \ell)}{h} \right) \quad (6)$$

$$\Delta\phi = \tan^{-1} \left( \frac{0, 5(\ell + 3\Delta x)}{h} \right) - \tan^{-1} \left( \frac{0, 5(\Delta x - \ell)}{h} \right) \quad (7)$$

$$\Delta\psi = 2 \tan^{-1} \left( \frac{0, 5(\ell + \Delta y)}{h} \right) \quad (8)$$

$$\Delta\phi = \tan^{-1} \left( \frac{0, 5(\ell + 3\Delta x)}{h} \right) - \tan^{-1} \left( \frac{0, 5(\Delta x - \ell)}{h} \right) \quad (9)$$

$$\Delta\psi = \tan^{-1} \left( \frac{0, 5(\ell + 3\Delta y)}{h} \right) - \tan^{-1} \left( \frac{0, 5(\Delta y - \ell)}{h} \right) \quad (10)$$

Where equation 3 and 4 are the angular uncertainties in scintillator I, equation 5 and 6 are the angular uncertainties in scintillator II, equation 7 and 8 are the uncertainties in scintillator III and equation 9 and 10 are the uncertainties in scintillator IV.

To get some more feel for these equations, we can Taylor expand these expressions to first order in  $\frac{\ell + \Delta x / \Delta y}{h}$

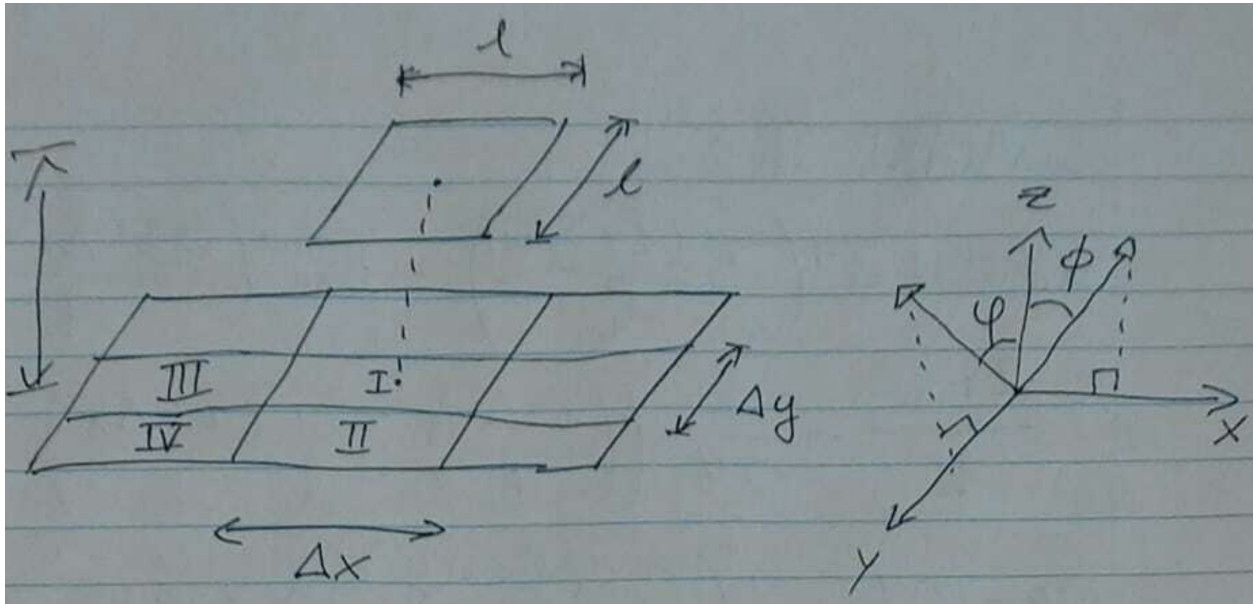
This yields:

$$\Delta\phi = \frac{\ell + \Delta x}{h} \quad (11)$$

$$\Delta\psi = \frac{\ell + \Delta y}{h} \quad (12)$$

When  $h$  is large compared to  $\ell$  and  $\Delta x/\Delta y$  these expressions give a good approximation to the angular uncertainties.

Figure 5: *Setup for uncertainty analysis.*



*A sketch of the configuration used in the uncertainty analysis.*

### 2.3.2 Geometry uncertainties of our detector

The detector setup for the experiment consists of three layers of 5 cm by 5 cm scintillators where the scintillators are placed at a distance of 4 cm apart. The uncertainty is then given by equation 3, using a height of 8 cm. This yields an uncertainty in the angle  $\phi$  and  $\psi$  of 1.117 rad.

## 2.4 Scintillators

The scintillators used in our detector are the ones of the cosmic watch, they are plastic scintillator of dimension (5x5x1)cm composed by a transparent part of polystyrene and a fluorescent part made by POP and POPOP. A detailed description of their role in a detector in general and of the process of testing different shapes of scintillators that led to this decision can be found in the Appendix. (See Section 8.4). The main motivation that justify the choice of this component is represented by a non sufficient time dedicated to the testing phase for

the other possibilities, this could be improved by running the simulations and comparing them with the observations earlier in the timeline of the project.

## 2.5 Coincidence

The scintillator of a CosmicWatch is sensitive to any particle travelling through it that can undergo electromagnetic interactions. Aside from muons, this comprises electrons, photons<sup>1</sup> and heavier charged hadrons, such as protons, pions and kaons. However, the final detector is solely interested in muons. In order to get rid of most of the noise, the CosmicWatches come with a built-in functionality referred to as coincidence mode. This mode allows multiple detectors to be connected to each other, where every detector can fulfill one of two roles: Master or Slave. Masters will count any incoming particle, as if the CosmicWatch is running on its own, while slaves only count within a very short time window if the master detector is triggered. Detectors set up in coincidence mode can make a distinction between muons and noise because of the different tracks these signals follow: due to their low mass, electrons are very prone to scattering effects and will rarely travel in a straight line between two detectors. Heavy particles with a low energy will not be able to travel through multiple scintillators as they are stopped by energy loss. For heavy particles with a high energy, a distinction is made between muons and charged hadrons. This is due to highly energetic charged hadrons being able to react through strong force in addition to the electromagnetic interactions, which can greatly affect their trajectory. Muons do not possess this property and as a consequence will travel with minimal deflection. The result of this will be that, while background particles can enter a single detector they will rarely go through a second detector, while muons are expected to travel in a straight line and penetrate multiple detectors [4].

### 2.5.1 Two detectors in coincidence

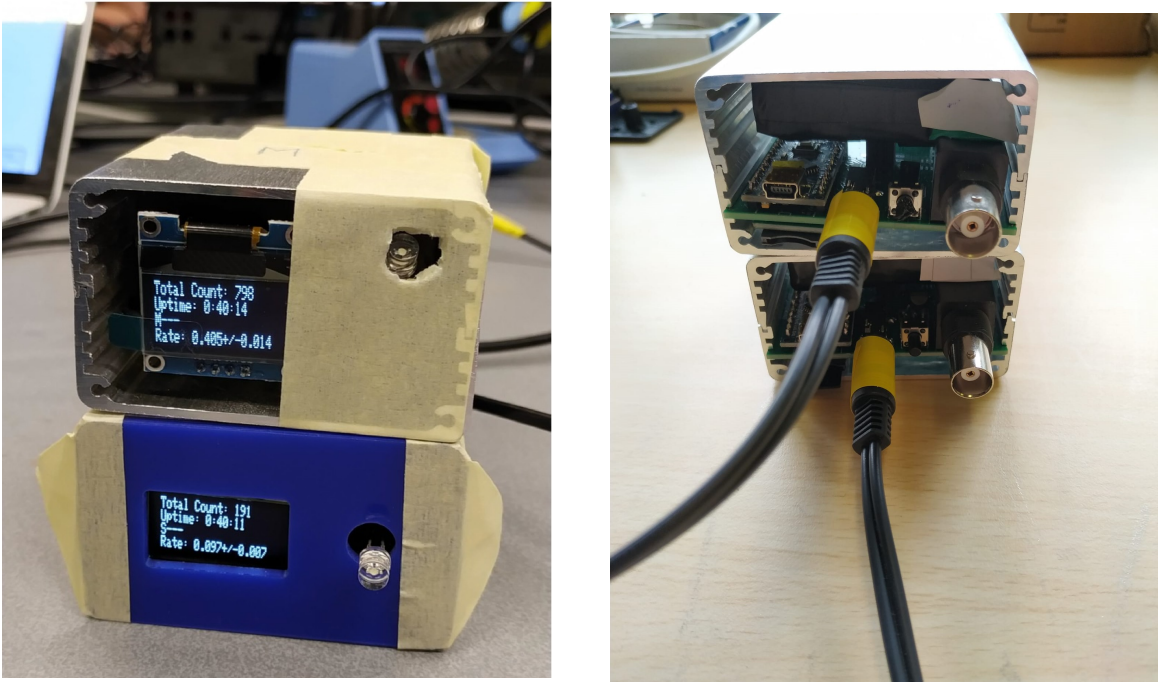
In order to put two detectors in coincidence mode we had to make use of the 3.5 mm jack, which is located on the main PCB right next to the Arduino. By using a male-to-male jack cable we connected at first only two detectors, as shown in Figure 6. With this set up, the power is only needed to be provided to one of them, since the jack cable itself serves as a power cable for the second detector. The original way to decide on the detector task division is written in the code provided with the CosmicWatch project. To decide which detector becomes the master and which becomes the slave, both have to be reset. In particular, the one that is reset first becomes the master, while the subsequent detector, as long as it is reset within a 10 ms to 2000 ms window, becomes the slave. This selection is not affected by either the name of the detector nor by which one of the two detectors is powered through the miniUSB cable. However, because this process is not handy when dealing with a lot of detectors, the code was altered in such a way that we could decide a priori which detector is going to be the master and which one the slave (see the paragraphs below for details 2.5.3). Regarding this setup, the data that is recorded are those signals that are recognized by the detector connected to the computer through the miniUSB cable. Therefore, in order to record signals from only muons, the slave has to be the one directly connected to the

---

<sup>1</sup>The scintillators are made light-tight so the photon noise should be minimal.

computer. However, in order to collect as much data as possible for a better simulation later, we also connected the master to the computer. This allowed us to gather all the signals from non-muon particles as well. Here one could pose the question whether the non-muon particles are not just electronic or thermal noise. When a functional CosmicWatch is connected to an oscilloscope, an always present 'random' noise can be seen in the BNC signal on a scale of approximately 2 mV. This fluctuation is the electronic and/or thermal noise and is an order of magnitude lower than the expected particle signals and can therefore easily be distinguished from actual particles. On top of that, the detector has a non-zero threshold that, when correctly attuned, should filter out this noise by being unresponsive in this signal amplitude regime.

Figure 6: *Two detectors in coincidence mode*



(a) *Two CosmicWatches in coincidence mode (front view). Note the difference in the count between the Master (on top) and the Slave (at the bottom). This difference is due to the fact that the slave can only count when the master is triggered.*

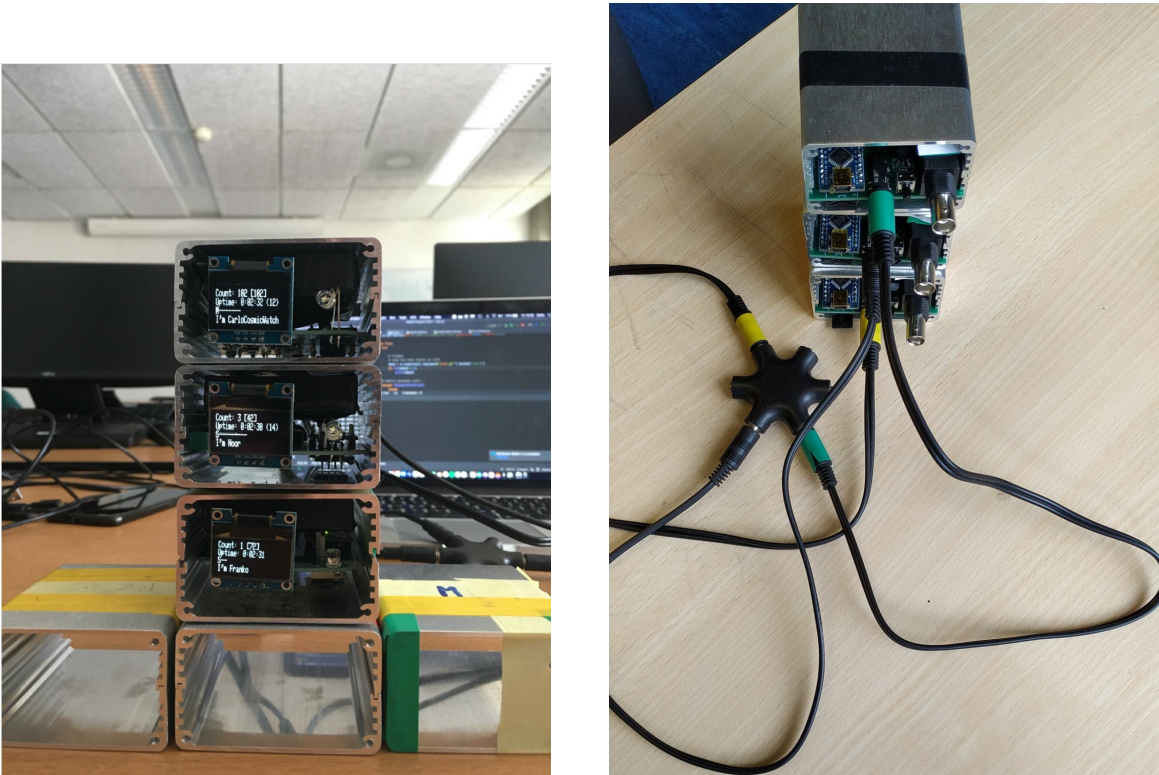
(b) *Two CosmicWatches in coincidence mode (back view). Note the audio m/m jack cable connecting the two detectors (black and yellow wire).*

*Two CosmicWatches Muon Detectors in coincidence mode.*

### 2.5.2 Multiple detectors in coincidence

To extend the coincidence mode to more than two detectors, new equipment was needed. By using an audio splitter we were able to connect more than two detectors to each other, see figure 7. In our first test session we connected three detectors to each other and experimented with assigning different roles to them. We appositely changed the Arduino code to achieve

Figure 7: *Three detectors in coincidence mode*



*Three CosmicWatches running in coincidence mode as seen from the front (left) and from the back (right). The right picture also shows the 6-way audio splitter that was used in order to connect more than two detectors to each other. On the left the master detector is on top, and even though the setup has been running for a few minutes only, it has a much higher count rate than the two slaves below it. Furthermore, the number of hits is shown in brackets. For the master this number is equal to the count rate, while slaves only count if the master opens its trigger window.*

this result (see section 2.5.3). With the setup of two masters with one shared slave, we found that the slave could count when either master opened its trigger window. Changing the setup to comprise one master and two slaves, we found that there is no hierarchy among slaves and both slaves could trigger individually when the master opened its trigger window. This was proven by putting the three detectors in coincidence mode but without stacking them (lay them out flatly aligned) and subsequently moving one slave at a time on top of the master. While the detectors were next to each other, no detections were made over

multiple minutes. In principle an air shower can trigger this setup, however, this is found to be very unlikely, which is backed by the setup not recording anything over multiple minutes. Subsequently moving a slave on top of the master would detect multiple events within a single minute. Moreover, we found that wherever one puts the master detector with respect to the slaves, the coincidence mode still works. However, putting the master at the top of the tower would first of all result in a more sensible and understandable choice and secondly in a higher number of recorded background particles. This is because when the master detector is at the bottom, the electrons entering at the top of the tower would be scattered away and wouldn't hit the detector at the bottom which would result in a lower counting. Along with that, the closer the slave detectors are to the master detector, the higher the coincidence rate is. This is because the further away you place the slave detectors the smaller the maximum angle of approach becomes. At this point one could wonder if the trigger window between the master and the farthest away slave can become too short to allow a coincidence detection. However, this should not be a matter of concern because it can be easily shown that the time needed to overcome the distance between the master and slave detectors in our setup is three orders of magnitude smaller than the window of the signal. In order to collect data within this setup, again one could only read out the signals detected from the detector at the bottom with one miniUSB cable, gathering in this way mainly signals from muons. However, we found it particularly interesting to get data also from the two above detectors. For this we needed two additional miniUSB cables and a USB splitter, depending on the number of USB ports a computer has. In order to collect data from more than one detector, all detectors should be connected to the laptop and multiple USB ports should be selected in the data recording program.

With our findings on a coincidental three detector setup, we could easily extend it to a setup of eleven detectors, as the audio splitting equipment accommodates six slots and we had four of them available. However, in the end we found out that coincidence mode misses a lot of supposedly coincidental detections, moreover in section 2.5.3. Instead, a new software tool was written that counts coincidental detections within a time window while all detectors are running in master mode.

### 2.5.3 Control Software (Arduino)

The Arduino is used to perform several tasks. The main code used is the OLED.ino script provided by Spencer Axani, but we implemented some modifications to make it easier to use. For example, we now define masters and slaves through the Arduino code and not via the reset button, that was becoming a more difficult task with the increasing number of detectors. Another important change was to modify what is printed on the screen, that made the troubleshooting part much easier to understand. In particular, the important things that are printed directly on the screen are: the current ADC value (to check that the baseline was not above the reset threshold), the number of counts both as an independent Master or as a Slave in coincidence (to test the rate of background and muons) or the number of times that one signal is received from the Master (to check that the jack connection was working properly).

The main task of the Arduino is to recognize a signal through a trigger with an ADC threshold on AnalogPin0. The end of the signal is then determined by a reset threshold:

when the ADC is below the threshold, the signal is finished and the script is ready to record a new one. The data is then sent to the computer via a mini USB cable and to the OLED screen inserted in the board.

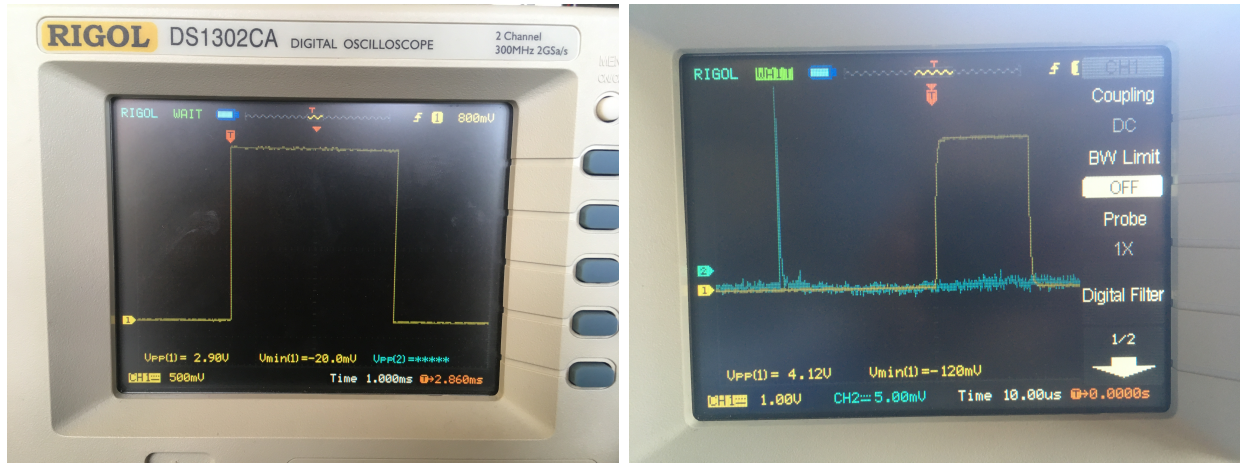
It is important to make some remarks on the timings of the Arduino. The clock of the Arduino is 16 MHz, to make a measurement we need between 5 and 8 microseconds and to send the data through the mini USB we add an uncertainty of the order of 10 milliseconds.

With this in mind, we can now also discuss the second important task of the Arduino, that is the possibility to determine if signals from different detectors came *together*. This is done through the jack port that is installed in every PCB. The idea is that we can use two (or more) detectors together and set one as the 'Master' and the other one as the 'Slave': the Master records every signal that it gets, while the Slave will trigger only if it gets a signal in the same time-window of its Master. What happens in practice is this: when the Master is triggered it will send a signal through the jack cable, when the Slave is triggered, it will first check if there is any signal coming from its Master through the jack and then eventually record the event. In all of this, timing is very important, but it should not be too difficult to deal with it. If a muon passes through two detectors, the two detectors will detect it almost simultaneously. There is a delay of around  $20\mu s$  between the time in which the Master detects an event and the time in which the Slave gets the signal through the jack, as showed in the right panel of Fig. 8 where one extra jack cable was connected, opened and directly connected to the oscilloscope. The solution is to add a time delay when the Slave detects an event before checking if the jack (digital) input is low or high.

There is one problem that we encountered in all of this. As the jack cable is connected to a digital pin of the Arduino, the reading of it can only return 0 or 1. What we think is that when we used a lot of detectors all together (but sometimes also with two or three detectors) the signal coming from the Master was very close to the threshold to be considered as high (that is around 3V) and so it was often read randomly. At the moment it is still not very clear why, when and how this happens, but looking at the signal in the jack through the oscilloscope and looking at some data that we print on the screen of the detectors, it is very likely that the signal coming from the master through the jack is not seen as a constant high signal, but more oscillating very quickly between high and low for the duration of the signal. The phenomenon can be observed in the left panel of Fig. 8. This can of course cause some big problems to the whole coincidence method as it is possible that the Slaves will not record some of the signals due to this oscillation.

To be extremely precise about the timings involved in our measurements and to be sure that this was not a cause of some problems, the difference in time between the detection of a muon signal in two different detectors (one on top of the other) was measured with the oscilloscope. As it is shown in Fig. 9, the reception of the signal is almost simultaneous. While studying this, we realized one big problem with the big scintillators that we did not test before. The blues line in Fig. 9 is from a detector with the small original scintillator, while the yellow one is from a detector with one of the new big scintillators that was built. It was clear from repeated measurements that the average amplitude of the signal in the big scintillators was much smaller (order 10) than the one coming from the original ones. This was not what was expected, and it is still not clear to us what caused this phenomenon to happen. One possible explanation is that the photons are scattered over a bigger volume and because of that less photons reach the SiPM. Given this, it was decided to revert back

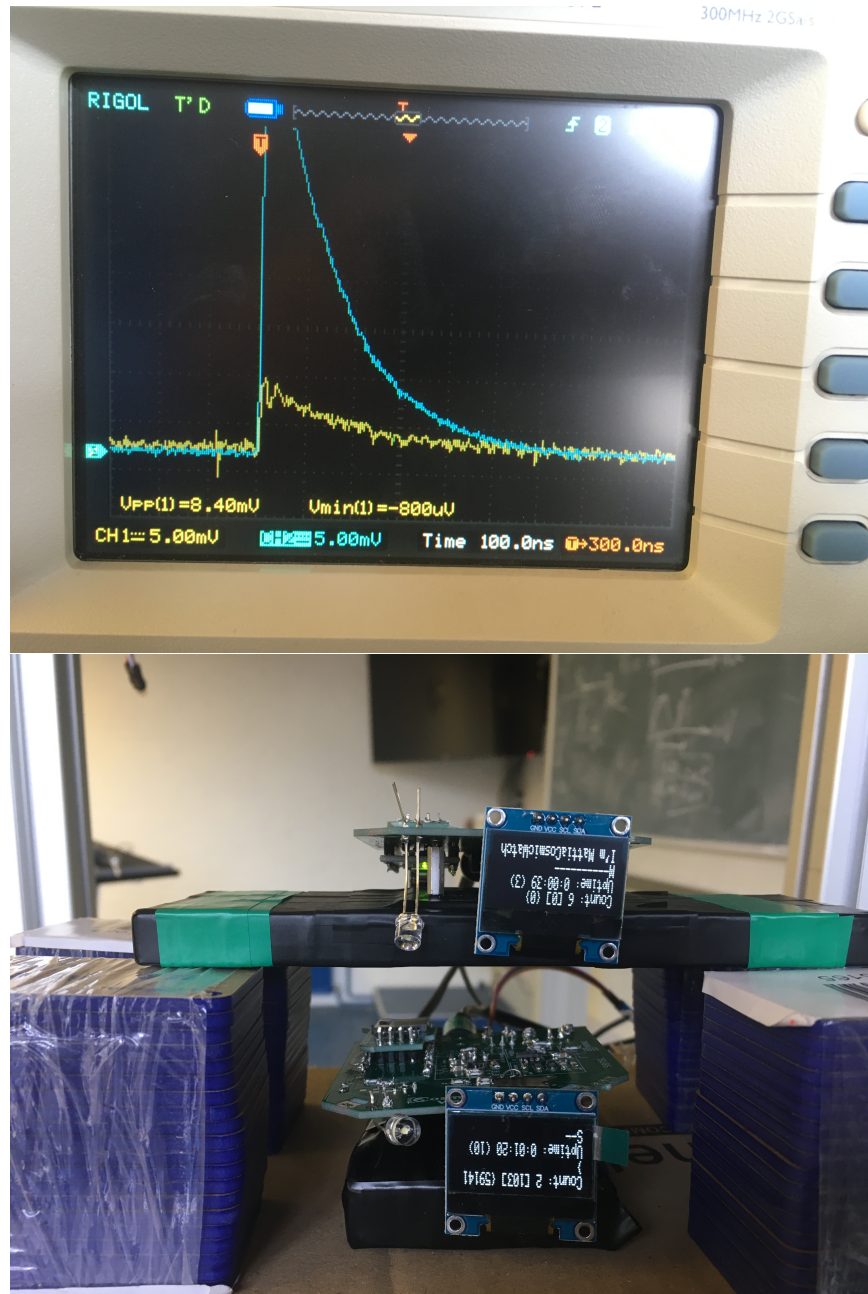
Figure 8: *Signal timing and jack connections*



*Studying timings and the jack signal with the oscilloscope. On the left: the signal received by the slaves, it is clear that the amplitude is oscillating around 3V (critical value). On the right: studying the delay between the detection of the signal from the master and the sending of the message to the slaves through the jack cable.*

to the small scintillators.

Figure 9: *Signal timing and amplitude*



*Studying timing and amplitude of the detection of the same muon with two different detectors stacked one on top of the other.*

### 3 Simulations

In order to restrict and evaluate the performance of the detector the system is simulated using the open-source framework Allpix<sup>2</sup> [9] for silicon pixel detectors. Visualisations are produced using the Geant4 toolkit. The simulations produce estimates on the number of photon-hits measured by the sensors of the detector, when a large number of events are taking place. In addition, the simulation yields estimates on the photons' energy, wavelength and travel time, derived from the interactions between a passing particle and the scintillator, and the time of detection and emission of both [10][11][12].

The aim of the simulation is to test the number of detectable cosmic muon events in the scintillator as a function of detector geometry and configuration. In addition, to indicate whether it is possible to extract information about the angular- and energy distributions of cosmic muons using the scintillator-based detector of this project. A combined analysis of the simulation results are used to adjust the cosmic watch detectors to increase efficiency and indicate potential improvements. Given that Allpix<sup>2</sup> is constrained to the use of only one source per simulation, we run the simulations for the case of incident cosmic muons as an isotropic source from all directions for all sky positions. I.e the simulation is performed on a grid of incident cosmic muons constructed from a distribution of possible  $(\Theta, \Phi)$ -directions and positions, and for a distribution of energy values at GeV-scale. There are three types of simulations performed to evaluate the detector: Scintillator tests using different geometrical characteristics (shape simulations), simulations of the cosmic muon energy range (Energy Simulations) and simulations of the final configuration (Final Configuration Simulation).

The shape simulations comprises simulations of scintillator-based detectors with different geometrical characteristics, such as different scintillator lengths and thicknesses, for both central and non-central hits. The goal of this simulation is to observe how different shapes of scintillators and different directions of passing muons affect the detection-capability and to illustrate some central limitations to the scintillators.

The energy simulations aims to evaluate how the detectability of the muons in the scintillators are dependent on the incident energy of the cosmic muons. That is, to simulate how different energy values produce differences in the amplitude of the observed output signal pulse, using the photon-hit distributions that the sensor measured. A strontium-90 simulation is used to simulate the shape of the pulse distribution and to calculate the correspondence between the simulated photon-hits and the energy values. In the end a lead simulation is performed, where a lead plate is put in-between the muon source and the detector in the simulated environment. The muon count rate is estimated, and then compared to the experimental data.

The final configuration simulation is based on the final detector that was constructed for this project. The main goal is to yield a large detection area using a combination of the individual scintillators described in the section above. This configuration has been shown to increase the angular precision of the detected muons for a small number of individual detectors [13] [14]. This configuration leads to an increase in length, from 5 to 15 cm. The results of the shape simulation will hopefully indicate that the new detector is as effective as the initial cosmic watch, and the energy simulation will predict if the different energy values of incident muons could lead to additional information through the detected pulses.

An additional Monte Carlo simulation was created in order to compute the expected theoretical values of cosmic muons that passes the detector. As well, for the number of events that is recorded in both layers of the detector, an additional Allpix<sup>2</sup> simulation estimate the photon-hits in order to create the detected pulses. A grid of the sources' parameters was created following the theoretical angular distributions of the cosmic muons in the angular range of muons passing all detector layers.

It should be noted that the scintillating material used in the simulation differs slightly from the one used in the actual detector. The above Allpix<sup>2</sup> simulations utilizes the Cerium Bromide scintillator, while the scintillator of the cosmic watch is BC408. As such differences are expected. The simulated scintillator has a vastly higher density than BC408, and thus the simulation should predict more photons than expected for the detector for the same number of events. In addition the maximum wavelength is observed at 380nm for the simulated scintillator, while it is 420nm in a BC408 scintillator [4]. The results can be evaluated and validated through comparison with previous work on the BC408 scintillator through simulations like for instance in reference [15]. It is expected that the behaviour although will be similar using either material for the cosmic muons.

The code for the simulations can be found at:<https://github.com/cfuselli/Nikhef-Project-2021/tree/simulation>

### 3.1 Shape simulations

The shape simulations are produced using Various scintillator lengths and thicknesses, which are evaluated for a block of scintillating material with a constant width of 10mm. The length is varied in the range  $l \in \{10, 20, 30\}$  mm, and the thickness is varied between  $t \in \{2, 4, 6, 8, 10\}$  mm. The simulated muons propagate along the central axis of the scintillator, passing the center of the sensor, with an energy of 1 GeV. The simulation is produced for 300 events, and the effect of the simulated material is demonstrated in figure 10 and the used parameters are presented in table 1.

Table 1: *Shape simulation parameters*

Fixed parameters:	Set Value
Number of events	300
Muons energy	1 GeV
Width	10 mm
Beam Direction (x, y, z)	0 0 -1 (vertical)
Scintillator position (x, y, z)	0 0 0
Source position (x, y, z)	0 0 20mm
Changing parameters	
Length	10 mm, 20 mm, 30 mm
Thickness	2 mm, 4 mm, 6 mm, 8 mm, 10 mm

*The parameters used for the Allpix<sup>2</sup> shape simulations.*

Figure 10: *Example of scintillator shapes*



*Simulated scintillator shapes using Allpix<sup>2</sup>. The scintillator (red block) is hit by a passing muon (red line) of 1 GeV in the center of the detector, inducing a shower of produced photons (green). The difference in the number of incited photons illustrate the effect of varying the scintillator shape.*

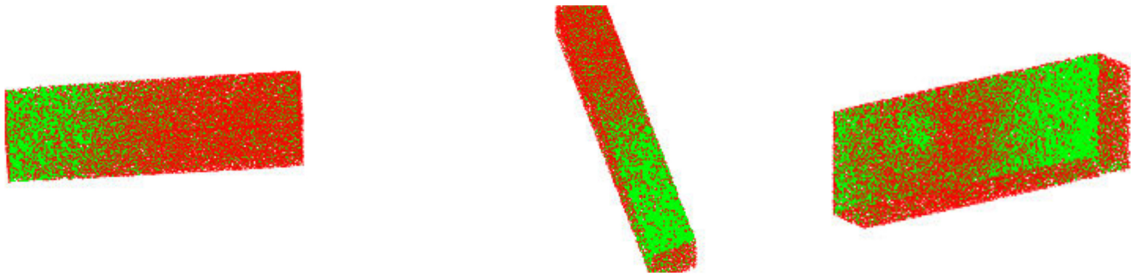
Off-center axis muon events can be simulated by keeping a scintillator of fixed dimensions [10mm x 100mm x 10mm] while varying the position of the source. The direction of muon propagation is still kept strictly parallel to the z-axis. As such, non-central hits are simulated at distances of  $l \in \{10, 20, 30, 40, 49\}$  mm off center-axis. Off-axis effects are demonstrated in figure 11 and the parameters are presented in 2.

Table 2: *Asymmetry simulation parameters*

<b>Fixed parameters:</b>	<b>Set Value</b>
Number of events	300
Muons energy	1 GeV
Width	10 mm
Length	100 mm
Beam Direction (x, y, z)	0 0 -1 (vertical)
Scintillator position (x, y, z)	0 0 0
<b>Changing parameters</b>	
Source position (x, y, z)	(0,0,10 mm) (0,0,20 mm) (0,0,30 mm) (0,0,40 mm) (0,0,49 mm)

*Parameters used in the off-central axis simulations*

Figure 11: *Non-central simulated muons events*



*The effect of non-central axis muon events in the simulated scintillating material, providing illustrations on how a signal is propagated in the material. The scintillator (red block) is hit by a passing muon of 1 GeV at an off-central axis position in the detector, inducing a shower of produced photons (green).*

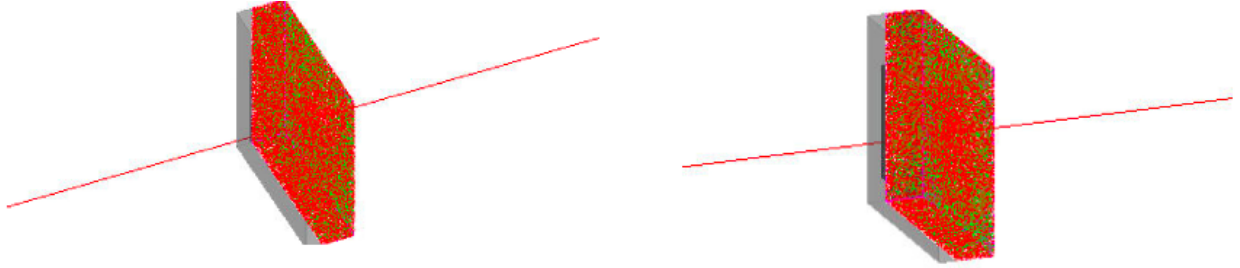
### 3.1.1 Energy simulations:

The energy spectrum simulations are performed for a fixed scintillator shape with cosmic watch dimensions of [50mm x 50mm x 10mm]. The simulations are performed using on-central axis muon hits for the muon energies  $E \in \{5, 10, 50, 100\}$  GeV, the simulations are demonstrated in figure 12 and the simulation parameters are presented in table 3.

Table 3: *Energy change simulation*

Fixed parameters:	Set Value
Number of events	300
Width	50 mm
Length	50 mm
Thickness	10 mm
Beam Direction (x, y, z)	0 0 -1 (vertical)
Scintillator position (x, y, z)	0 0 0
Changing parameters	
Muons energy	5 GeV 10 GeV 50 GeV 100 GeV

Figure 12: *Muon energy simulations*



*The effect of two different muon energies in the simulated scintillating material, providing illustrations on how the energy changes the produced photon signal. The scintillator (red block) is hit by a passing muon of 1 GeV at an on-central axis position in the detector, inducing a shower of produced photons (green).*

The strontium-90  $\beta$ -decay produces electrons with a maximum energy of 2.2 MeV. An electron source with energy in the range [0,2.2 MeV] is simulated in a position just above the scintillator with an incident vertical direction parallel to the z-axis. This simulation were performed for a scintillator of dimension [50mm x 50mm x 10mm], with electrons hitting at the center region of the scintillator, and for a scintillator of dimension [50mm x 150mm x 10mm] hitting both on the central axis as well as at the edge of the material. The maximum possible electron energy event is predicted to be very rare according to the indicated energy spectrum [14], but is valuable in order to observe if the photon-hits measured by the sensor are high or low relatively to the measured muons. The simulation parameters are presented in table 4.

Table 4: *Strontium-90 Simulations*

<b>Fixed parameters:</b>	<b>Set Value</b>
Number of events	100
Width	50 mm
Length small scintillator	50 mm
Length big scintillator	50 mm
Thickness big scintillator	10 mm
Thickness small scintillator	11.1 mm
Beam Direction	0 0 -1 (vertical)
Scintillator position	0 0 0
Housing	Aluminium
Housing Thickness	0.03mm
Housing Reflectively	0.85
<b>Changing parameters</b>	
Source position (small scintillator)	0 0 1.1cm
Source position (Big scintillator)	0 0 1.1cm 7.4cm 0 1.1cm
Electrons energy	0.2MeV 0.9MeV 1.6MeV 2.2MeV

*Simulation of energy ranges using a Strontium-90 source.*

The lead simulations are performed in two parts. Initially a lead plate (passive material) was simulated for values of varying thickness  $t \in \{10.6, 40.0, 86.0, 136.0, 182.0\}$  mm, with muons hitting vertical on the center. The muon energies are varied in order to define the minimum energy values for passing muons (cut-off energy).

The second part covers the Allpix simulation of two values of lead thickness for the configuration presented in table 10, with the photon-hit distributions. The position of the detectors change due to each individual configuration of lead thickness.

Table 5: *Lead simulation*

<b>Fixed parameters:</b>	<b>Set Value</b>
Number of events	50
Width	5 cm
Length scintillator	5 cm
Thickness scintillator	1.1 cm
Beam Direction	0 0 -1 (vertical)
Scintillator1 position	0 0 0
Scintillator2 position	0 0 lead thickness + 5 cm
Scintillator3 position	0 0 lead thickness + 7.5 cm
Lead position	0 0 lead thickness/2 + 2.5 cm
Housing	Aluminium
Housing Thickness	0.03mm
Housing Reflectively	0.85
Muons energy	4GeV
<b>Changing parameters</b>	
Source position	0 0 lead thickness + 15 cm
Lead thickness	4 cm 8.6 cm

*Simulation using a lead plate passive material.*

### 3.1.2 Final configuration detector simulations:

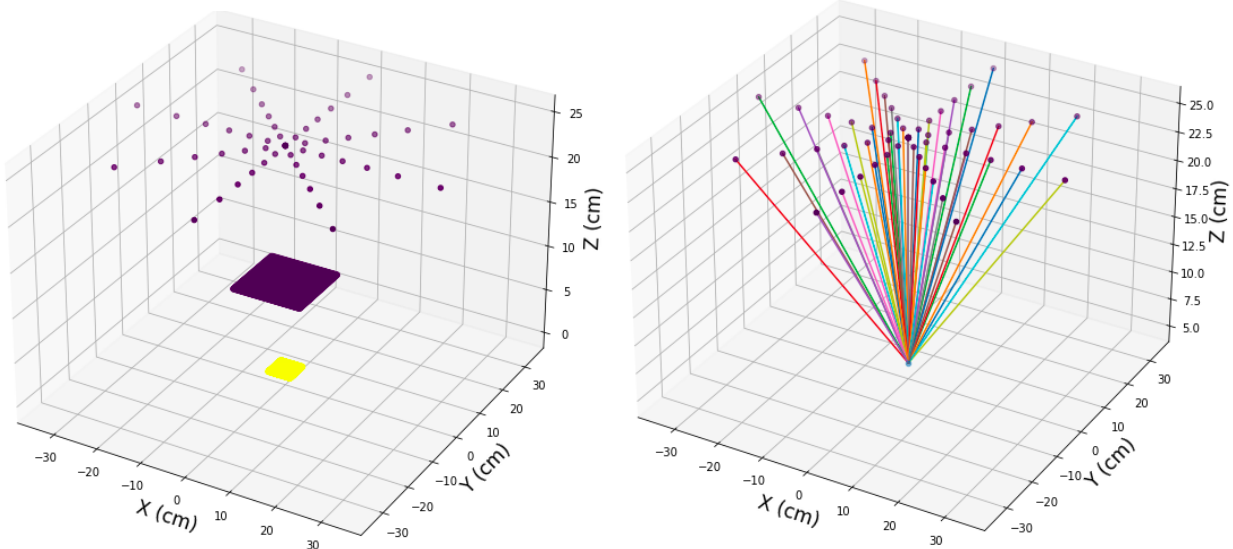
Table 6: *Final configuration simulation*

<b>Fixed parameters:</b>	<b>Set Value</b>
Width Layer Scintillators	5c m
Length Layer Scintillators	15cm
Thickness Layer Scintillators	1 cm
Width Low Scintillator	5c m
Length Low Scintillator	15cm
Thickness Low Scintillator	1 cm
Lower layer Orientation	0 0 90deg
Scintillator 1 position	0 5 cm 11 cm
Scintillator 2 position	0 -5 cm 11 cm
Scintillator 3 position	0 0 11 cm
Lower layer Orientation	0 0 0
Scintillator 4 position	5 cm 0 10 cm
Scintillator 5 position	-5 cm 0 10 cm
Scintillator 6 position	0 0 10 cm
Low Scintillator:	
Scintillator 7 position	0 0 0 mm
Muons' energy	4 GeV
Housing	Aluminium
Housing Thickness	0.03mm
Housing Reflectively	0.85
Total number of events	1992
<b>Changing parameters</b>	
Theta angle	0-90 degree
Phi angle	0-360 degree

The positions and directions of the muon sources are estimated using a function that calculates the above values by drawing a line through the upper scintillator, the lower scintillator and from a central point on the  $(x, y)$  plane at half of the height between the upper and lower scintillator, for leading to symmetric hits to the vertical symmetric line of our configuration. The energy was defined as the mean muon energy of 4 GeV. A singular energy was utilized since the energy variations are negligible at GeV-scale, as demonstrated by the energy simulations.

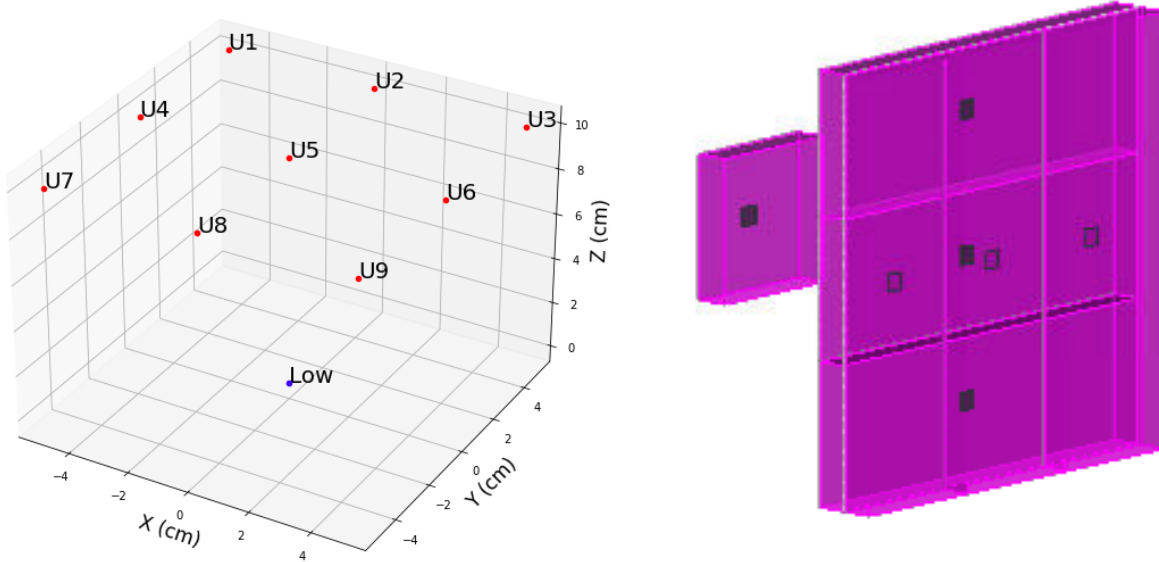
An angular range of  $\theta \in [0, \theta_{max}]$  was used, where  $\theta_{max}$  is the maximum angle that can be measured for selected parameters through the available range of  $\phi$ -values. The distance between the upper and lower scintillator were set to 10 cm, yielding the exact values used  $\theta \in [0, 11, 22, 33, 45]$  and  $\phi \in [0, 315]$  deg. The number of events for each combination of  $\phi$  and  $\theta$  follows their theoretical distributions [13] [14]. The parameters used in the final configuration simulations are presented in table 6 and a graphical illustration is provided in figure 13 and 14

Figure 13: *Incident positions and direction of simulated muons.*



*Positions (left) and directions (right) of muon sources using Allpix<sup>2</sup>*

Figure 14: *Final Configuration*



*Final configuration in pixels representation and in Allpix<sup>2</sup> simulation.*

For each event one of the above detectors triggers and then one of the three detectors of the low layer can be activated. So that passing muon can travel through one of 3 possible areas in the overlapping surface that is defined by the detectors of the low layer. The whole two layers of scintillators define 9 pixels as the picture shows above, with each one to correspond to values of  $\theta$  and  $\phi$  for each event's trajectory as shown below for an event that passes the layers and the low scintillator.

Figure 15: *Angular information*

```
For height: 10 cm
Maximum theta measured (in degrees): 45.0
```

Theta measurements (in degrees) for different pixel triggered:

	Pixel 1	Pixel 2	Pixel 3	Pixel 4	Pixel 5	Pixel 6	Pixel 7	Pixel 8	Pixel 9
Theta:	35.26	26.57	35.26	26.57	0	26.57	35.26	26.57	35.26

Azimuthal measurements (in degrees) for different pixel triggered:

	Pixel 1	Pixel 2	Pixel 3	Pixel 4	Pixel 5	Pixel 6	Pixel 7	Pixel 8	Pixel 9
Phi:	135	90	45	180	0	0	315	270	225

*Final configuration's pixels' angular information*

The Monte Carlo simulation was utilized in order to predict the number of measured events, that covered the muons trajectories following the theoretical angular distribution:

$$I(\theta) \sim \cos(\theta)^2, I(\phi) \sim Uniform[0, 2\pi], I_0 \sim 1\text{cm}^{-2} \cdot \text{min}^{-1} \quad (13)$$

The tracks traversing the upper layer utilize that the every point is hit with the same probability, as such the tracks are produced using a uniform distributions with  $x \in [-7.5, 7.5]$  and  $y \in [-7.5, 7.5]$ . The total number of events is 1000000 and configured to propagate through the upper layer. To produce a random sample of  $\theta$  values a simple Metropolis-Hastings algorithm was used, which is in good agreement with the 13. The probability for the muon to hit the lower scintillator was calculated, and the number of coincidence events (events that detected by both layers and the low scintillator) derived, the false events and also the number of detected events of each layer. We expect to have false events because of the relatively high distance between the low scintillator and layers, a muon from trajectories that do not pass the above layer can hit the low scintillator and an independent event to trigger the same time the top layer leading to a false detection. In this simulation we are interested only in the geometrical properties of the final configuration, since we assume the dead time of the detector to be several ms while the events rate is relatively low for lost events.

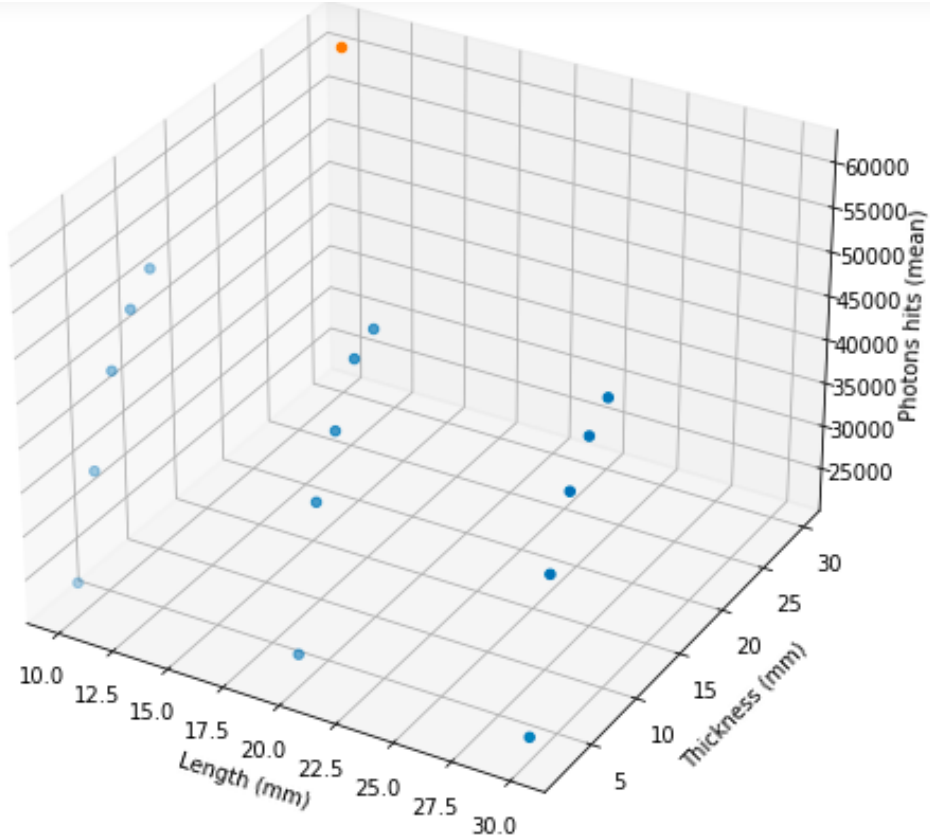
Table 7: *Final configuration Monte Carlo simulation*

<b>Fixed parameters:</b>	<b>Set Value</b>
Upper layer position	0 0 0cm
Lower layer position	0 0 -1cm
Low scintillator position	0 0 -12cm
Upper layer detector 1 x	[-2.5cm, 2.5cm]
Upper layer detector 2 x	[2.5cm, 7.5cm]
Upper layer detector 3 x	[-7.5cm, -2.5cm]
Upper layer scintillators y	[-7.5cm, 7.5cm]
Lower layer detector 1 y	[-2.5cm, 2.5cm]
Lower layer detector 2 y	[2.5cm, 7.5cm]
Lower layer detector 3 y	[-7.5cm, -2.5cm]
Lower layer scintillator x	[-7.5cm, 7.5cm]
Low scintillator x	[-2.5cm, 2.5cm]
Low scintillator y	[-2.5cm, 2.5cm]
$\theta$	$[0, \pi/2]$
$\phi$	$[0, 2\pi]$
muons hit on upper layer x	[-7.5cm, 7.5cm]
muons hit on upper layer y	[-7.5cm, 7.5cm]
Total number of events	1000000

### 3.2 Simulation results

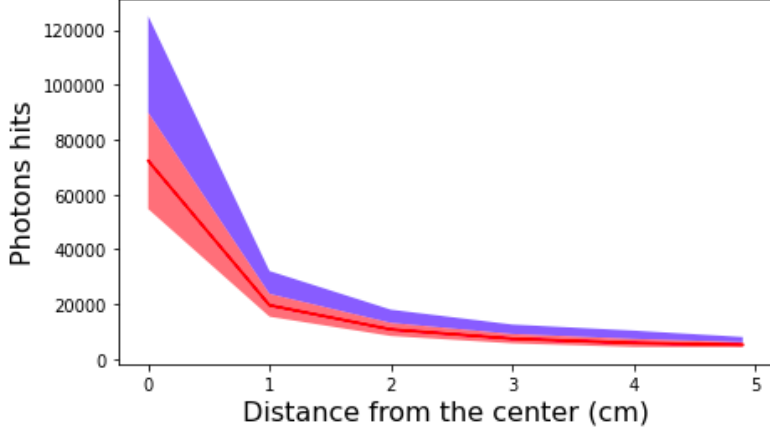
The below figures summarizes the results of the simulation of 300 events for 1GeV muons on different shapes of scintillators. First of all we observe that the change of length does not change by a large value the photons hits mean value but the thickness do, which is explained by the fact that it is equal to the travelled distance of muons inside the scintillator. As we can see the mean value of the photons hits, as the thickness of the scintillator increases , tend to reach a plateau. From these results no differences are expected between the initial cosmic watch scintillator and the new one for central muons' hits.

Figure 16: *Photons hits with shape changes*



The below figures summarizes the results of the simulation of 300 events for 1GeV muons on a fixed shape scintillator for non-central vertical hits. As we can see the number of photons are decreasing rapidly with the increase of hitting distance from the center and it is obvious that scintillators with very large length have limitations on their detection ability.

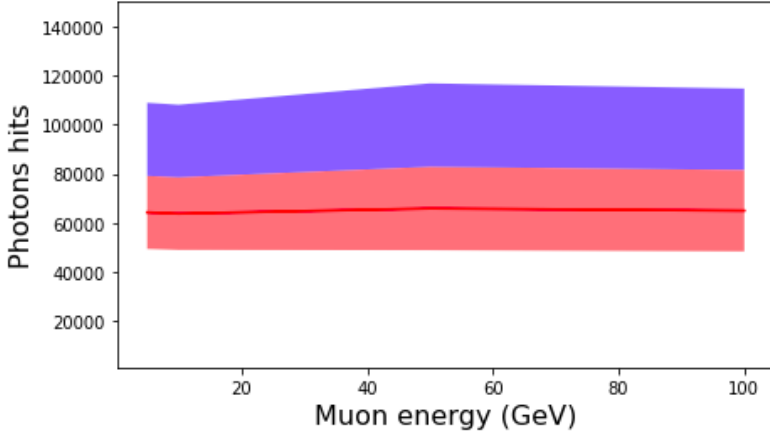
Figure 17: *Asymmetric hits*



*Photons hits:* The red line is the mean while the soft red and blue are the one and two sigma areas respectively.

Energy simulation: The below figure shows that the photons hits are almost equal for the given energy range. Both mean and standard deviation values of photons hits are almost identical for the GeV scale muons and so no extra information on muons' energy is expected by the measured pulses. These results are in good agreement with previous work [15].

Figure 18: *Photons hits for different energy values.*



*Photons hits:* The red line is the mean while the soft red and blue are the one and two sigma areas respectively.

We observe that the energy cut-off for the range [10.6mm,182 mm] lead thickness is very low for the cosmic muons with mean 4GeV energy. So from the simulation the difference on count rates does not expect to change significantly within this thickness range, as it is also obvious from the photon hits counts.

Figure 19: *Energy cut-off of muons passing lead .*

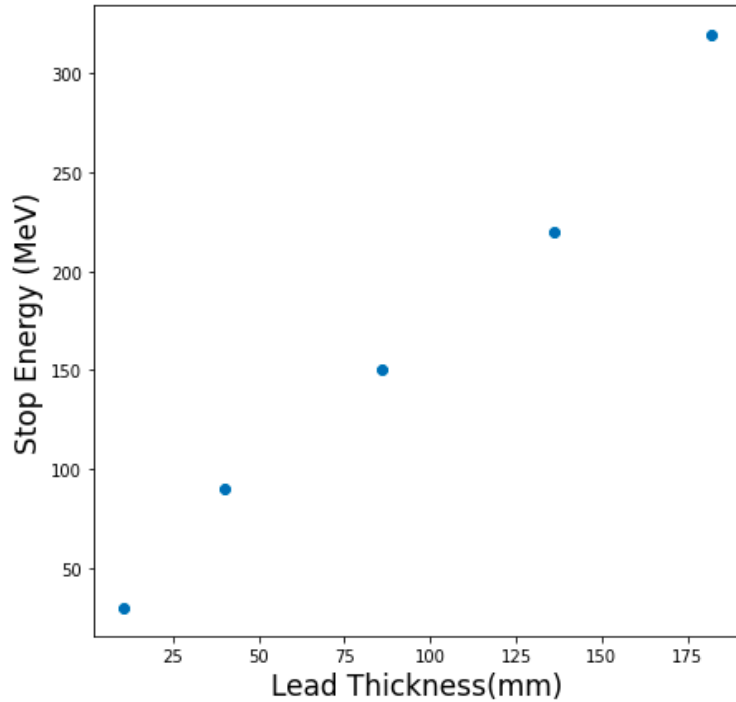
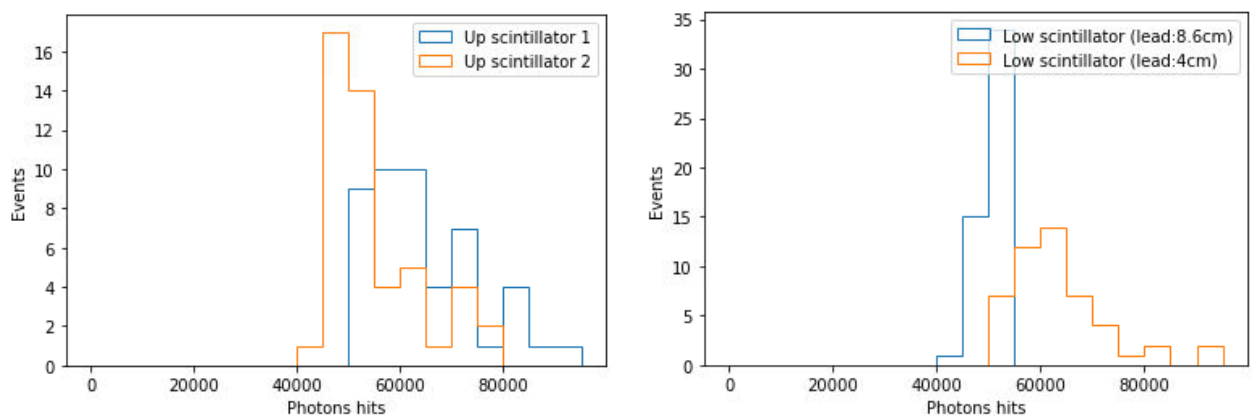


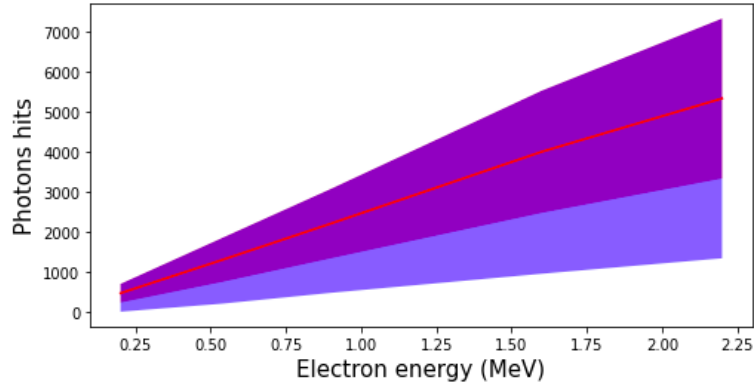
Figure 20: *Upper photons hits for energy lead simulation.*



*Photons hits for the upper scintillator (left) and the one below it (right), both are on top of the lead.*

The below figures shows the photon hits for strontium-90 source leading to electrons that hit the the big scintillator at the center and at the edge and the small scintillator at the center. First of all we observe that there is a linear relation between the mean photon hits and the energy of the detected electron, so the measured pulses contain information on the electron's energy. Also, electrons with higher energies causes more photons hits. But it seems that one electron event with MeV energy causes much less photons hits relatively to cosmic muons, especially for the case of the edge of the big scintillator.

Figure 21: *Electrons' photons hits.*



*Photons hits for electrons hits for different energies with the red line being the mean value and the purple and blue being the one and two sigma respectively.*

Figure 22: *Strontium-90 small scintillator.*

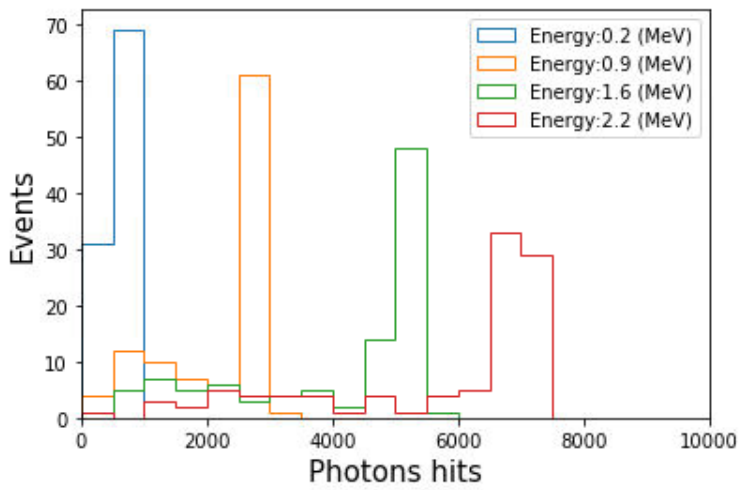
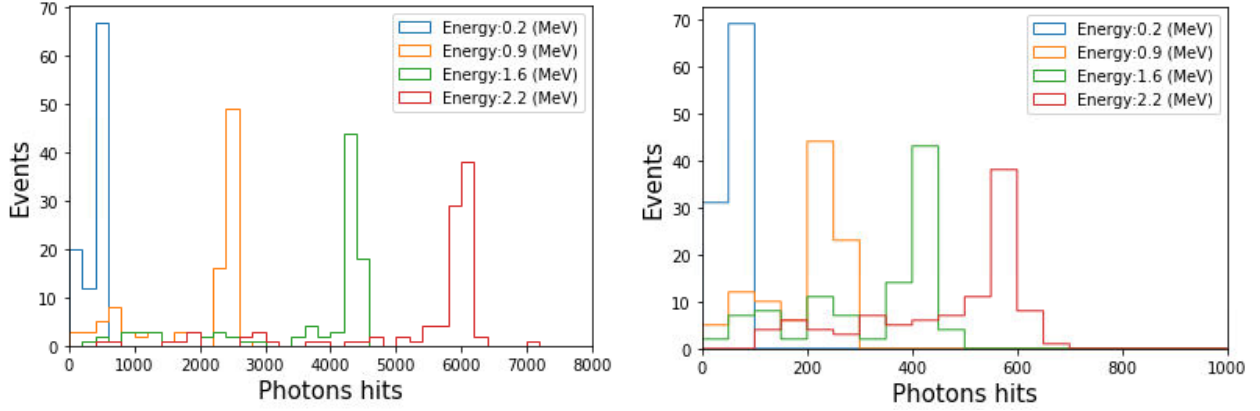


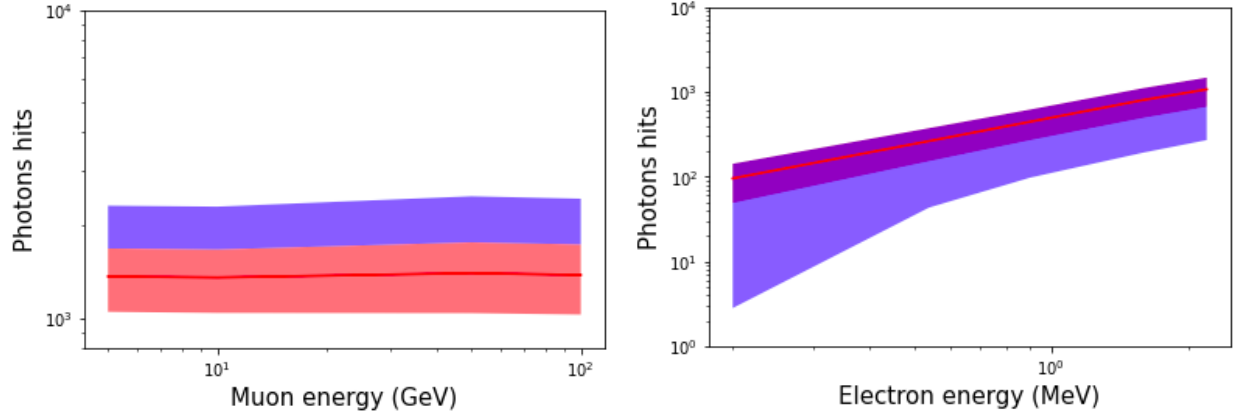
Figure 23: *Strontium-90 big scintillator.*



*Photons hits with source of strontium-90 on the big scintillator at the center(left) and at the edge(right).*

Since in this simulation we observed the same behavior of the scintillator with [15] for both electrons and muons we can normalize the photons hits that the sensor measures to the realistic case of the scintillator material. In comparison to the results of [15] in our simulation the photons hits are 47 times higher for muons and 5 times higher for electrons. By the normalization of our values of photons hits according to those values the results are almost identical with [15] as the picture shows below.

Figure 24: *Normalized photons hits for electrons and muons*

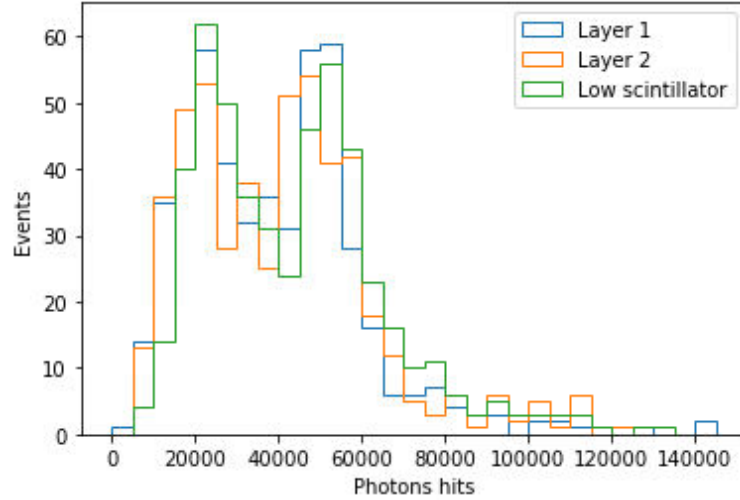


*Normalized photons hits for muons(left) and electrons(right) according to [15]*

### 3.3 Simulation final configuration

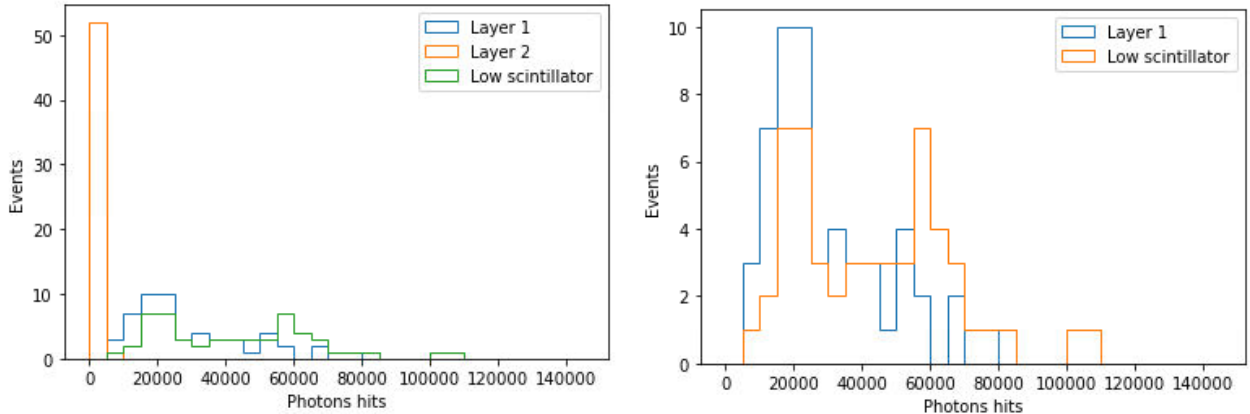
The below figures shows some of the photon hits for some representative directions:

Figure 25: *Photons hits for  $(\theta, \phi)=(0,0)$ .*



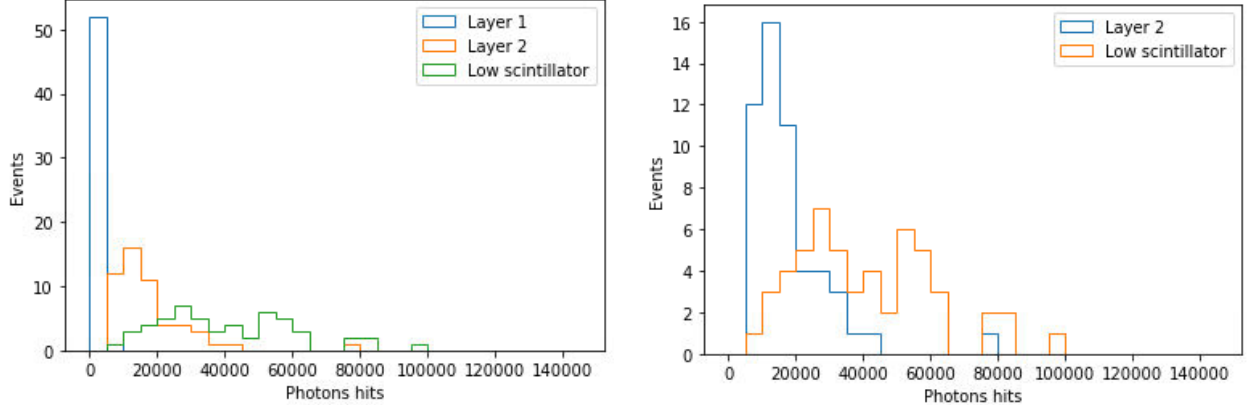
*Photons hits for  $(\theta, \phi)=(0,0)$ , pixel 5, all three triggered detectors.*

Figure 26: *Photons hits for  $(\theta, \phi)=(22,0)$ .*



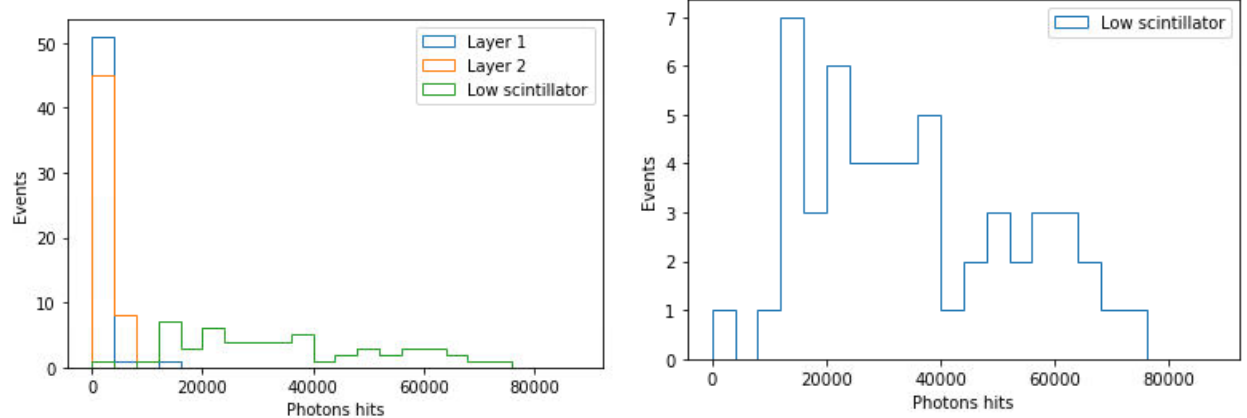
*Photons hits for  $(\theta, \phi)=(22,0)$ , pixel 6, all three triggered detectors(left) and the two triggered detectors with high number of photon hits(right).*

Figure 27: Photons hits for  $(\theta, \phi) = (22, 90)$ .



Photons hits for  $(\theta, \phi) = (22, 90)$ , pixel 2, all three triggered detectors(left) and the two triggered detectors with high number of photon hits(right).

Figure 28: Photons hits for  $(\theta, \phi) = (22, 45)$ .

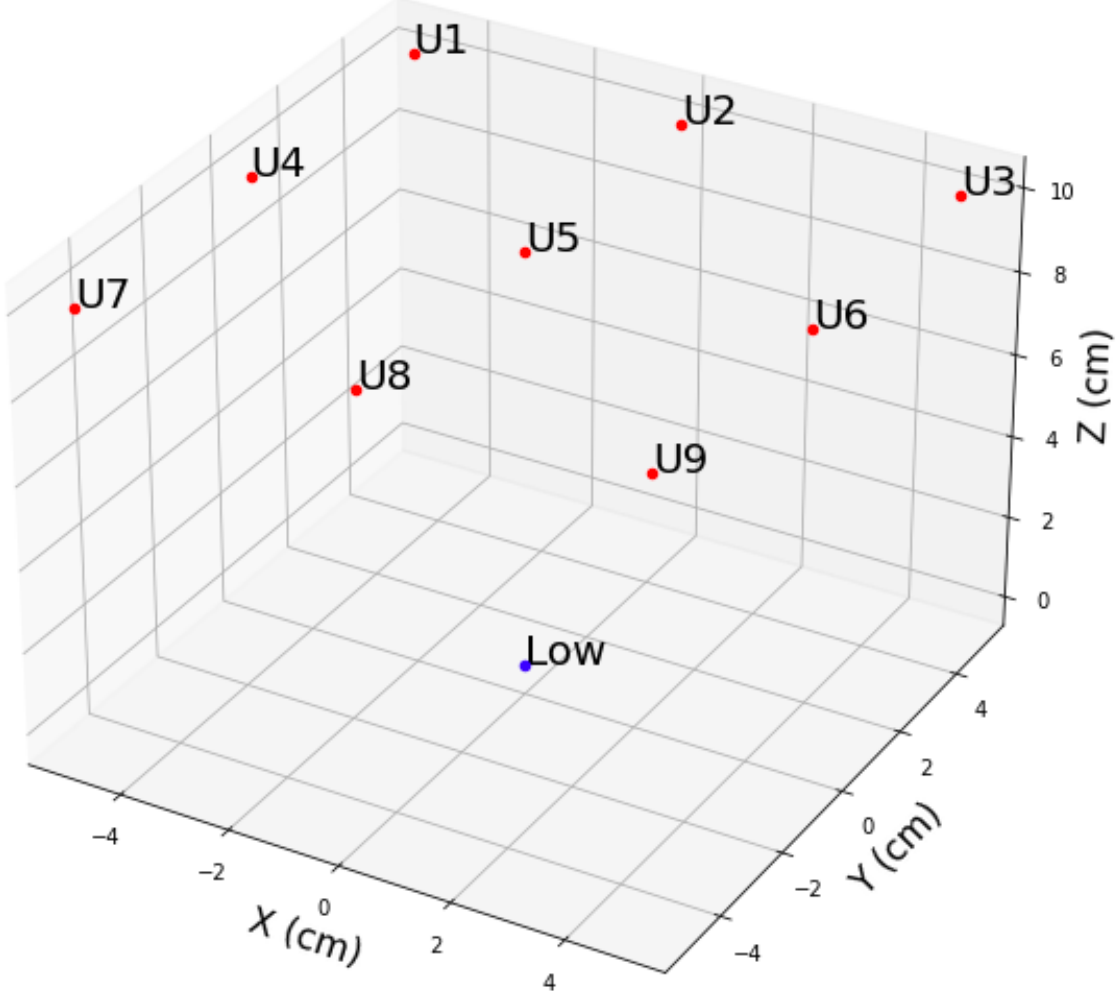


Photons hits for  $(\theta, \phi) = (22, 45)$ , pixel 3, all three triggered detectors(left) and the one triggered detector with high number of photon hits(right).

The above results shows that in the worst case only the central pixel that covers a small range of angles can measure coincidence events(muons that passes through the two scintillator's layers and the the low scintillator).For the case of pixel 6 (and also 4) we have detection for the first layer and for the second layer not,while for pixel 2 (and also 8) the situation is reversed between the layers.The worst area of detection is expected to be the edge pixels (1,3,7,9),where the scintillators do not measure anything at all as we can see for the case of  $\theta = 22$  and  $\phi = 45$ .The above events where chosen because we expect the same measurements from their anti-symmetric area(pixel) due to uniform distribution of muons' azimuthal angle.So we do not expect to measure events that passes all the scintillator layers leading to a coincidence event for hits outside the central vertical area since in reality the photons hits are much more smaller(due to lower housing reflectivity and the different scintillator material).The pixels that are referred above are,as mentioned at the set up section, the

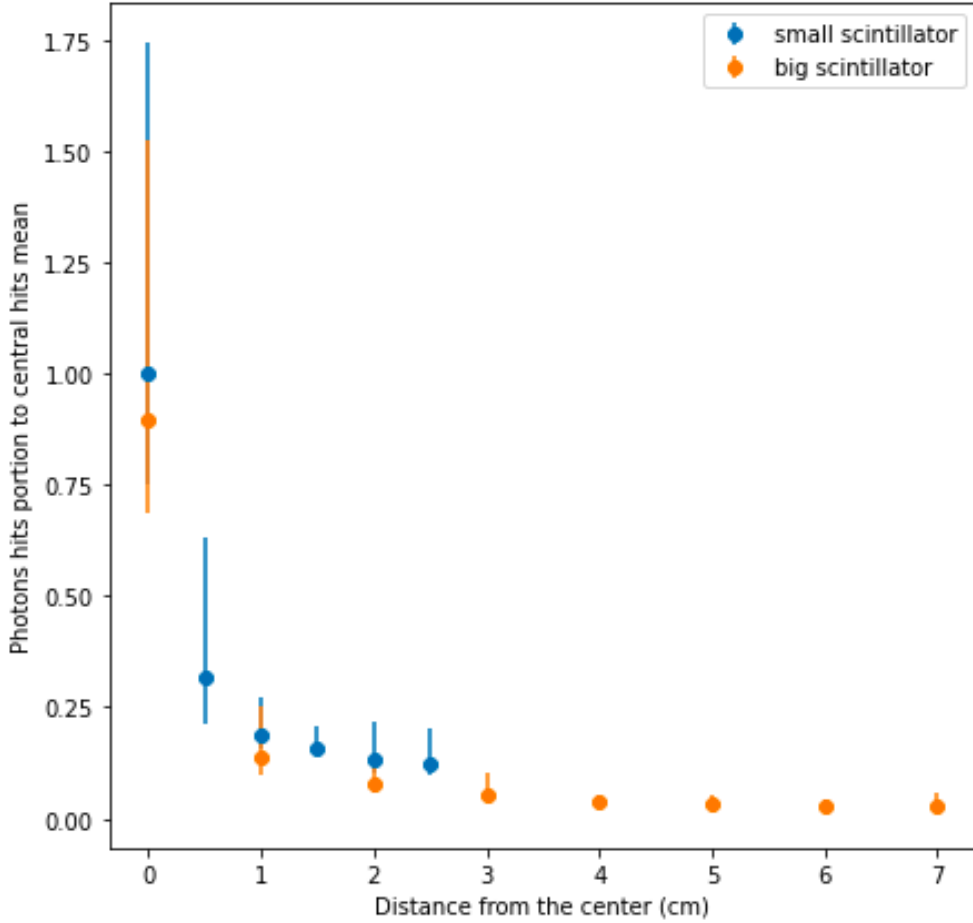
top scintillator's layer overlapped areas as below. Each pixel covers  $\frac{1}{3}$  of the big scintillator's surface and correspond to 1 of 9 possible trajectory( $\theta, \phi$ ) measurements.

Figure 29: Final configuration with pixels.



The low number of photons we observe is explained by the figure below, where there is the number of photons hits for muons hits at different distance from the center for the small and the big scintillator. We observe that the muons that hit the detector at non-central areas lead to a measured number of photons that are very low relatively to the central hit value. For the big scintillator the bigger portion of its surface leads to very low number of photons, at smaller than 10 % for hits at hit distances higher than 2cm from the center. Given that the reflectance that was used (0.85) was higher than the reflectance of aluminium foil in reality the value of non-central hits are smaller, leading to a big area of the surface that practically cannot measure events effectively.

Figure 30: Final configuration scintillators asymmetry hits.



Photons hits ,normalized to central hit mean photons number of the small scintillator, in 2 sigma range for different distance from the center of the scintillator for the big scintillator (orange points) and the small scintillator (blue points).

The Monte Carlo simulation showed the measurements for the case of the big scintillators working perfectly and measuring all along their length .

Because of the expected non-central hits effects the above simulation is expected to not be realistic.A second simulation was made,adjusting the first simulation to the assumption that the detector can detect a muon hit inside the cosmic watch surface's dimensions only(with that area being centered to the center of the scintillator).For this case the big scintillators measured only the hits inside this area,otherwise they do not trigger.

Count measurements with both small and big scintillator showed that the small detector measures around 10 times more counts.If the large scintillator worked sufficiently it should have three times higher counts as a result of its dimensions.An extreme case is considered,with the simplest assumption for this result to be that the surface that can lead to a detection on the large scintillator is 10 times smaller than the cosmic watch's surface(detectable events cover only muons that pass at distance smaller than 7.5mm from the center or sensor).

Table 8: *Monte Carlo simulation results (1hr)*

<b>Parameter:</b>	<b>Value</b>
Number of events top layer	13500
Number of events low layer	12783
Coincidence events	982
False events	282

*Measurements of the final configuration for 1 hr of exposure.*

Table 9: *Adjusted Monte Carlo simulation results (1hr)*

<b>Parameter:</b>	<b>Value</b>
Number of events top layer	3976
Number of events low layer	1147
Coincidence events	365
False events	135

*Measurements of the final configuration for 1 hr of exposure.*

Table 10: *Extreme case Monte Carlo simulation results (1hr)*

<b>Parameter:</b>	<b>Value</b>
Number of events top layer	398
Number of events low layer	120
Coincidence events	31
False events	6

*Measurements of the final configuration for 1 hr of exposure.*

## 4 Calibration

### 4.1 Radioactive calibration

#### 4.1.1 Sr-90 energy spectrum calibration

To calibrate the energy of the signal we used a radioactive source for which the energy spectrum is known. We found the relation between the ADC count and the energy by comparing the known energy spectrum of the source with the ADC distribution measured by our detector. For our measurement we used the radioactive source Strontium-90 (Sr-90), which decays into Yttrium-90 (Y-90) through  $\beta$ -decay.

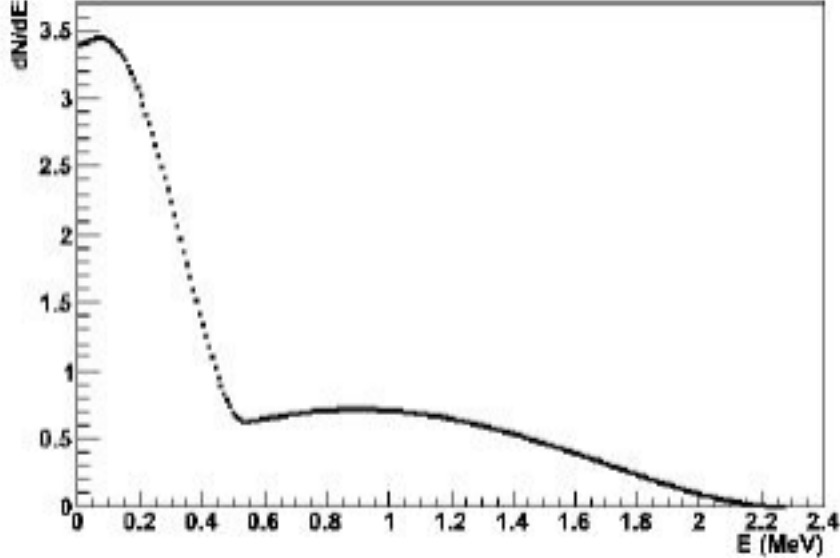


Since the half-life time of Sr-90 is 28.5 years and the half-life time of Y-90 is 64.1 hours we also include the decay spectrum of Y-90.



The energy spectrum of Sr-90/Y-90 is shown in Figure 31. For this calibration, only one

Figure 31: *The energy spectrum of Sr-90/Y-90 [1]*



*The energy spectrum of Sr-90/Y-90 [1]*

point of comparison was possible, and this was the endpoint. This is due to the energy spectrum of Sr-90 not being in the same range as the energy spectrum of a typical cosmic muon passing through our detector. The Sr-90 spectrum has an endpoint energy value of 2.27MeV [1]. According to [4], a cosmic muon typically has an energy of 4GeV at sea level,

and loses energy at an almost constant average rate of 2.2MeV/cm in a material of density  $1g/cm^3$ . Therefore, the mean energy deposited by muons in our 1 cm thick scintillator is 2.2MeV. The initial idea was to use these two datapoints to fit the ADC function, however since the energies are approximately the same, we use it for cross checking.

As will be shown in section 4.2, the ADC distribution will be different for every individual detector. For this reason we used the same detector for our measurements. We took a 1-hour measurement with the source held above the detector inside a dark test box and covered with lead plates to reduce background, see figure 32. We also took a background measurement of

Figure 32: *The setup of the radioactive measurements inside a blackbox.*

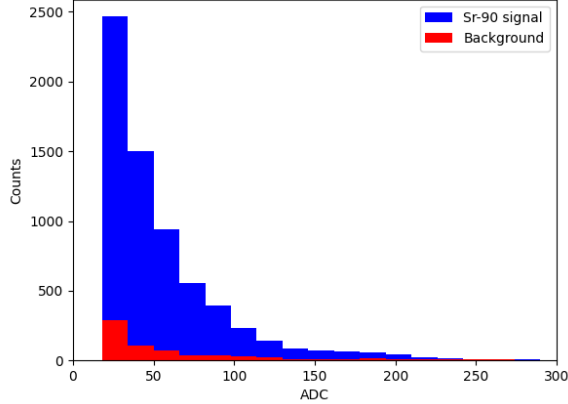


*The setup of the radioactive measurements inside a blackbox. The source was placed on top of the collimator.*

the same setup without the source, in order to obtain the ADC distribution for the source. The source and background ADC distributions are shown in Figure 33. The final ADC distribution was taken as the source distribution minus the background distribution, and an exponential fit to the data of the form  $Ae^{bx}$  was performed. The final ADC distribution and fit is shown in Figure 34. The fit parameters were found to be  $A=2757.84$  and  $b=21.65$ , and the fit had a reduced  $\chi^2$  statistic of 10.64 with respect to the data. The final ADC distribution has a long tail due to background. Consequently, to determine the endpoint of the distribution in order to compare it to the Sr-90 spectrum, we had to set a threshold for the signal to background ratio. We chose a signal-to-background ratio threshold of one. The endpoint of the distribution was therefore found by taking the first bin for which the ratio of signal to background is less than 1. This gives an endpoint bin center value of  $224 \pm 8$  ADC. This ADC value therefore corresponds the aforementioned Sr-90 spectrum endpoint of 2.27MeV. The error on this value is the half bin width.

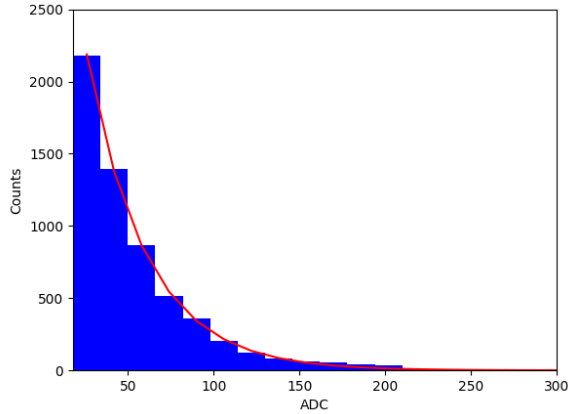
Since we know that the average energy that muons deposit in our detector is 2.2MeV we use this to cross check the ADC value found for the endpoint of Sr-90, which is approximately 2.2MeV. We found that the average energy value of 2.2 MeV for muons, measured by our detectors, corresponds to  $148 \pm 8$  ADC. This difference in ADC value for the same energy value for muons and electrons can be explained by bremsstrahlung photons. Since electrons

Figure 33: *ADC distribution measured by the detector over 1 hour with and without the Sr-90 source.*



*ADC distribution measured by the detector over 1 hour with and without the Sr-90 source*

Figure 34: *Background subtracted ADC distribution of Sr-90 source with exponential fit*



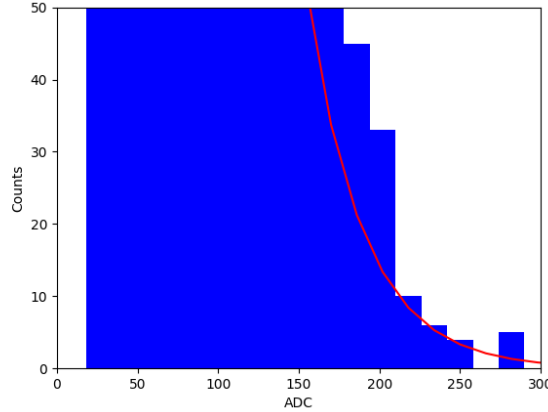
*Background subtracted ADC distribution of Sr-90 source with exponential fit*

create much more photons inside the scintillator than muons, much higher energies are recorded.

#### 4.1.2 Spatial properties of the scintillator

The effect of the positioning of the source on the ADC distribution was also determined by taking additional measurements with the source placed at the center and off-center on the side of the large scintillator. These results were compared to simulation and it was found that a significant amount of the photons are lost when particles pass through the side of the scintillator, see figure 36.

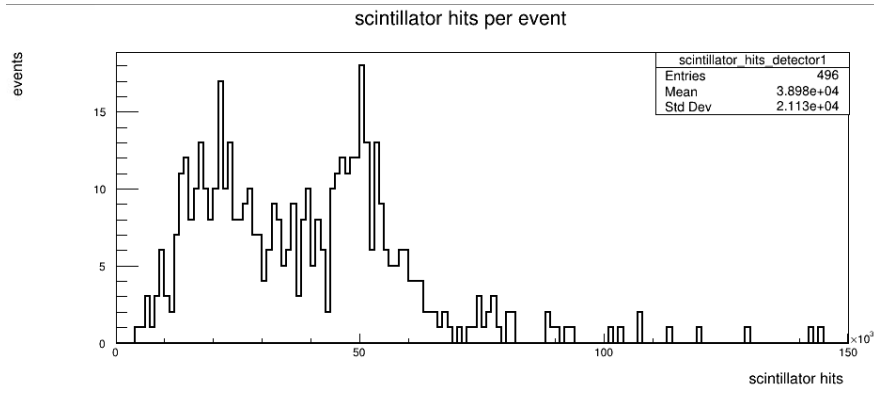
Figure 35: *ADC distribution zoomed in on endpoint*



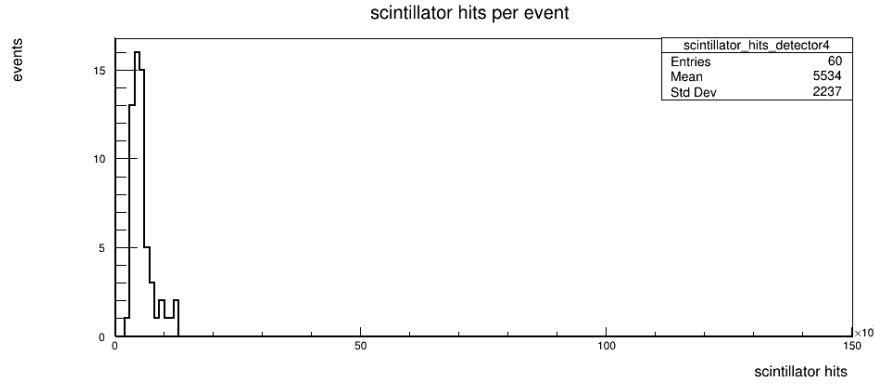
*ADC distribution zoomed in on endpoint*

This results in a higher count rate at low ADC values compared to particles that pass through the center of the scintillator, see figure 37. The central measurement in figure 37 shows high count rates in the region 75-175 ADC, which is remarkable since it does not show this on the Sr-90 spectrum in figure 33, where we measurement with the source approximately at the center. We tried to reproduce the central histogram of figure 37 with the small scintillators, however we repeatedly obtained the exponential spectrum. One possible explanation for this is also bremsstrahlung, since photons are lost in the long scintillator side measurements and the small scintillator has less volume to capture the photons, it makes sense that their spectrum is shifted towards the lower ADC values.

Figure 36: *Simulation of muons hitting the detector at the center (top) and side (bottom) of the scintillator.*



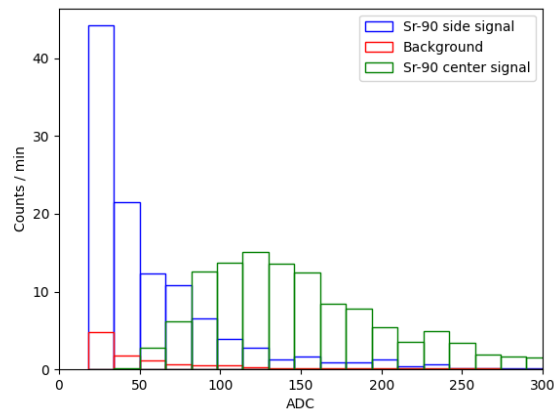
(a) Simulation of muons hitting the detector at the center of the scintillator.



(b) Simulation of muons hitting the detector at the side of the scintillator.

*Simulation of muons hitting the detector at the center (left) and side (right) of the scintillator.*

Figure 37: *ADC distribution of long scintillator with the Sr-90 source.*



*ADC distribution of long scintillator with the Sr-90 source at the center (green), the Sr-90 source at the side (blue) and the background (red).*

## 4.2 Electronic calibration

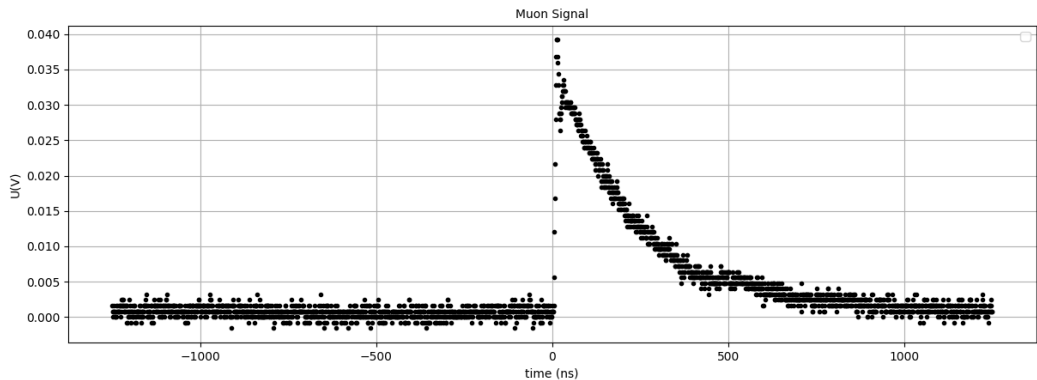
The Arduino Nano on the main PCB (Printed Circuit Board) converts an incoming, analog, signal into a digital number, this is called the ADC (Analog to Digital Conversion) value. The Arduino Nano has a maximum resolution of 10 bits and an operating voltage of 5 Volts [16], which means that an incoming signal with a peak voltage between 0 and 5 Volt will be converted to a number between 0 and 1024. The analog signal that enters the Arduino does not directly come from the SiPM (Silicon Photon Multiplier). The signal that leaves the SiPM is amplified and stretched before it enters the Arduino. And this amplified and stretched signal is converted into the ADC value.

When a signal travels through the amplifier and peak detector, the final analog signal differs, dependent on the board it travels in. In this experiment we used 11 different main PCBs, and in order to compare the measurements of each board, the ADC values of each board must be coupled to the mV they represent and this is what the electronics calibration does.

The main goal of the electronics calibration is to mimic a muon signal with a known peak value, inject it in the circuit, let it travel through the amplifier and peak detector and measure the ADC value. Now if we determine the ADC value as a function of injected peak voltage (in mV), we can fit this function and can calculate from each ADC value, the corresponding peak voltage and compare results from different detectors.

### 4.2.1 Generating a Muon Signal

Figure 38: *Muon Signal on Oscilloscope*



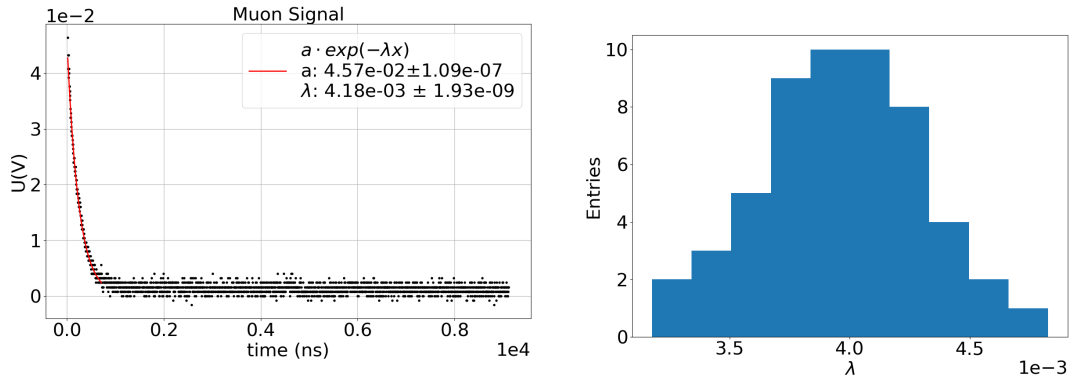
*A muon signal as measured from the BNC output.*

The first step in calibrating our detectors is digitizing the muon signal and injecting it into the main board. The injection is done through the BNC, so at this point we want to mimic the muon signal. This is done by analysing muon signals from the BNC on the oscilloscope, generate a similar waveform, feed this waveform to a pulse generator and inject

this pulse through the BNC into the main board.

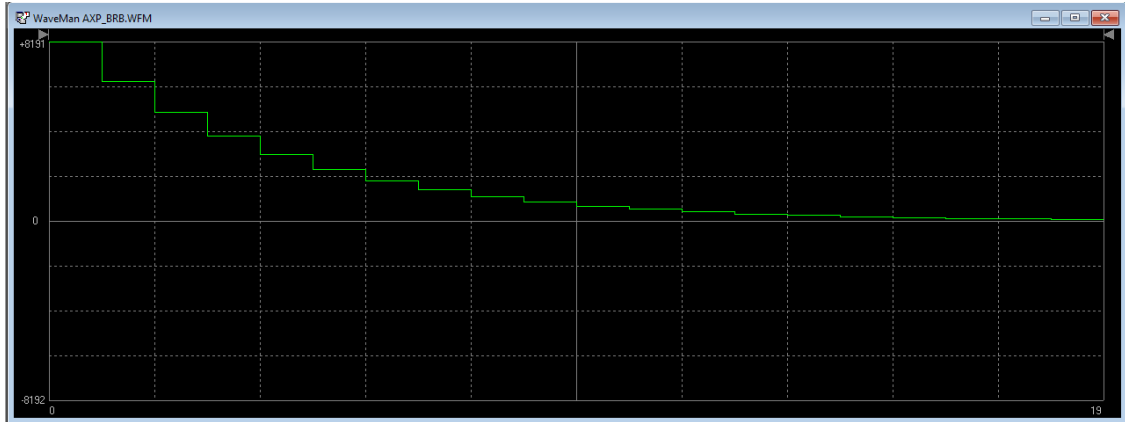
Muon signal analysis done by displaying and saving muon signals as .csv files from the oscilloscope (Model: Tektronix TDS 2022B), the manual can be found in ref [8]. The data is visualised in figure 38. The data of 63 muon signals is fitted with an exponential function and the time constant ( $\lambda$ ) is determined for each signal, see figure 39. From the distribution of  $\lambda$  we used the mean value to generate the muon signals, this value lies around  $4 \times 10^{-3}$ . We used the TTi TG5011 pulse generator to inject the waveforms and used the program TTi Waveform Manager Plus to construct the right waveforms, see figure 40, the manual can be found in ref. [17].

Figure 39: *Calibration Analysis*



On the left we see a muon signal as seen from  $t = 0$  fitted with an exponential function. The right figure displays the configuration of  $\lambda$  obtained from 63 different muon signals.

Figure 40: *Waveform Generator*



The digitized muon signal. The signal has to be created in 20 bins in order to be compatible with the required input of the used pulse generator.

### 4.2.2 Injecting Pulses

To calibrate the detector, pulses are injected with their peak amplitude between 10 mV and 1.0 V. A dedicated python script controls the signal generator and triggers the calibration signal waveform. The serial commands were extracted from the manual [17], the correct communication specifications had to be found by trial and error. The script also reads the detector signals and stores them in a .csv file. The Arduino was programmed in a way that only the ADC value is printed, which is all the necessary data needed for calibration. During the calibration, the baseline of the muon signal (before and after the pulse) increases with increasing pulse amplitude. This means that the reset threshold and the signal threshold in the Arduino code cannot be too low. If the thresholds are too low, the ADC values will never go below the reset threshold and the Arduino stops measuring. Therefore we looked at what value the Arduino started measuring pulses, and set the signal threshold to this value (between 60 and 90) and set the reset threshold at a value of 15 less, for example: 60 and 45 respectively.

### 4.2.3 Analysing the data

The calibration data is fitted with a polynomial function. To minimise the relative (and not the absolute error), the  $\log(\text{mV})$  is fitted. In figure 41 and 42 we show the data and fits of one example detector. Higher degree order fits show divergences for  $\text{ADC} < 100$ , but describe the data better for  $\text{ADC} > 500$ . We find, that in general, a low degree (2 or 3) degree fit is enough to describe the data sufficiently as the majority of hits is to be expected for low ADC values. Most importantly, the calibration fit must be monotonously increasing over the full ADC range, which excludes the higher degree fits. A possible improvement would be a distinction in low and high ADC areas with corresponding conversion based on different polynomial fits. The fit parameters obtained from this plot are used to determine the mV amplitudes of the measured muon signals.

### 4.2.4 Voltage analysis

Injecting a muon-like signal with the signal generator needs to account for the different impedances of the various components and circuits, e.g. a BNC jack with  $50\Omega$ . When a muon signal is injected into the main PCB from the SiPM, the signal is not passing through the BNC jack. Therefore, we need to take into account that the signal is modified when passing through the BNC jack instead of directly being injected into the PCB. The solution is to measure the voltage directly at the BNC jack and use this voltage to make the ADC count vs. voltage plots instead of the input voltage of the pulse generator. Another issue is that, when the signal is injected and the impedance of the pulse generator, transition medium and the PCB mismatch, the signal deflects back to the source which causes noise and makes the signal to very difficult to read out on the oscilloscope. For this reason we used a  $50\Omega$  radio-frequency feedthrough terminator to connect the pulse generator to the PCB. This terminator dampens these noise components. The schematics of the calibration including the oscilloscope test points is presented in figure 43.

With this setup, multiple pulses were injected with a peak amplitude ranging from 30 mV to 980 mV. This was done for two PCB's (Rens' and Carlo's). Then the voltage was measured and with this, the ratio of the measured voltage to the input voltage was plotted against the input voltage. The plots were fitted with the function  $y(x) = \frac{a}{x} + b$ .  $a$  and  $b$  were determined by using a least squares fit. The resulting plots can be seen in Figure 44 and Figure 45. It is observed that the two plots are almost identical, indicating that there is no significant difference between two PCB's.

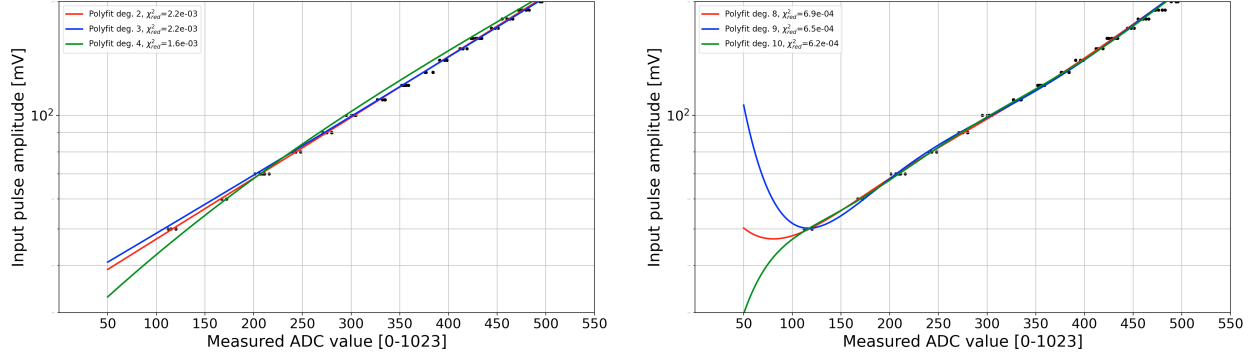
The reason why we used the function  $y(x) = \frac{a}{x} + b$  for the fitting can be explained as follows. We expect the voltage measured to be a constant times the input voltage of the signal generator. In our fitting function, this constant corresponds to  $b$ . Furthermore, at low input voltages, we expect the noise to dominate the signal and the SNR (signal to noise ratio), to increase proportional to  $\frac{1}{x}$ . In our fitting function  $a$  corresponds to this factor of proportionality. The parameters of the fit are summarized in Table 11. The value  $a$  is a measure of the average noise and  $b$  is the conversion factor of the input voltage to the voltage behind the BNC port.

For the energy reconstruction, when the voltage injected by the pulse generator into the PCB is plotted against the ADC count, the voltage first has to be converted to the voltage behind the BNC by multiplying by the factor  $b$ . This is the voltage that then should be compared to the radioactive calibration where the energy is plotted against the output voltage.

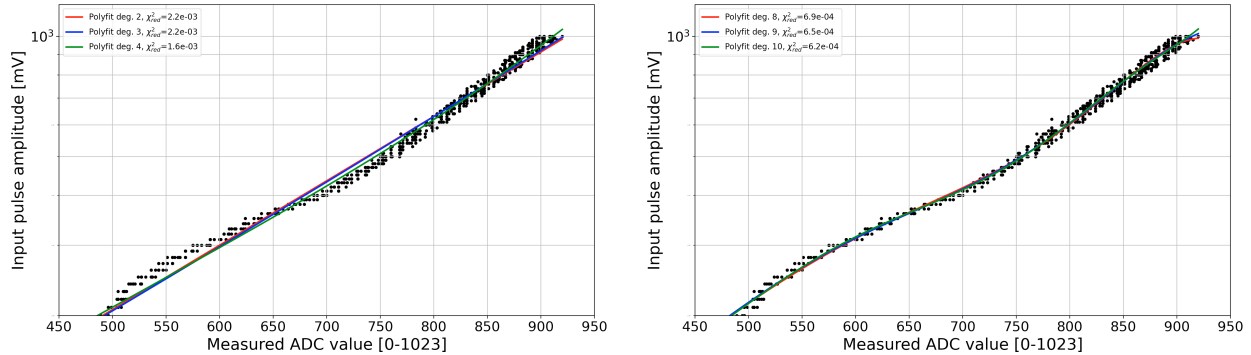
Table 11: *Fit parameters*

parameter	value
a	1.981
b	0.437

Figure 41: Electronics calibration fits polynomial degree study

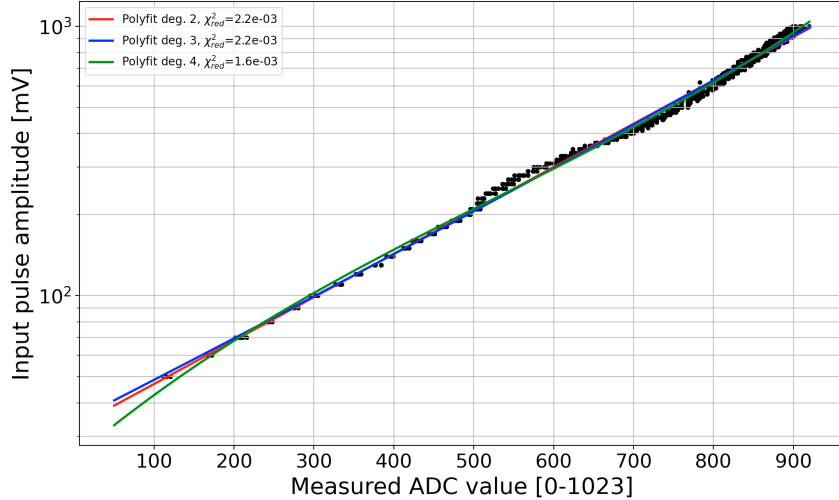


The input pulse amplitude in mV as a function of ADC value for the detector Florian zoomed in to the lower ADC range. The fits model  $\log(mV)$  to minimise the relative error. The  $\chi^2_{\text{red}}$  values indicate an overfit for all models given the large amount of data points which is desired for a calibration curve. For  $ADC < 100$ , the higher degree polynomial degrees clearly do not agree with the expected data. The 2-degree fit appears the best description of the data



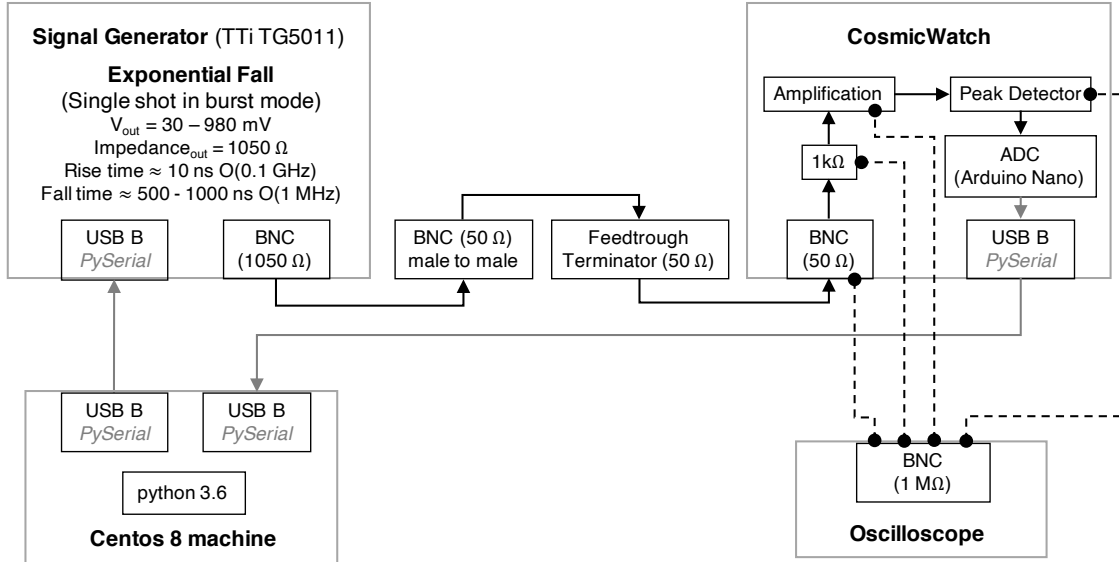
The input pulse amplitude in mV as a function of ADC value for the detector Florian zoomed in to the higher ADC range. The fits model  $\log(mV)$  to minimise the relative error. The  $\chi^2_{\text{red}}$  values indicate an overfit for all models given the large amount of data points which is desired for a calibration curve. For  $ADC > 500$ , the higher degree polynomial degrees describe the data better, however, as seen above, these fit diverge for values close to the signal threshold. Since the majority of counts are to be expected in this low regions, a sufficient description is given by the low degree fits. A possible improvement would be the distinction in a low and high ADC region to convert the ADC to mV.

Figure 42: Electronics calibration fits



The input pulse amplitude in mV as a function of ADC value for the detector Florian. The fits model  $\log(mV)$  to minimise the relative error. The  $\chi^2_{\text{red}}$  values indicate an overfit for all models given the large amount of data points which is desired for a calibration curve. For this specific detector, a second degree fit describes the low ADC region of interest best.

Figure 43: Calibration schematics



Calibration schematics including the test points with an oscilloscope. Analog signals are drawn with black solid arrows. Dashed black lines indicate test points with an oscilloscope which can be removed or switched and are thus not permanent. Digital signals are shown by dark-gray solid arrows. Individual units are encased in light-gray boxes, with the corresponding units in black boxed are

Figure 44: *I/O plot of Rens's PCB*

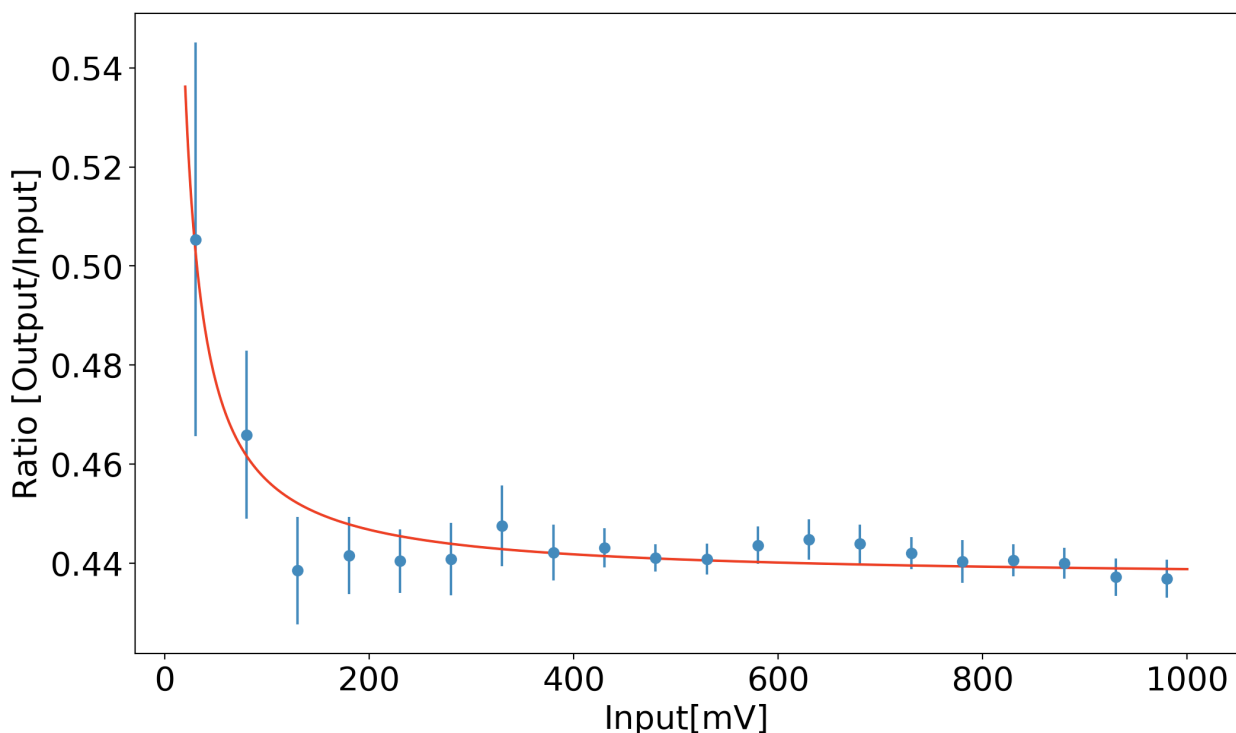
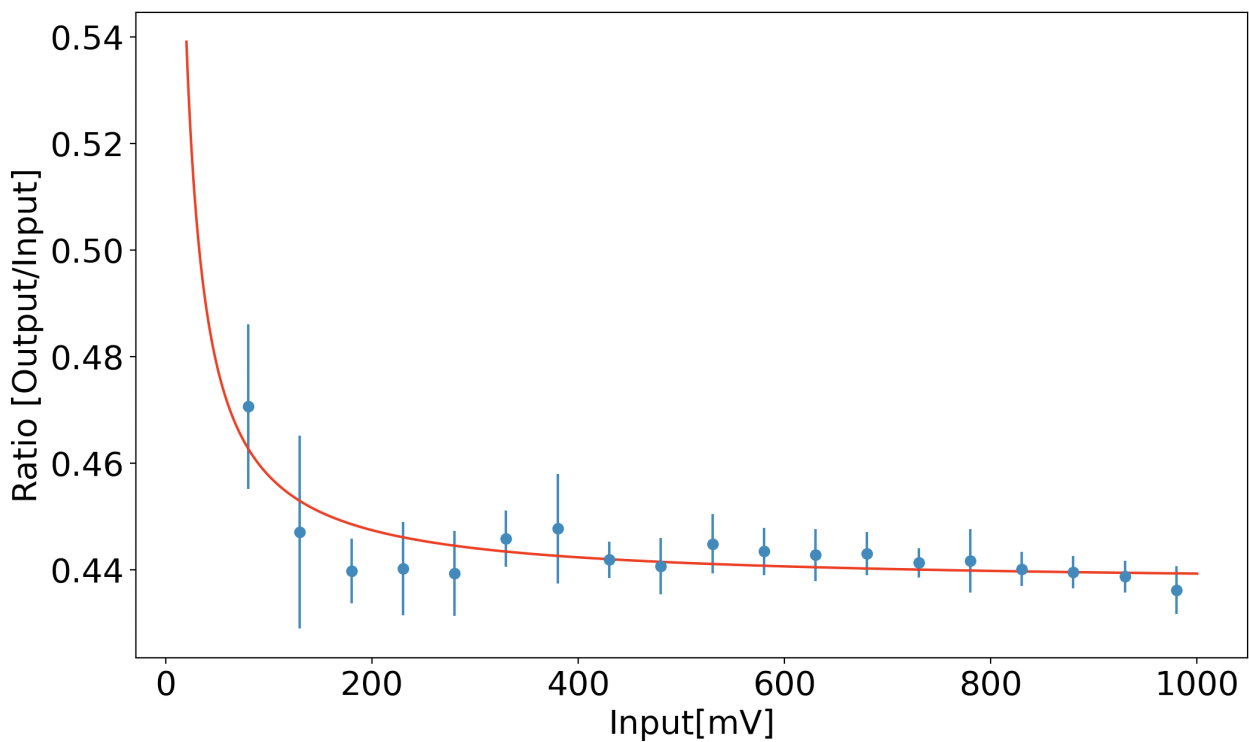


Figure 45: *I/O plot of Carlo's PCB*



## 5 Data Acquisition

### 5.1 Methodology

The data acquisition is performed through a Python script (available on GitHub)<sup>2</sup>. The main task was that of building a module with some classes to define our *Grid of Detectors*, and to describe what is a *Signal* and a *Muon*. The program communicates with the detectors through the USB connection on the Arduino. As every detector has a specific name, the program is made in such a way that, reading from a configuration file the names and the positions of the detectors, is able to automatically connect and recognize which detector is connected to which serial port. The crucial information to include in the configuration file is the layer of the detector, where a layer comprehends all the detectors that are at the same level (height from the ground).

The requirements to take the data is then to just define the initial configuration of the grid in the file, and to connect every detector to the computer via the USB (we had a very useful USB hub with 7 ports to handle all the detectors at once.)

The code loops through all the detectors continuously, and checks if there is a signal coming through the serial port. If there is a signal coming, this is recorded with all its information: ADC, temperature, up-time, time difference, the name of the detector and other pieces of information. If two signals are recorded within a short window of time (that after some testing was set to 0.1 seconds), they are considered as coming from the same particle passing through the two detectors. If, as in this case, there is a total of three layers, a signal is considered to be a muon only if there is at least a signal recorded in all of the three layers. There are some additional checks on the script that avoid having a signal from two detectors of the same layer in the same muon signal: this is because we expect the muons to come from 'above' and it will be then not reasonable to have a signal going through more than one detector per layer.

It is important to stress that the clocks on the different detectors are not synchronized. When a signal is recorded, the time assigned to the signal is the time of the machine where the program is running. This avoids a lot of problems with trying to synchronize the different Arduinos, but it introduces an important loss of information: as the script can't read from all the detectors in parallel but just 'ask' the detectors if they have a signal one after the other, the order of the detection of a muon from the different layers is just random. This is not a very big problem, as it will anyway be assumed that the muon is coming from the top, but it is still important to stress that as some types of measurements are not possible because of this.

Another interesting remark is that this script works both if the detectors are set in Master and Slave mode and connected through the jack, but also in the Master-only mode and no jacks at all. The difference is that in the first case, only the signals of the Slaves that are triggered together with the Master are sent to the computer, while in the other case every single event recorded by the detectors is sent via the serial port. This second option worked quite well for our case, but it can become trickier if the number of detector grows, in which case a first hardware filtering of the background will definitely help to track the

---

<sup>2</sup><https://github.com/cfuselli/Nikhef-Project-2021>

correct muon signals.

Figure 46: *Example of configuration*



*An example of a configuration of detectors with three layers.*

## 5.2 Live plotting

As a final result of the project, it was decided to provide the detector with a live visualization of the incoming muons. Even if the initial plan was to have some sort of screen to place in front of the detector and really being a hardware part of it, it was decided to opt for the easier and cheaper solution to just to show a live plot on the screen of the computer. This has been achieved through a simple Python script that shows the live animation of the detector.

The program gets the information about the configuration of the specific run from the setup file that is saved in the folder: there it is possible to find the coordinates of the centers of the detectors as well as the dimensions of the scintillators. These are then plotted in a 3-dimensional graph, where every layer has a different colour. On top of every detector in the plot it is possible to read the name of the detector itself (the names are just an ID of the detector, and everyone decided to name the detector randomly and without any criteria).

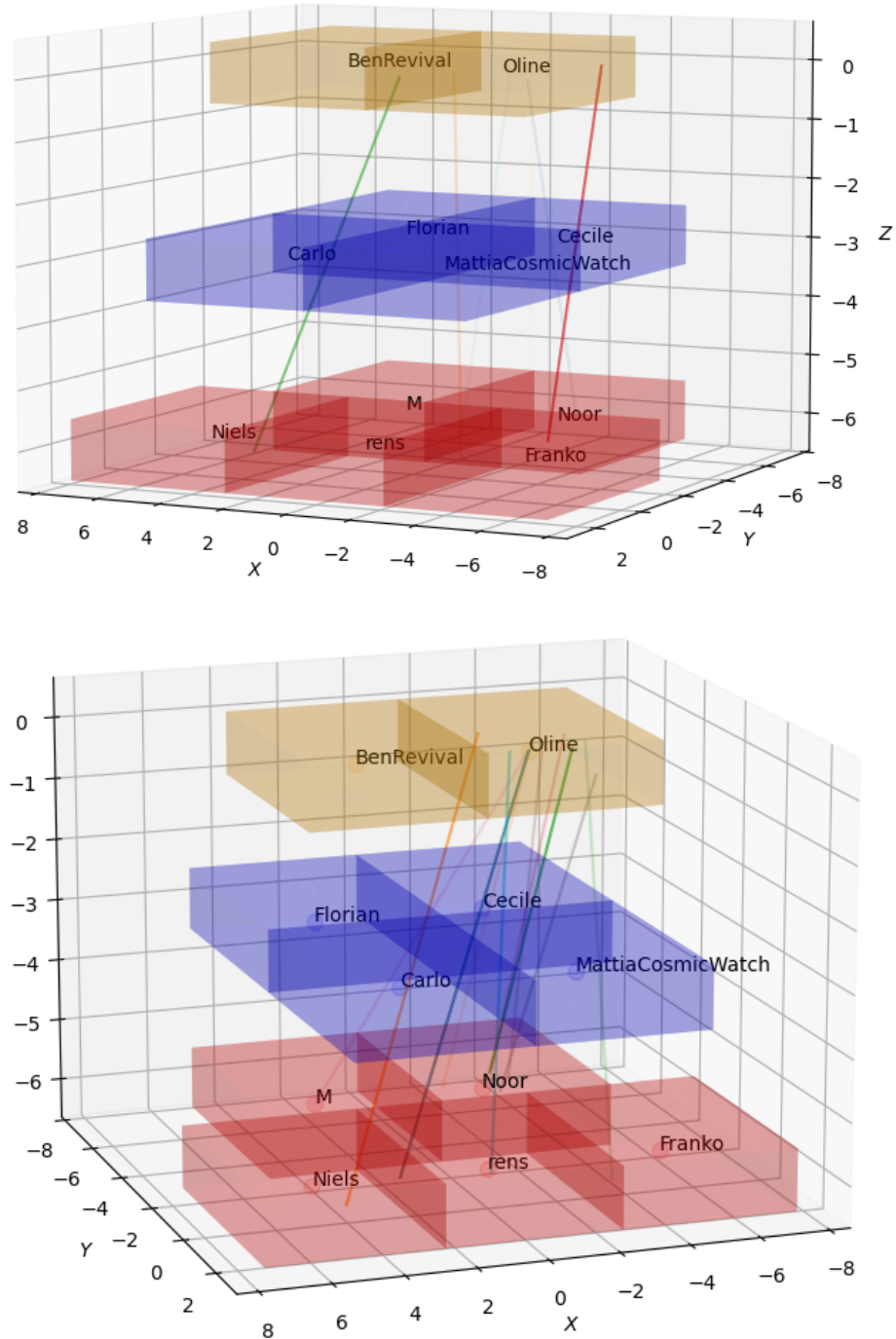
The plot is then populated with some lines that connect the centers of the detectors that were triggered by a muon (at the moment, it does not show any information about background signals). The thickness of the line is proportional to the energy that is deposited in the detectors by the muon (actually, it is proportional to the maximum value of the ADC in the three triggered detectors). The lines then fade-out after few seconds to leave the floor to their successors. As the spatial resolution of the configurations is quite low, it was decided

to insert some random shift from the center of the detector, to make it clearer that the muons are obviously not going straight through the centers but that there is a big uncertainty on the real path followed by a muon. This also makes the whole plot a bit more interesting, and makes it possible to easily visualize - for example - two muons that go through the same detectors in a short time window (otherwise they will be just one on top of each other). One configuration that can be considered is shifting the detectors to overlap by half to be able to more accurately determine where the track passes through.

This script can be ran in parallel to the main data readout script, and it will automatically switch file when the maximum number of events per file is reached. There is no need to start the two programs together, because this script will just locate the last file that is being written and wait for it to be updated to print muons in the plot.

In Figure 47 it is possible to see some examples of the result of the live plotting script, for a configuration made of 11 detectors distributed in the three layers. The dimensions and the units of the axis are arbitrary, and this is supposed to be just a visualization tool.

Figure 47: *Live plotting*



An screenshot from the live animation of a configuration of 11 detectors distributed into three layers. The lines represent the muons going through the detector. The names are the ID of every little detector, and it is set via the Arduino.

## 6 Detector results

### 6.1 Zenith Angular Distribution

The measurement setup of the count rate per zenith angle with three muons in software-based coincidence - that is, all three detectors hits are recorded by the lab machine within a relative time window of 0.1s with respect to the others accounting for the serial communication and python-based non-threaded readout delays. To further reject background, the detectors are inside a light-tight black box, with the screens and LEDs turned off. The measurement error for the count rate is given by  $\frac{\sqrt{N}}{\text{time}}$ , the angular uncertainty is  $\leq 0.005$  rad. The latter is thus ignored by the  $\chi^2$  fits. The data points are fitted with two models, see figure 48.

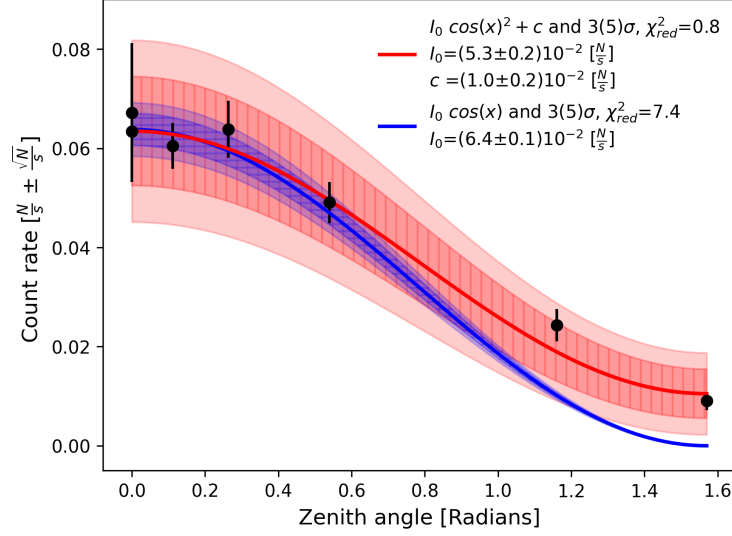
It is evident that there is a significant background additional to theoretical prediction of  $\Theta(\theta) = I_0 \cos^2 \theta$  as given by [18], the reduced chi-squared is significantly larger than 1 (7.4) and indicates that a model underfits if no background degree of freedom is provided (blue). The model is able to catch the measurements for less than 0.5 rad. The two measurements for zenith angles 1.1 rad and 1.57 rad lie outside the models  $5\sigma$  prediction. The obtained value of  $I_0 = (6.4 \pm 0.1) \cdot 10^{-2} \frac{\text{N}}{\text{s}}$  is thus not a reliable estimator. The fit with an additional degree of freedom in the form of a constant offset describes the data well, all data points lie within the  $3\sigma$  uncertainty of the model, the reduced chi-squared value indicates an overfit which is likely due to the large error bars of one the 0 rad data points.

The model shows the cosine-squared dependence of the cosmic muon flux due to the different path through the atmosphere. Similar to Axani et al, we see that the count rate does not vanish for angles around 1.57 rad ( $\pi/2$ ). They suggest that this effect might originate from large cosmic ray showers, showers developing in the roof above the detector or muons producing either high energy electrons or photons along the track that can trigger the detectors [4]. A potential improvement is to repeat the experiment outside under the clear sky. Another issue might be that the opening angle of the configuration is too small. The configuration with three horizontally stacked detectors was chosen in order to accommodate the detectors safely inside the dark box and to obtain enough data points within a one hour long measurement time (versus 10h each by Axani), see figure 49. Orientating them vertically as done by Axani (but with only two detectors) will decrease the rates but will decrease the 'wrongly attributed' counts from smaller (and to a lesser degree larger) angles.

#### 6.1.1 Zenith-angle-dependent ADC and mV distribution

We can analyse the ADC and the mV spectrum under different angles, to see whether we observe a change in the energy distribution. Muons lose some of their energy when they traverse the atmosphere. So when we increase the angle of our detector, we measure muons that have travelled larger distances through the atmosphere. This could leave an imprint in the ADC and consequently the mV spectrum. The ADC and mV spectra in figure 50 do not immediately seem to support this hypothesis. For all three detectors, see figure 50, the highest ADC and mV values are reached at an angle of 0.57rad and not at the expected 0rad. These discrepancies could be caused by the fact that we did the angular measurements inside a building. By tilting the detector to the side, which was towards a window, we decreased the amount of material in between the sky and detector and this material can

Figure 48: *Angular distribution of cosmic ray muons*

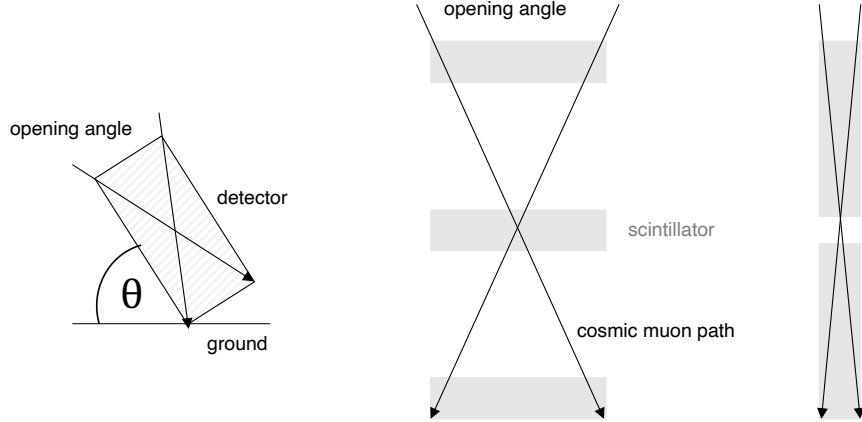


*Count rate per zenith angle, fitted once with  $I_0 \cdot \cos x^2$  (blue) and  $I_0 \cdot \cos x^2 + \text{offset}$ . The coloured hatched areas indicate the  $3\sigma$  uncertainty band, the solid coloured areas the  $5\sigma$  uncertainty bands.*

make the muons lose energy as well. In order to test this hypothesis, the measurements could be repeated outside and a theoretical calculation could show whether the energy losses caused by the atmosphere or the building can be determined significantly with our setup. This is however not done in this study, but can be a very interesting topic for further research.

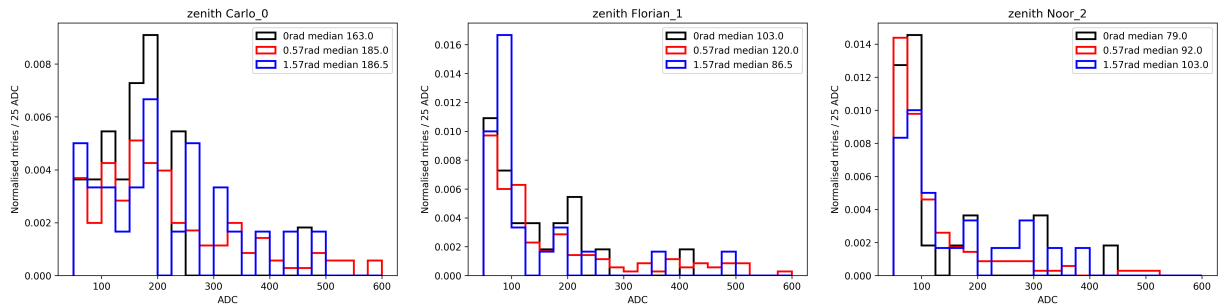
Figure 51 shows the background measurements for the same angles as figure 50. Here we do not see significant differences in the shape of the spectrum and the ADC and mV values cover the same range. This is what we would expect, since the background radiation is expected to be independent of direction.

Figure 49: Angular distribution setup

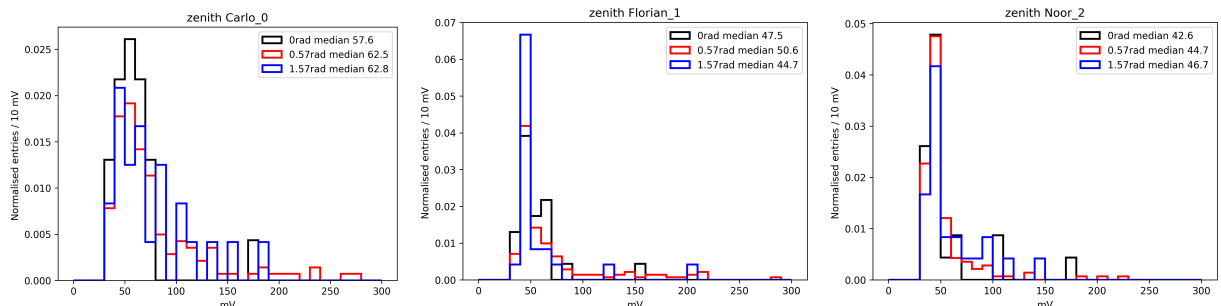


Angular distribution setup (left) and orientation of the three scintillators used by this group (center) and as used by Axani et al (right) [4] including the maximal opening angle for detected muons.

Figure 50: ADC and voltage distributions per detector for different zenith angles.

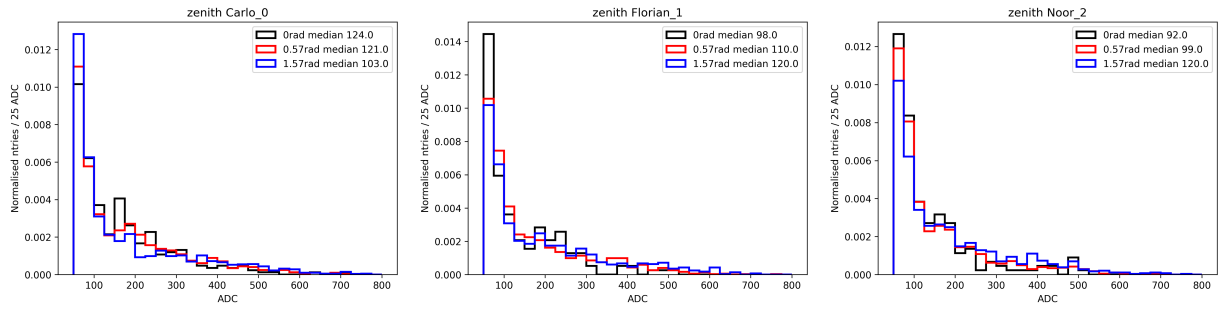


ADC distribution for three stacked detectors inside a dark box for varying zenith angle.

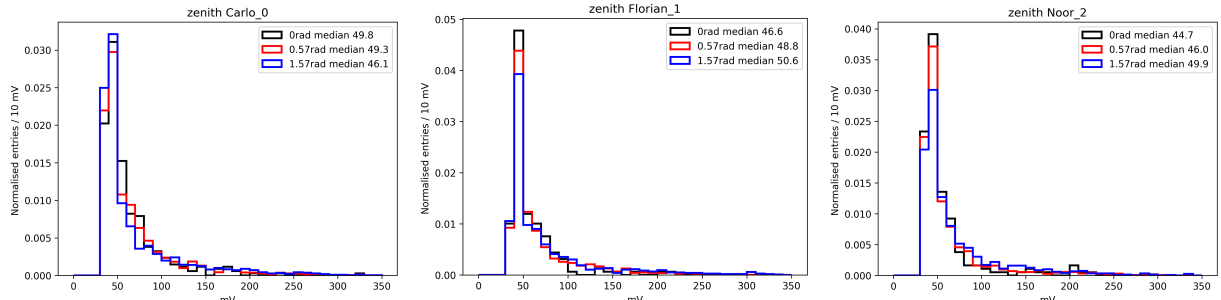


mV distribution for three stacked detectors inside a dark box for varying zenith angle obtained by electronics calibration.

Figure 51: *Background ADC distribution for zenith angles.*



Background distribution for three stacked detectors inside a dark box for varying zenith angle.



Background mV distribution for three stacked detectors inside a dark box for varying zenith angle obtained by electronics calibration.

## 6.2 Muons passage through lead

Muons lose energy as they pass through materials due to ionization. The energy loss of muons in lead as a function of their energy can be found in [19]. The count rate of muons that passed through zero, one (4cm) and two (8.6cm) layers of lead was obtained. Three detectors were used for this setup, with 2 on top of and one below the lead blocks. A muon was counted if it was detected by all three detectors. The setup for one layer is given in Figure 52. Measurements were taken over 30 minutes.

The muon count rate for each thickness of lead is given in Figure 53. It can be observed from the graph that with one layer of lead, the count rate drops by almost 50%. The stopping power of lead for muons at their mean energy at sea level (2GeV) is  $1.386\text{MeV}\text{cm}^2/\text{g}$  [19]. The density of lead is  $11.35\text{g}/\text{cm}^3$ . A muon should therefore lose  $15.73\text{MeV}$  per centimeter of lead traversed on average. This gives an energy loss of  $62.92\text{MeV}$  in one layer and  $135.29\text{MeV}$  in two layers of lead. The observed steep drop in muon count rate cannot be explained by energy loss alone, but also by the increasing distance between detectors, as explained in Section 8.3.1, which gives an attenuation factor to the count rate to account for distance between the detectors. The distance in this case is equal to 4cm and 8.6cm for one and two layers of lead respectively.

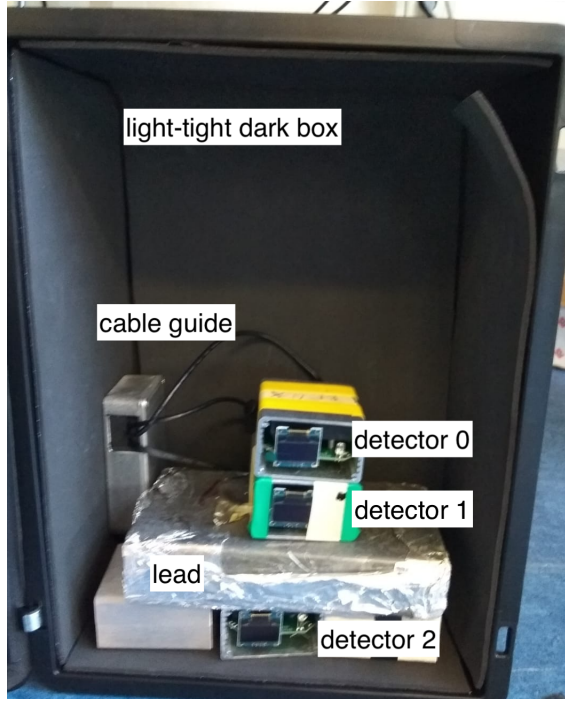
### 6.2.1 ADC and mV spectrum analysis

Besides the analysis of count rates, we can study the ADC and the mV spectra of the different detectors. In figure 54 we see the ADC and mV spectra for the three detectors used in the setup of figure 52, measured with three different layers of lead between the second and third layer. The lead absorbs some of the muons' energy and the more lead we put, the more energy can be absorbed. We expect the ADC and mV distribution in the bottom layer, underneath the lead, to shift to lower values and we expect to measure less events as well, since the low energy muons might be stopped and not reach the lower layer at all. However, we observe the opposite in figure 54.

If we look at figure 54 we see that the maximum ADC and mV values somewhat decrease for increasing lead thickness. This behaviour is most evident in the two left plots that represent the upper detector and the detector in the first layer. However, this is not what we would expect. The layer of lead only affects the energy of the muon when it passes the third layer and if only higher energy muons pass, we would expect relatively more high ADC measurements in the upper and first layer. What we do see is that the ADC distribution for 40mm lead (in orange) is flatter than the 0mm (blue) distribution, this means that relatively more high energy muons are measured, and this is in line with what was expected. It must be noted that this observation does not apply for the 86mm distribution but this could be caused by the limited time of measurement and therefore high statistic uncertainties. If we look at the figure on the right, that displays the data from the detector below the lead, we do see that the median slightly decreases for increasing lead thickness, this is not in conflict with what we expect, but we need more data to be more certain of this behaviour.

The peaks around ADC values below 100 leave the impression that part of the measured muons are actually caused by random coincidences of uncorrelated background. These

Figure 52: *Set-up of the lead measurements*



*3 detectors stacked with one lead plate on the bottom detector*

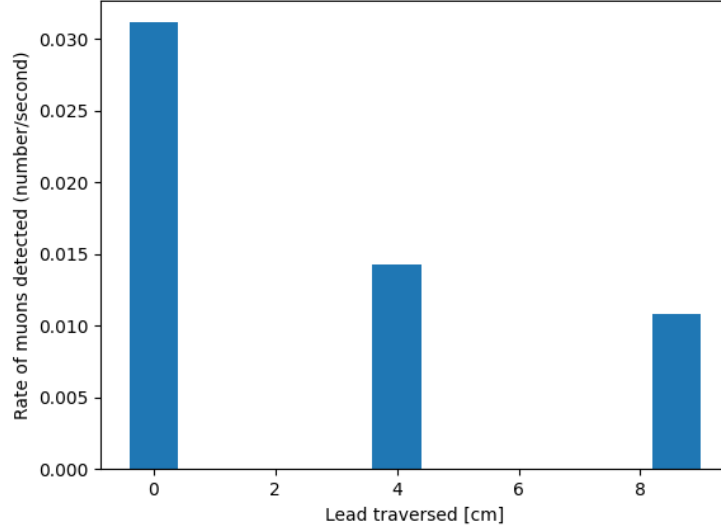
false-muon measurements interfere with the spectra and toughen the interpretation of the plots. The data could be improved by putting a cut on the lowest ADC values, so that the background is eliminated as much as possible. Determining the best ADC value to put this cut could be interesting to improve the measurements.

In figure 55 we show the background signals for the same configurations as discussed above. And we see no significant differences between them.

### 6.3 Time Window

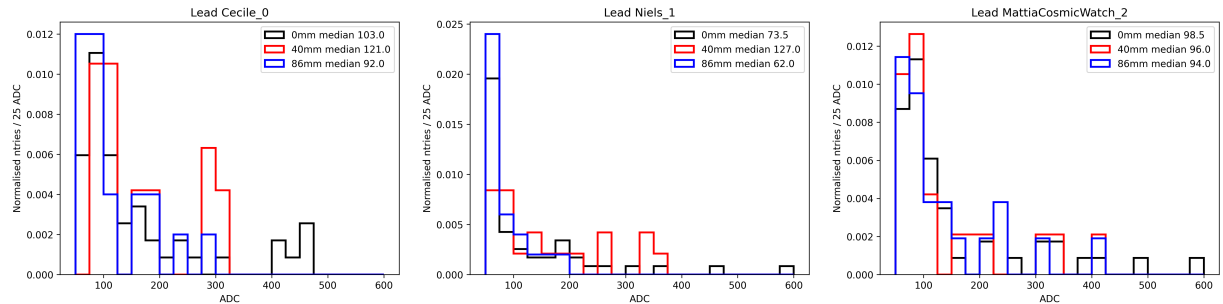
As a final analysis we can look at the time differences between serial readings from muon-like events. An event is labeled muon-like if all three detectors measure a signal inside a time window of 0.1 s. We can see in figure 56 how these time differences are distributed. The time window of 0.1 seconds could cause a higher fake signal rate, where the detectors all measure background at the same time, but this signal is measured as a muon. Due to the somewhat long calculation time of the Arduino, we were limited to this time window.

Figure 53: Muon count rate versus amount of lead traversed

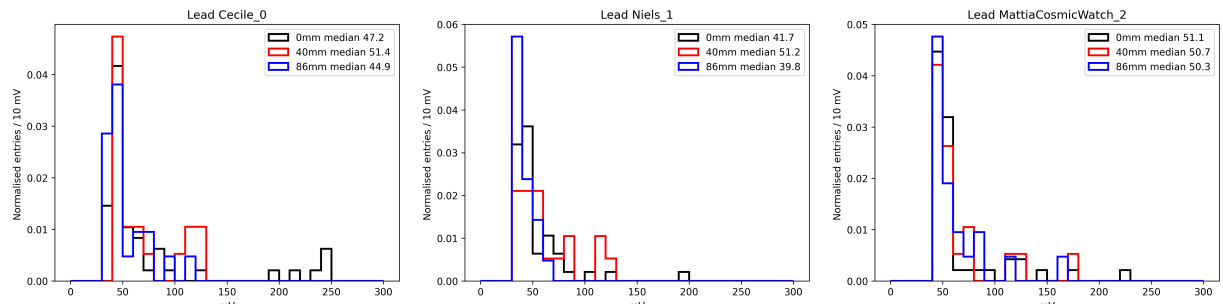


The number of muons per second that were detected after passing through 0,1 and 2 layers of lead

Figure 54: ADC distributions per detector for lead measurements.

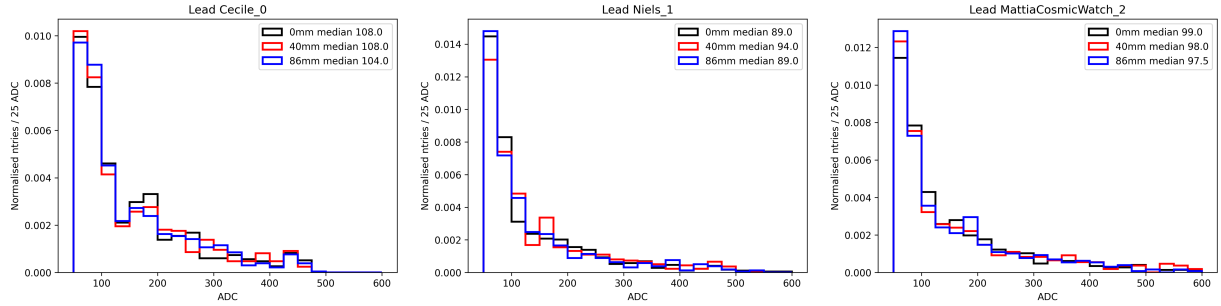


ADC distribution for three stacked detectors inside a dark box for varying lead thickness between the second and third detector layer. Detector 0 (Cecile) is on top.

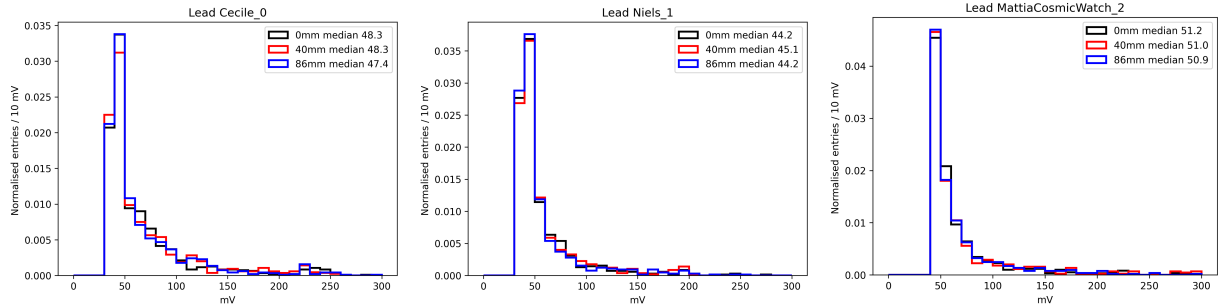


mV distribution for three stacked detectors inside a dark box for varying lead thickness between the second and third detector layer. Detector 0 (Cecile) is on top.

Figure 55: ADC background distributions per detector for lead measurements.

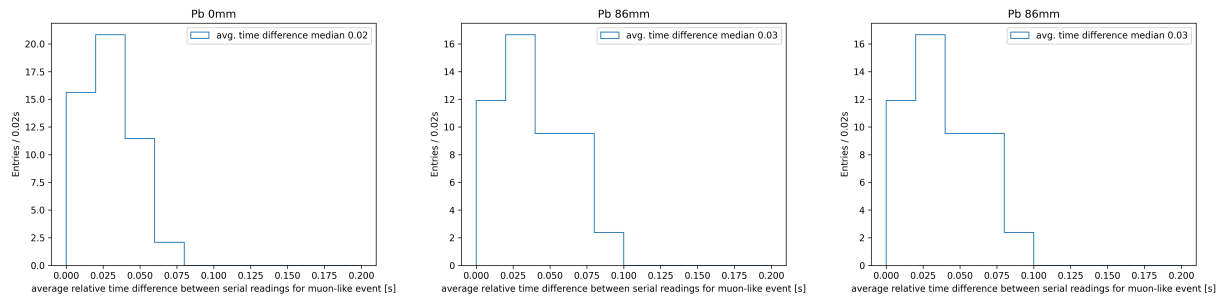


ADC background distribution for three stacked detectors inside a dark box for varying lead thickness between the second and third detector layer. Detector 0 (Cecile) is on top.



Background mV distribution for three stacked detectors inside a dark box for varying lead thickness between the second and third detector layer. Detector 0 (Cecile) is on top.

Figure 56: Time difference between events for lead measurements.



Time difference between events for three stacked detectors inside a dark box for varying lead thickness between the second and third detector layer.

## 6.4 Comparison between simulations and data

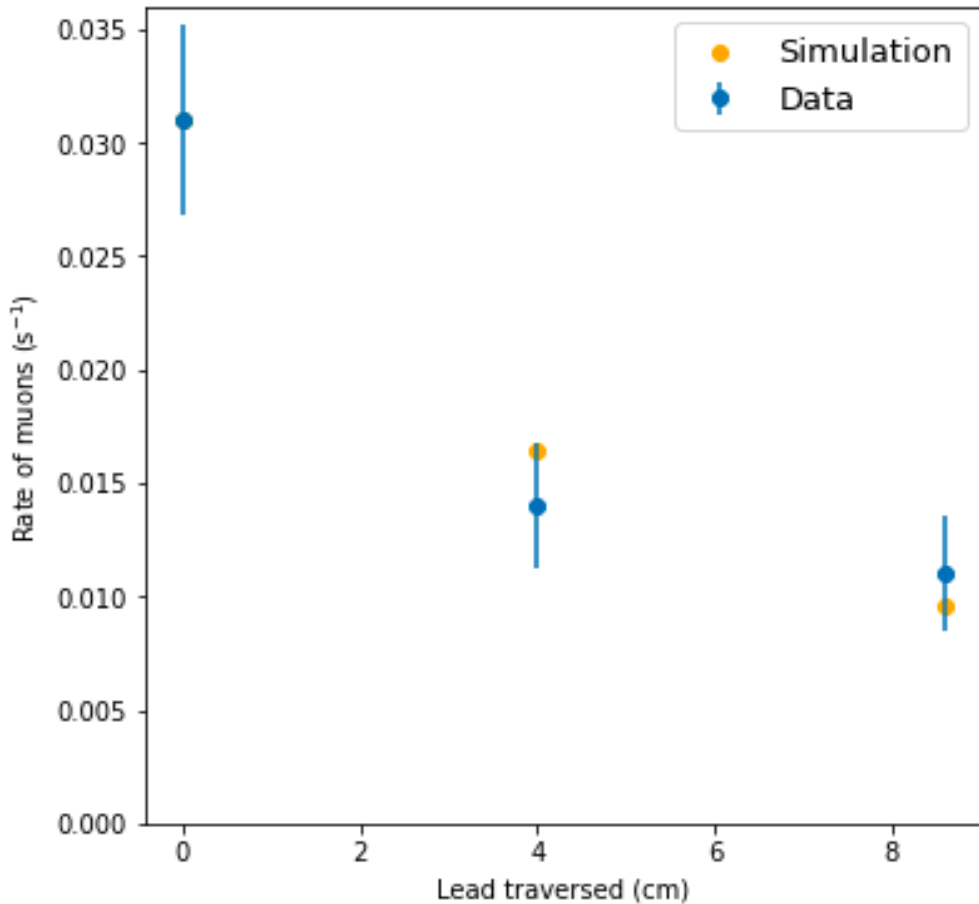
The main results to be compared with the simulation results are the strontium-90 measurements, the measurements of muon's count rate with the lead plate and the final configuration of the 7 detectors.

For the case of the measurements with the lead plate from the simulation there was not expected any differences for the given range of lead thickness. The difference between muon's count rates with different values of lead is expected to come from geometrical effects (the height between lowest and highest scintillator changes) of the configuration. For this reason the count rates were calculated approximately, normalized to rate without lead, as shown below:

$$I(\theta) = I_0 \cos(\theta)^2, I(\phi) \sim Uniform[0, 2\pi] \quad (16)$$

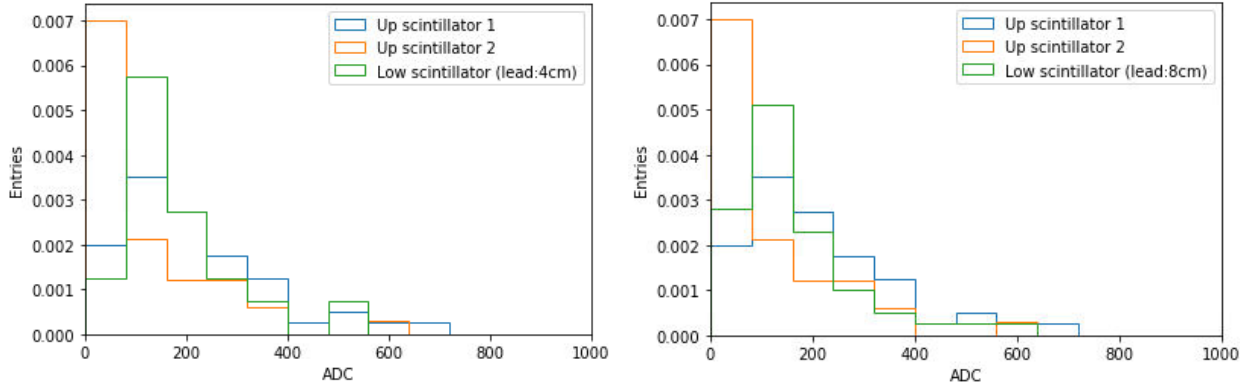
$$\frac{R_i}{R_0} \sim \frac{\int_0^{\theta_i} \cos(\theta)^2 d\Omega}{\int_0^{\theta_0} \cos(\theta)^2 d\Omega}, \theta_i = \arctan\left(\frac{H_i}{2.5}\right), i = 1, 2 \quad (17)$$

Figure 57: *Simulation comparison, lead case rate*



From the figure above we can see that the simulation and the measurements are in good agreement and so at the given lead thickness range no muon stops. Given that the photons hits distributions can be normalized in order to have accurate values, the photons hits distribution, after normalization, was shifted in order to fit to the range  $[0, V_{out_{max}}]$  in order to recreate the expected pulses. The physics aspect of this shift is a result of the fact that the detector loses more photons than the Allpix<sup>2</sup> results (lower housing reflectivity in reality) and also the sensor, even at its detection peak's wavelength, have a maximum of 40% probability to measure a photon's hit.

Figure 58: *Simulation comparison, lead case pulses*



*Expected measured pulses for a lead plate with thickness 4cm (left) and thickness 8cm (right)*

From the simulated output pulses distributions no important changes are expected for one or two lead plates of 4cm thickness. These results are similar to the measurements and so small differences that occurred should be a result of statistical uncertainties due to small number of events. The calculation of the event rates was calculated successfully by a similar Monte Carlo simulation of three detectors on a column as a check and validation.

In the following tables the comparison between the Monte Carlo simulations and the measurements of the final configuration are shown.

Table 12: *Monte Carlo comparison*

Parameter:	Simulation	Data
Number of events top layer	13500	4179
Number of events low layer	12783	130
Coincidence events	982	35

Table 13: *Adjusted Monte Carlo comparison*

Parameter:	Simulation	Data
Number of events top layer	3976	4179
Number of events low layer	1147	130
Coincidence events	365	35

Table 14: *Extreme Monte Carlo comparison*

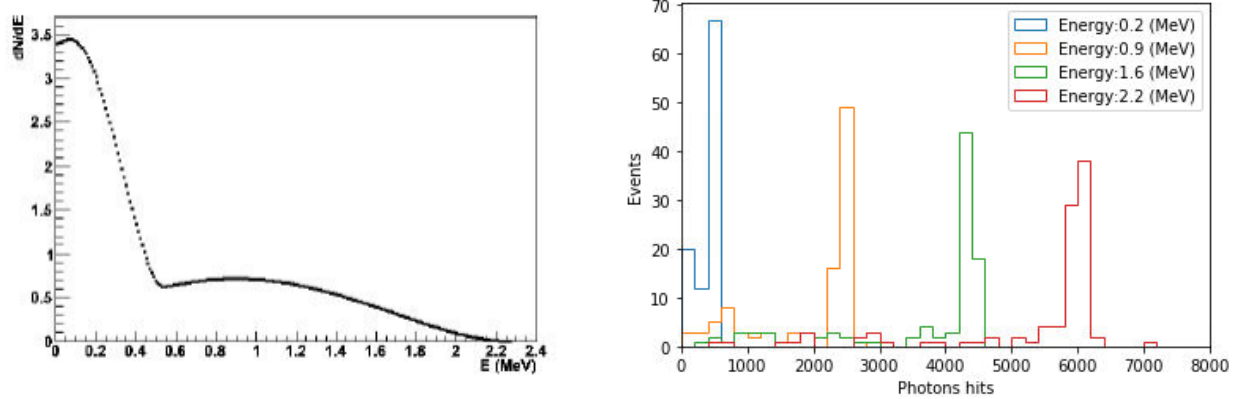
Parameter:	Simulation	Data
Number of events top layer	398	4179
Number of events low layer	120	130
Coincidence events	31	35

From the experimental data it is obvious that the final configuration failed, since the main reason for using a big scintillator's layer is the high number of detectable events. These measurements are in agreement with the Alpix<sup>2</sup> results for the final configuration, which showed that only the central area of the layer can lead to detection.

It seems that the big scintillators that was used for the layers are not effective, since a large portion of their surface cannot detect events due to the small number of measured photons from the sensor, as the simulation showed. This assumption was checked experimentally with a source with very low rate that was positioned at the center and at non-central positions of the surface of the detector. The detector only measured events with the source very close to its center. The comparison between the Monte Carlo simulation of the final configuration and the experimental data seems not in agreement by a larger amount of events. The Adjusted Monte Carlo also failed by large number of events except for the measurements of the first layer. But we expect to observe higher differences on this value between the simulation and the experimental data since no background source was considered. Especially for those data the background events are expected also to be high because the scintillators did not have the aluminium case or other type of shielding. The extreme Monte Carlo case shows quite good agreement to the measurements for the low layer and the low scintillator. The big difference on the events of the first layer can be a result of the background as mentioned before, but more measurements are needed for defining the exact values.

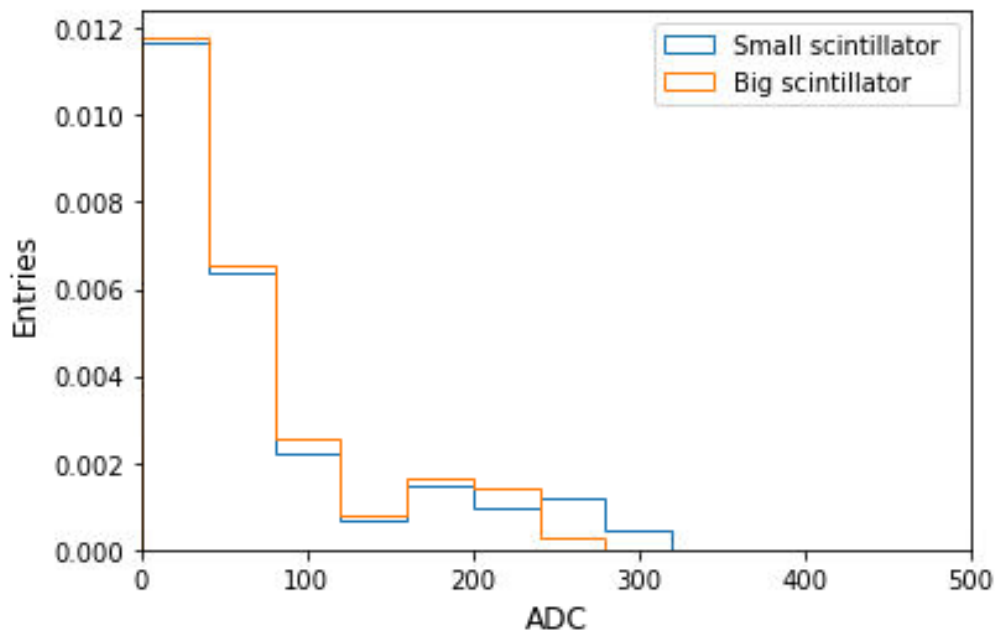
For the source of strontium-90 measurements, the output pulses were calculated with the same way as at the lead simulation case. The only difference in this case is that the total photons hits had also to follow the energy spectrum of the source as below. The photons hits for different electrons' energy values, after the correction by [15] again, were multiplied with the energy spectrum for realistic results and then got shifted to the expected range.

Figure 59: *Simulation comparison, strontium*



The energy spectrum of strontium-90 (left) and the electron's photons hits for different energies in the range of strontium-90 beta decay energy(before correction) for the small scintillator.

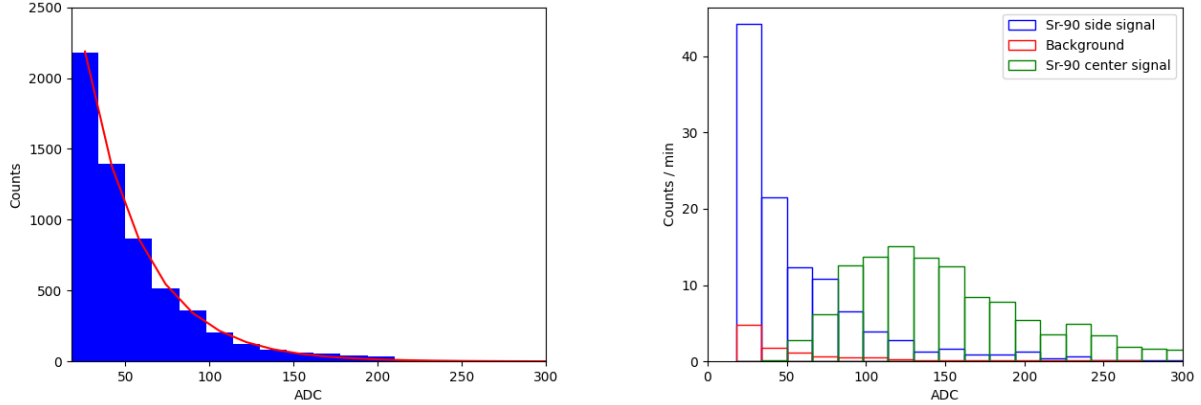
Figure 60: *Simulation comparison, strontium pulses*



Simulated output pulses for strontium-90 beta decay on the small and the large scintillator.

In the picture above we can see the output pulses distribution for central hits at the small and the big scintillator. The output pulses of the small scintillator is expected to have higher maximum value and also the output values of both cases are expected to be lower from the muons' ones. The simulation result is in good agreement with the results of the small scintillator but not for the case of the large one.

Figure 61: Strontium-90 experimental data



Measurements of strontium-90 beta decay with the small(left) and big scintillator(right).

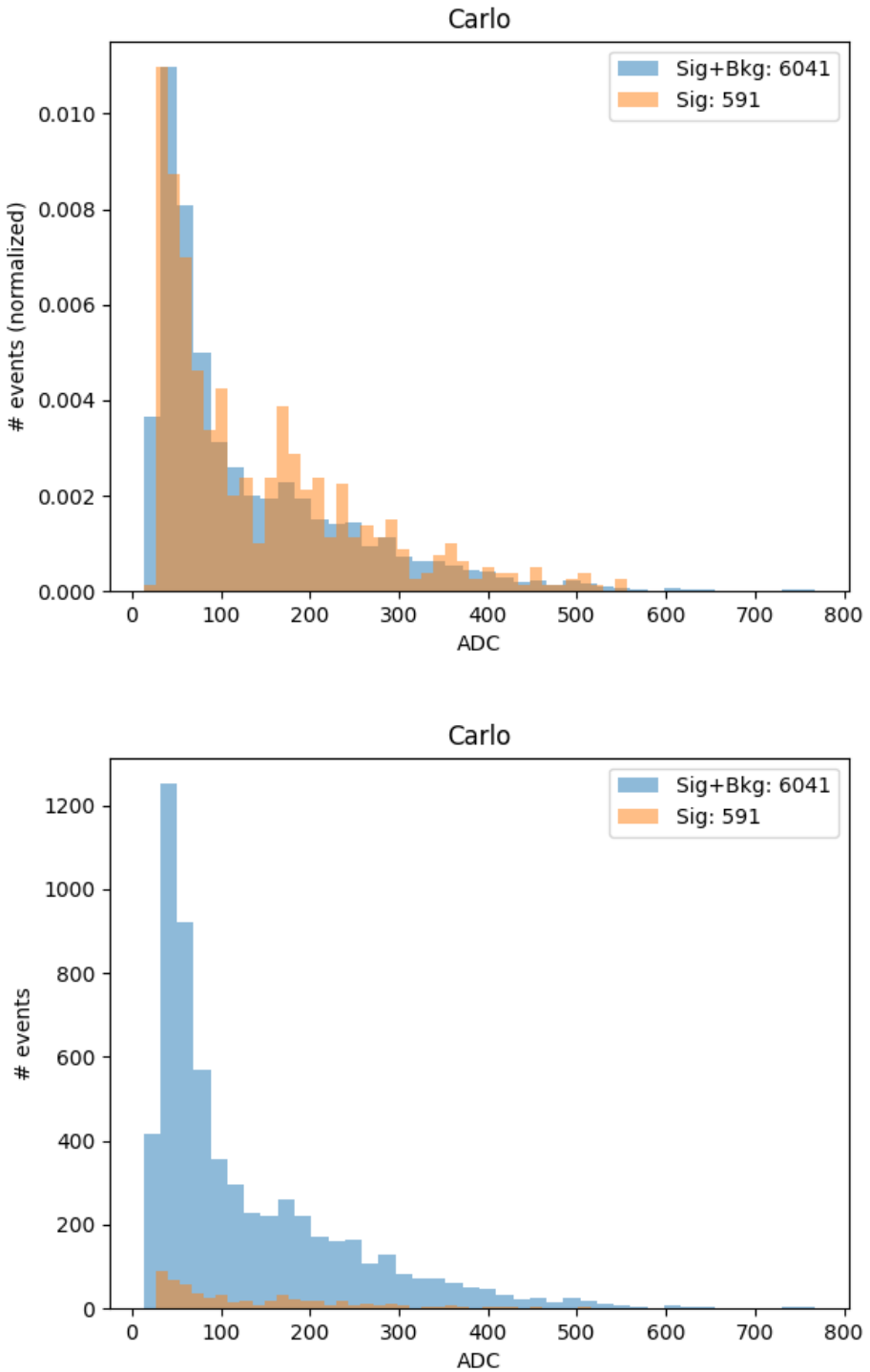
In the plot of the big scintillator we observe that the measurements with the source at the center have different values and distribution's shape from the results of the simulation and the measurements from the small one. Additionally, the measurements with the source at the edge has relatively very high pulses values, from the simulation it is expected to observe lower values since there are 10 times lower photons hits from sources at the center. Knowing that the big scintillator is not as efficient as the small one, also the measurements did not happen at the same day and those results do not agree with similar measurements as [15] there is a possibility of mistake or the detector was dysfunctional. A possible explanation could be the measurement of the photons from more than one events per detection due to a very high decay rate of the source, since the large scintillator has several times higher travel time of the produced photons.

## 6.5 ADC distribution

We now show the distribution of the ADC values for one single detector. The detector was inside a configuration with other 10 detectors, as showed in Figure 5.2. We can then show the ADC distribution for background ( + signal ) and signal only. It is important to mention that different detectors can have very different signal to noise ratios: this is because the scintillators are not all exactly the same, some have been polished more than others, some might be more irregular or, in particular, some might have been wrapped in more tape to reduce the background. The results are shown in Figure 62. On the upper panel the two densities are normalized, while in the bottom one it is possible to see the total count difference: the detector counted 6041 signals of which 591 belonged to a muon. We can observe that there is not a big difference between the two distributions. They both start from a minimum of 30 that is the lowest value of ADC that is accepted (i.e.: the signal threshold that we set in the Arduinos) and they both peak at around 80 ADC. The maximum value for the ADC is 1023 but in this case there are no signals with more than  $\sim 700$  ADC. The only difference in the two distributions is that the signal distribution has a second peak around 180. This value is in line with what was predicted with the measurements with the radioactive source, in which two peaks were measured at 148 and 224 ADC. It is interesting to notice that also the background has a little peak around 180: this is in part due to the signal (what we show is background and signal together) but, as the peak is more pronounced than in the signal only distribution, it is possible that that peak is due to muons that were not recognized by the whole detector (for example if a muon went through the examined detector but not through the other ones, so not being recorded as a muon). It would be in principle possible, with some further analysis, to estimate the rate of muons that went through the single detector without being labeled as muons.

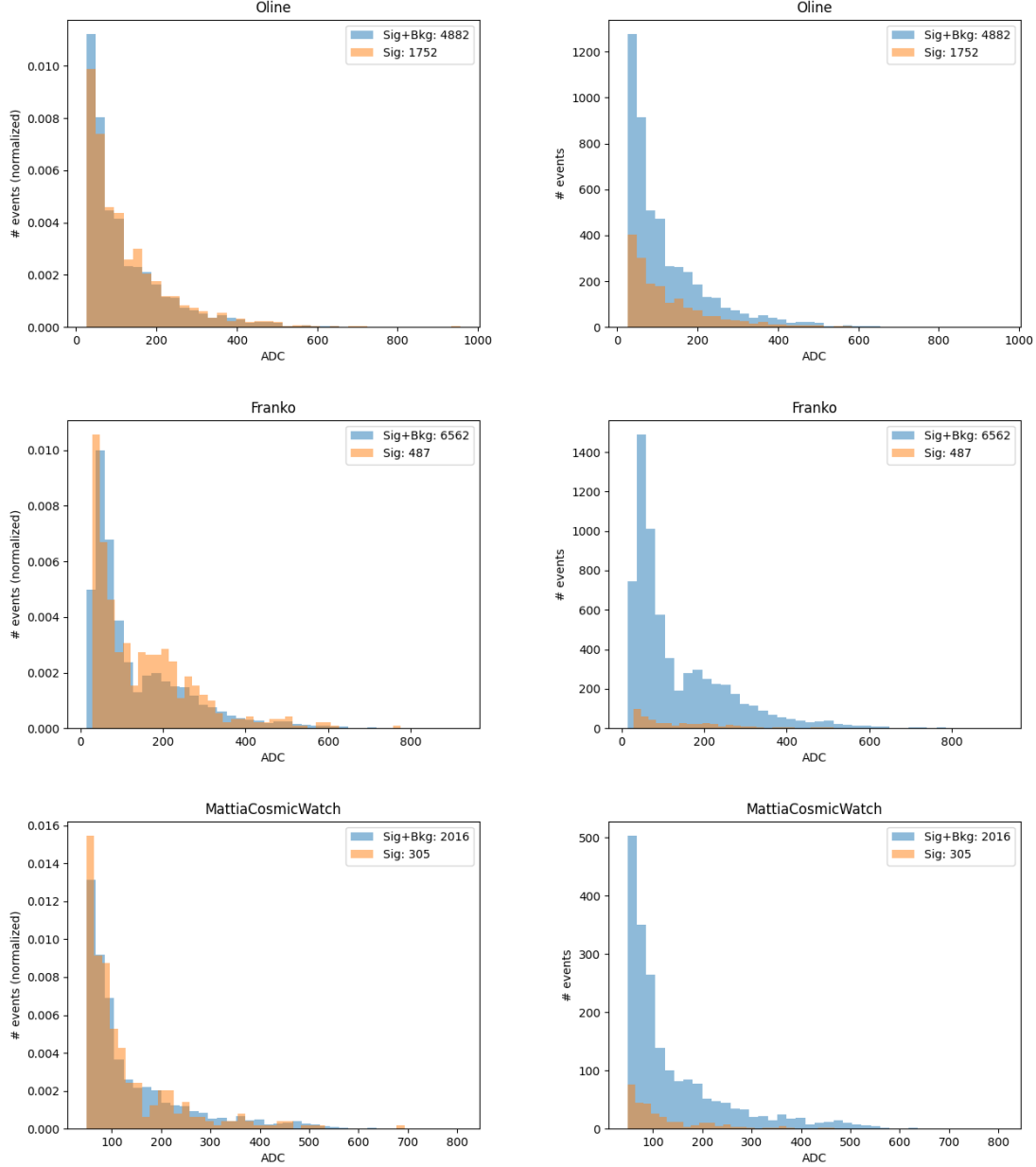
It is also interesting to notice some similar behaviours in the other studied detectors. The position of the detectors is as in Fig. 5.2.

Figure 62: *ADC distribution*



*Signal and background distribution for ADC values of one detector.*

Figure 63: *ADC distribution, more detectors*



*Signal and background distribution for ADC values of multiple detectors.*

## 7 Conclusion and future prospects and improvements

### 7.1 Conclusion

Eleven muon detectors were built, based on the CosmicWatch desktop muon detectors [4], as described in section 2, and combine them with the purpose to measure the angular distribution of cosmic ray muons and to reconstruct and visualize their tracks in 3D.

The detectors can be operate in coincidence mode to filter out more background events and therefore improve the purity of the muon signal. We managed to get coincidence to work for up to 3 detectors, but larger setups were troublesome due to the acceptance window being too small. Instead the code was used to determine coincidental detections.

The expectations and restrictions of the detector were simulated using Allpix<sup>2</sup> [5]. A grid was constructed of possible directions ( $\theta, \phi$ ) and energy values and the simulation was run for each combination of the parameters. The scintillator simulations fall into three main categories: Layered scintillator tests, muon count rate with the lead plates, initial muon energy tests and detector shape configuration tests. The detector shape configuration tests show that the length does not have a large impact on the photons hits, however the thickness does, which is explained by the fact that it is equal to the travelled distance of muons inside the scintillator. The energy simulations show that the number of measured photons are decreasing rapidly with the increasing hitting distance to the center. This was also confirmed by the measurements, see section 4.1.

The detectors were calibrated in different ways. The electronic calibration was used to convert the output signal of the detector, ADC, to mV and Sr-90 was used for the energy calibration.

We used three detectors, 2 on top of and one below lead blocks to measure the angular distribution and the ADC distribution. The plotted muon count rate over the angular distribution shows that the distribution followed the expected cosine squared trend.

The Lead analysis shows that the count rate with increasing lead decreases more than expected with calculated energy loss. This can be partially explained by the distance between detectors.

We managed to create a live visualization of the incoming muons.

## 7.2 Discussion and outlook

For the radioactive calibration it would be nice to have a higher count rate to be able to measure individual decays from the radioactive source. Furthermore to be able to see the whole energy spectrum of the Sr-90 source, either the minimum threshold of the detector should be lowered or a different radioactive source is needed that corresponds more to the energy spectrum of muons. The final configuration of the detector needed to be changed because of the malfunctioning of the scintillators we used. The choice made for the solid scintillator 5x15x1 at the end of the project was not a successful one because of the too short time spent testing them. This implied going back to the scintillators 5x5x1 of the cosmic watch. However, the research done while testing the different shapes of scintillators was still extremely useful because it led to new conclusions regarding the differences in their internal behaviour for what concern both the reflection of light inside them and the emitted light with respect to the energy deposit. See section 8.4.

## References

- [1] S. Satyal. Absorption of beta particles beta end point decay energy, 2021. Available at University of Texas Arlington: <https://www.uta.edu/physics/labs/nuclear.html>.
- [2] S.H. Neddermeyer and C.D. Anderson. Note on the nature of cosmic-ray particles. *Physical Review*, 51, 1937.
- [3] Yi-Hong Kuo. *Determination of the angular distribution of cosmic rays at sea level*. PhD thesis, Massachusetts Institute of Technology, 2010.
- [4] Spencer N. Axani. The physics behind the cosmicwatch desktop muon detectors, 2019.
- [5] LHCb collaboration, R. Aaij, C. Abellán Beteta, T. Ackernley, B. Adeva, M. Adinolfi, H. Afsharnia, C. A. Aidala, S. Aiola, Z. Ajaltouni, S. Akar, J. Albrecht, F. Alessio, M. Alexander, A. Alfonso Albero, Z. Aliouche, G. Alkhazov, P. Alvarez Cartelle, S. Amato, Y. Amhis, L. An, L. Anderlini, A. Andreianov, Y. Zhou, X. Zhu, Z. Zhu, V. Zhukov, J. B. Zonneveld, Q. Zou, S. Zucchelli, D. Zuliani, and G. Zunica. Test of lepton universality in beauty-quark decays, 2021.
- [6] T. Aoyama, N. Asmussen, M. Benayoun, J. Bijnens, T. Blum, M. Bruno, I. Caprini, C.M. Carloni Calame, M. Cè, G. Colangelo, and et al. The anomalous magnetic moment of the muon in the standard model. *Physics Reports*, 887:1–166, Dec 2020.
- [7] Semiconductor Components Industries, LLC, 2011. *Introduction to the Silicon Photomultiplier (SiPM)*, 2018. Available at: <https://www.onsemi.com/pub/Collateral/AND9770-D.PDF>.
- [8] Tektronix, Inc. *TBS1000, TBS1000B/TBS1000B-EDU, TDS1000B/TDS2000B, TDS1000C-EDU/TDS2000C, and TPS2000B Series Digital Storage Oscilloscope*. Available at: <https://www.tek.com/oscilloscope/tds2022b-manual/tds2022b-and-tds2024b>.
- [9] S. Spannagel and Wolters *et. al.* Allpix2: A modular simulation framework for silicon detectors. *Nuclear Instruments and Methods in Physics Research Section A: Accelerators, Spectrometers, Detectors and Associated Equipment*, 901:164–172, Sep 2018.
- [10] S. Agostinelli *et al.* Geant4—a simulation toolkit. *Nuclear Instruments and Methods in Physics Research Section A: Accelerators, Spectrometers, Detectors and Associated Equipment*, 506(3):250–303, 2003.
- [11] J. Allison *et al.* Geant4 developments and applications. *IEEE Transactions on Nuclear Science*, 53(1):270–278, 2006.
- [12] J. Allison *et al.* Recent developments in geant4. *Nuclear Instruments and Methods in Physics Research Section A: Accelerators, Spectrometers, Detectors and Associated Equipment*, 835:186–225, 2016.

- [13] S. Cecchini and M. Sioli. Cosmic ray muon physics. In *5th ICTP School on Nonaccelerator Particle Astrophysics*, 6 1998.
- [14] Stefano Cecchini and M. Spurio. Atmospheric muons: experimental aspects. *Geoscientific Instrumentation, Methods and Data Systems*, 1, 08 2012.
- [15] Lucía Coll Alicia Pérez José Bazo Alberto Gago Joaquin Masias, Franco Delgado. Using a portable muon detector for radioactive source measurements and identification, 2019.
- [16] Arduino official website, June 2021. Available at: <https://www.arduino.cc/>.
- [17] Aim and Thurlby Thandar Instruments. *TG5011 & TG2511 Function Arbitrary Generators*, 8th edition. Available at: <https://www.aimtti.com/resources/tg5012a-2512a-5011a-2511a-instructions-issue-8>.
- [18] Prashant Shukla and Sundaresh Sankrith. Energy and angular distributions of atmospheric muons at the earth, 2018.
- [19] Donald E. Groom, Nikolai V. Mokhov, and Sergei I. Striganov. Muon stopping power and range tables 10 mev–100 tev. *Atomic Data and Nuclear Data Tables*, 78(2):183–356, 2001.
- [20] Tektronix, Inc. *Digital Multimeter TEKTRONIX TDS2012 Datasheet*. Available at: <https://www.testequipmenthq.com/datasheets/TEKTRONIX-TDS2012-Datasheet.pdf>.
- [21] L. Aliaga et al. Design, calibration, and performance of the minerva detector. *Nuclear Instruments and Methods in Physics Research Section A: Accelerators, Spectrometers, Detectors and Associated Equipment*, 743:130–159, Apr 2014.

## 8 Appendix

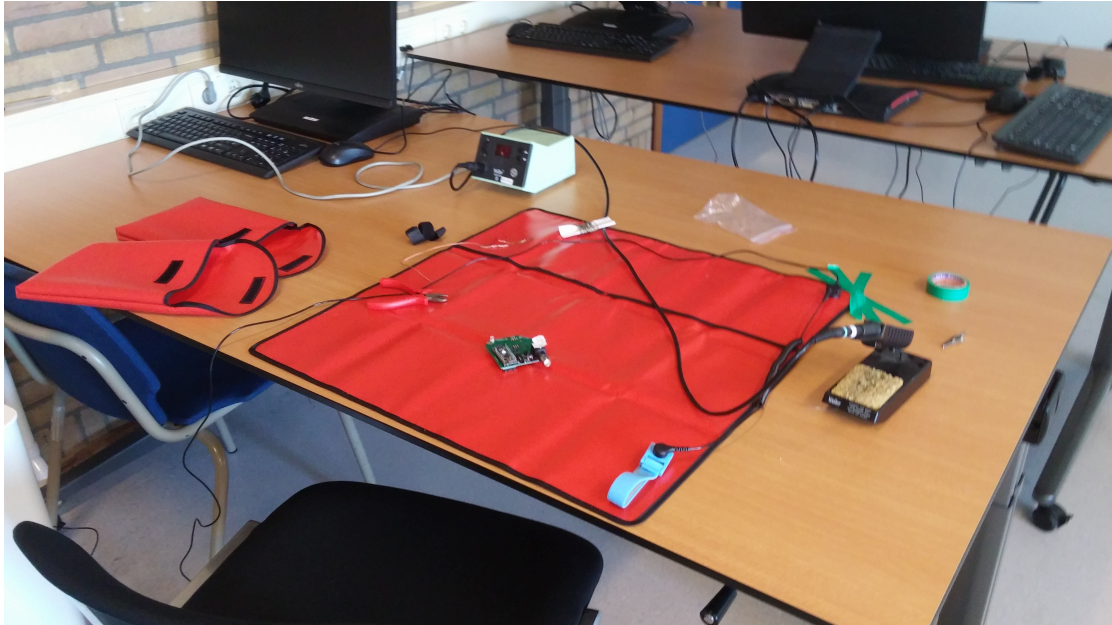
### 8.1 Guide to building and soldering the CosmicWatch

*"320°C is soldering, 380°C is cremating".*

-Wim Gotink

As the very first step, before starting handling the boards and the relative components, it is important to touch the ground of an electric plug, especially when not using proper electrostatic discharge (ESD) safe shoes and an ESD safe workplace. Not doing this could in fact result in a sudden flow of current through the component one is handling and subsequently can result in breaking the latter. Another way to prevent this is to use an ESD Mat as in figure 64.

Figure 64: *ESD Mat*



*An ESD safe workspace. The blue bracelet is connected to the ground through a wire. Wearing this will discharge the user at all time, making it safe to handle ESD sensitive equipment.*

As it can be seen in the above picture, the ESD Mat consists of a mat (the red squared towel in our case) and two cables, one connecting the mat itself with the ground of a socket and the other one connecting the mat with the person who is going to solder by a bracelet (the light blue ring in the picture). In this way, one is always connected to the ground, or, in other words, always discharged.

Each component that we are going to solder is uniquely labelled both on the boards and on the reference manual, so that placing the components on the board can be easily done. When placing the components, we recommend not to follow the order in the reference list, but rather to start by those that are in the center of the board. In this way it will be

easier to install the components with a lot of small legs. Moreover, we found easier to start with the smaller components, such as resistors and capacitors, and then progressively solder bigger ones. This is because good soldering can be achieved more efficiently if a lot of space is accessible when handling the soldering iron. We set the soldering iron to a temperature of 320° Celsius. This temperature can be slightly adjusted based on the tin that is being used, however, without ever reaching a temperature above 340° Celsius. Soldering above this temperature, even if done very briefly, can cause the components great damage, resulting in a high possibility of component failure. As for the actual SMD application, the procedure we found most successful is as follows:

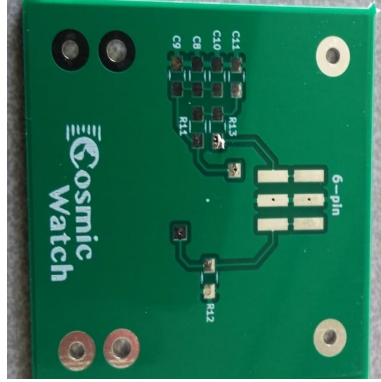
1. Heat up one pad on the board by using the tip of the soldering iron for a couple of seconds.
2. Melt a very small amount of tin on the hot pad while still holding the soldering iron on the pad, so that the tin can melt and slowly flow.
3. Place one side of the component on the pad by making use of tweezers.
4. Carefully remove the soldering iron and hold the components in place until the tin has solidified.
5. Heat up the other pad for a few seconds, with the soldering iron, where the component has to be attached to.
6. Melt the tin on this second pad making sure it flows and connects the component to the pad.

Given the tiny dimensions of the majority of the elements, holding them in place just with bare hands is neither practical nor safe. This is why we suggest to use proper tweezers to place and hold them in place on the board. Moreover, be sure to never apply too much pressure on the pads when using the soldering iron, as they could easily slide away and the establishment of the connection between the component and the board will be harder to create (see the respective troubleshooting section when running into such a problem). Along with this, one should never touch the component with the tip of the soldering iron, this would result in the component to break and it will have to be replaced. Never apply the tin on top of the component, as otherwise, when injecting current in the circuit the component will heat up and subsequently loosen or even burn, so that it will have to be replaced (when one component has to be replaced and/or some tin has to be removed, see the respective troubleshooting part). The amount of tin needed to establish a connection between a component and a board is very small, so that too much tin should never be applied, otherwise there is a possibility of creating a short between two different pads, which should not happen if not clearly stated. The resistors and the capacitors do not have a polarization direction, so that the direction they are placed with is not important, as long as the metal strips at the edges match with the underlying pads of the board. With regard

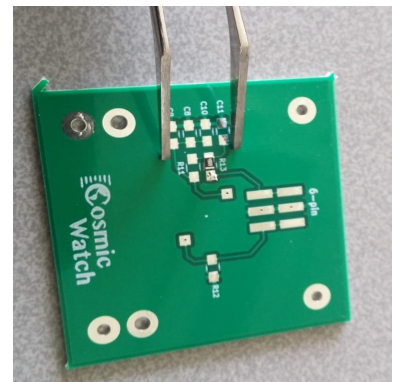
Figure 65: *Soldering steps*



(a) *Heat the pad.*



(b) *Melt some tin.*



(c) *Move the component into place.*



(d) *Melt tin and solidify component into place.*



(e) *Apply tin to the other pad.*



(f) *Finish both sides with a bit more tin.*

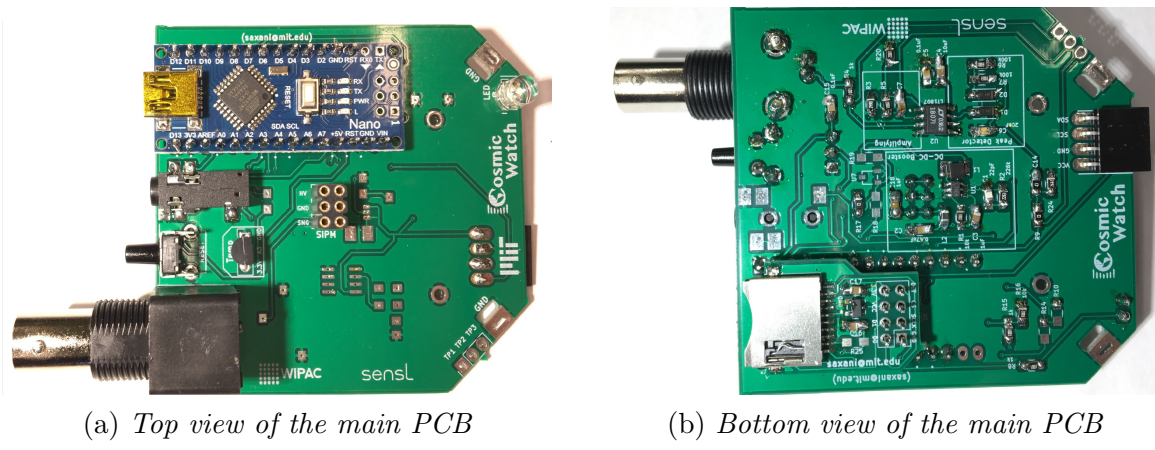
*Representation in 6 steps of the soldering technique on the SiPM board.*

to the other components, such as the LED and the diodes, their placement direction on the board cannot be chosen arbitrarily, so that particular attention should be used when placing them. Generally, pin one is indicated both on the component as well as on the board. Moreover, in order to facilitate the soldering process described above, one can make use of the soldering flux. This is a chemical substance that both protects the metal surfaces from re-oxidation during soldering and helps the soldering process by altering the surface tension of the molten solder. Applying a tiny amount of flux on the board pad before starting soldering will in fact make the tin much easier to handle when using the soldering iron. Finally, in order to get a very rough impression if a connection has been established, one can use a multimeter. This tool allows the user to measure several electrical properties of a circuit or an individual component, such as voltage, current, resistance and capacitance. For a full overview on the functionality of it we refer to its manual [20]. In our case we used it to measure the resistance between two points. If there is no resistance between two points, the multimeter will produce an audio signal. By taking a look at the circuit in the schematic

provided in the instructions, one has to check that the tin is in contact with (and only with) the relative component side, which in turn has to be in contact with the pad on the board. However, we found this method of checking the connection to be very naive: the beeping of the multimeter does not guarantee that a connection is steady. On the contrary, this is a very powerful method when checking whether a short has been created by a connection that is not supposed to be there.

By carefully following the procedure described above one should eventually be able to create a fully populated PCB, as shown in figure 66. However, if anything should go wrong, the following section outlines the common problems and how to solve them.

Figure 66: *Populated main PCB*



*Completely populated main PCB for the CosmicWatch Muon Detector.*

## 8.2 Troubleshooting

A CosmicWatch consists of many delicate components and, as outlined above, proper soldering is of utmost importance. However, even while taking proper care, when building a CosmicWatch for the first time, there is a high probability of something going amiss. During troubleshooting CosmicWatches, we found common issues to be:

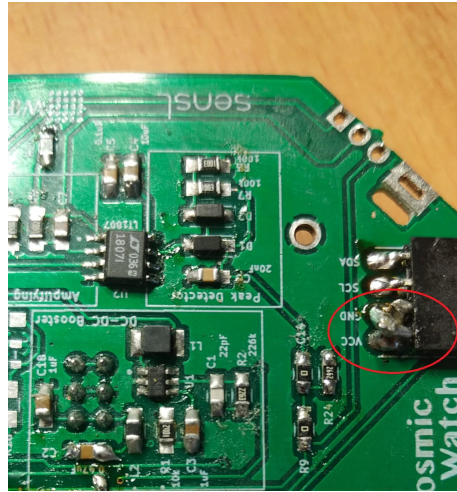
- **No output on the OLED screen:**

Many detectors we built have a very unstable OLED screen. This is due to a shipment error where the OLED screen connector on the main PCBs and OLED screens had pins that did not align. In order to circumvent this problem, we manually cut the OLED screen connector pins and built a custom bridge (see figure 67). However, this crossed connection proved difficult to solder and many screens became unstable or did not work. The only way to fix this problem is to properly resolder the crossed connection, while taking care of not burning into the plastic casing of the connector.

- **The 3.5mm jack is not responding:**

We noticed it was quite common for the 3.5mm jack to have one or multiple pins not

Figure 67: OLED screen connector crossed wire



The crossed wires on the OLED screen connector are indicated with a red circle. The GND and VCC pins on the board are mirrored compared to the pins of the ordered OLED screens. In order to still use the screens, the pins on the connector were cut and using small scrap metal pins, a custom crossed connection was soldered on.

making proper connection, by either too little tin application or because the tin got stuck underneath the legs. We think the reason for this was that a 3.5mm jack only serves a purpose in connecting multiple detectors in a setup. So when troubleshooting a single detector, everything may look fine, while the audio jack does not work. To fix this issue, (re)solder all legs of the connector to the board. Pay careful attention to placing tin on and around the connector of the legs. The legs may tend to turn slightly up, so when applying solder to them, use the soldering iron to push the legs down, which will melt through any tin that might be stuck underneath it.

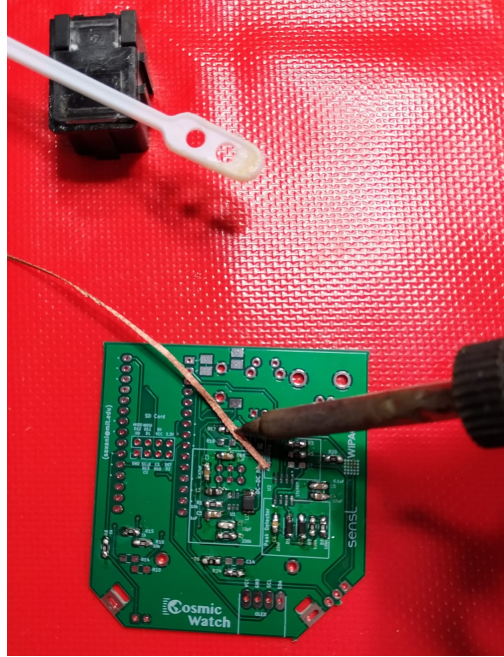
- **Replacing a component:**

Sometimes it happens that a component is misplaced or even breaks, for example due to too much heat applied and therefore it has to be replaced. In order to desolder one component, the tin previously applied has to be carefully removed by making use of the soldering wick. Place the soldering wick over the tin that has to be removed and place the soldering iron tip over it. Be careful when holding the wick with bare hands: it heats up quickly. At this point, the tin will melt and will be absorbed automatically by the wick, desoldering the relative component. Depending on the amount of tin that was previously used, this process might have to be repeated more than once. Be sure not to apply too much pressure nor heat, because the underlying pad could slide away, resulting in damaging the board.

- **No correct voltage between VH and GND of the 6-pin header:**

Once all the components have been soldered on the main PCB, there should be a voltage difference of around 29.4V (see figure 70) between the VH and GND pins of

Figure 68: *Wick utilisation*



*Representation of how to use wick. The wick (copper wire) is placed on top of the component that has to be removed. The soldering iron is placed on top of the wick, which heats both it and the tin underneath it. When the tin melts it will be absorbed by the heated up copper.*

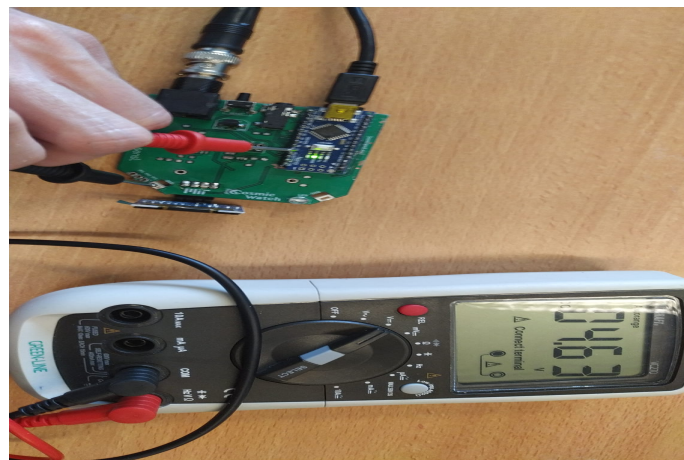
the 6-pin header, when providing the Arduino with the correct 5V through a miniUSB cable. If this is not the case, several causes may lie behind this issue.

When reading a voltage difference of exactly 0V, the most common issue was found to be that the circuit previously built is not closed, so that current cannot flow, either through a broken component or through a connection that was not properly established. In this case, starting from the Arduino pins and following the schematic of the circuit thoroughly, every single connection between the board and the relative component has to be checked, reheated and, in case, re-established. Most of the times the components that were not properly soldered were found to be the Arduino and/or U1 and U2, so that starting by checking their pins may save quite a lot of time. If all connections are correctly established but the voltage is still 0V, one component might be broken. To check which mount has to be replaced, by using the multimeter or the oscilloscope, one has to measure the voltage on each pin of each component (always following the circuit in the schematic). If one component receives a certain voltage as input but does not return anything, while it is expected to provide at least a non-null voltage, it probably means it has been damaged and has to be replaced.

In the case the voltage difference between VH and GND is instead a non-null value, but still different from 29.4V the circuit is closed, but some mounts are not working as expected. Check first of all that the Arduino works properly and it provides the board with approximately 5V (use the multimeter to measure the voltage on the +5V (figure

69) pin of the Arduino itself, we found that many Arduinos supply the board with approximately 4.6-4.8V). If not, check the relative connection with the board. If the connection is there, the Arduino might have been damaged and it has to be replaced. Proceed by measuring the voltage on U1 and U2 components: they should amplify the signal. If they are not working as expected, check all the connections between the board and the pins again, making sure there are no shorts. If this doesn't solve the problem, one or both of them have to be replaced (usually the problem is in U1). However, we want to underline that replacing a component must be the very last solution to adopt, as in fact it requires first of all more work and secondly a greater probability of damaging the board. Most of the problems usually lie in some connections that are not properly established, either because of a short or because of a missing junction.

Figure 69: *Measurement +5V Arduino pin*



*Measurement of the voltage on the +5V pin of the Arduino with the digital multimeter. Note on the digital multimeter screen the voltage of 4.63V, which falls nicely within the expected range of 4.6V to 4.8V.*

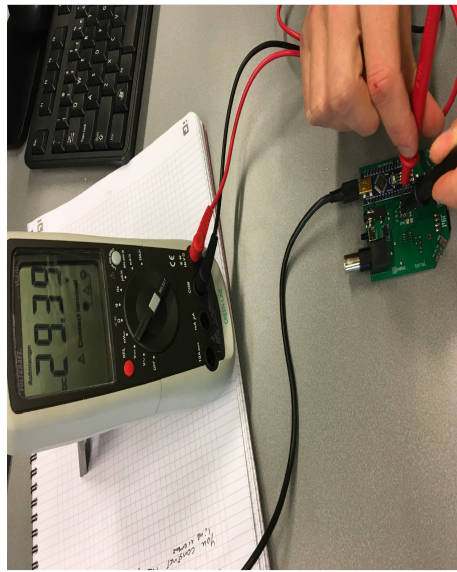
- **Pads sliding away from the board:**

When applying too much heat or pressure on a board pad, the pad is likely to slide away. This would result in serious damage of the board, which is hardly fixable, especially for non-experts. If one runs into such a problem the connection between a component and the board has to be established manually. This can be achieved by using a thin conductive cable connecting the component with the circuit inside the board. Under most of the pads there is in fact a small hole, which can be used to reach the inner circuit and successfully establish the connection.

- **Problems with uploading the code to the Arduino:**

Sometimes it may happen that, when trying to upload the code to an Arduino, the latter returns the error "Programmer is not responding". Even though we did not find the source of this error, we still found a way to bypass it by following the subsequent steps:

Figure 70: Measurement VH and GND 6 pin header



*Measurement of the voltage between the VH and GND pins of the 6-pin header with the digital multimeter. Note on the digital multimeter screen the voltage of 29.39V, which is in agreement with our expectations.*

1. Make sure to select "ATmega328P (Old bootloader)" as the processor, "Arduino Nano" as the board and the correct USB port in "Tools" of the Arduino application.
2. Hold the reset button on the Arduino while uploading the code.
3. Let go of the reset button the moment the IDE gives the message "uploading code..." .
4. The red light on the Arduino should light up for a few seconds.
5. Code uploaded successfully.

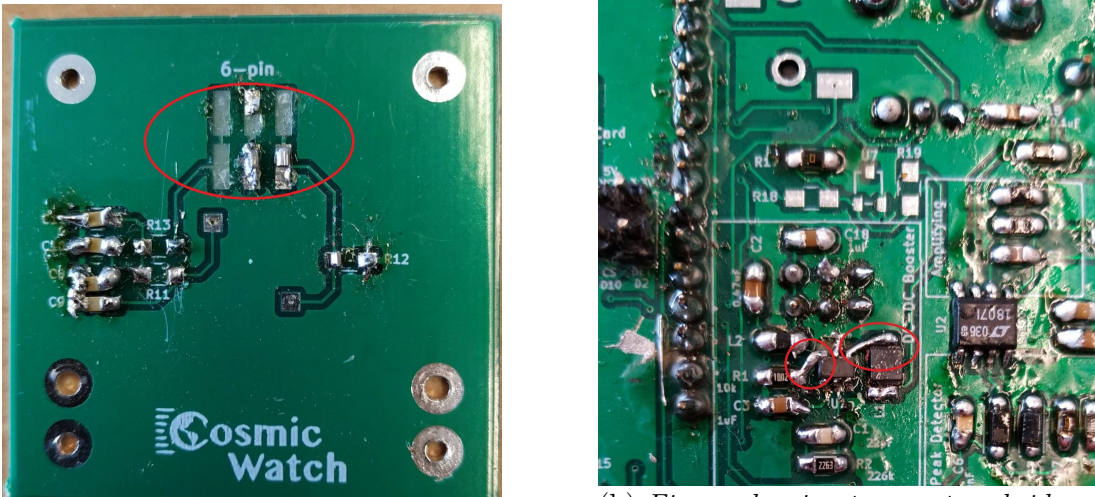
- **Arduino stuck in reset loop:**

An issue we ran into once, is that an Arduino got stuck in a reset loop. The cause of this event is still unclear. Upon connecting the Arduino with power, the LED light would flash indicating that the board successfully receives power and the OLED screen would show the CosmicWatch boot screen. Shortly after this, the board would reset, giving another flicker of the LED light and showing the boot screen again. This would continue for as long as the board is connected to a power source. Reheating the tin on all the reset button relevant pads solved this issue.

- **Random noise on the signal output:**

It can be quite common for the output signal to present itself accompanied by a noise

Figure 71: Missing pad: problem and solution



(a) Figure of a board with 3 and a half pad missing on the 6-pin connection indicated by a red circle.

(b) Figure showing two custom bridges, both indicated by red circles, that can establish relevant connections when pads are missing.

*SiPM PCB with a few missing pads on the left and solution (rewiring) to the same problem in the main PCB on the right.*

with a large amplitude. This problem was found to be due to the presence of a light leak in the scintillator, as in fact photons can be a disturbing source of noise, as the scintillator itself is transparent to photons. This issue can be easily solved first of all by screwing the scintillator on the SiPM board a bit more tightly. This reduces the space between the board and the SiPM, which reduces the amount of light that can enter in the gap. During this process, however, it is fundamental not to apply too much pressure, else it might be screwed in too deeply and the SiPM would be crushed. Additionally, if this does not solve the problem, it might mean that the leak comes from the wrapping and adding another layer of black tape can make it light tight and hence significantly reduce the noise. A well wrapped scintillator normally has two layers of black tape, which both cover the full block.

- **The detector does not register any particles:**

This problem is very broad and requires to be split up further. The board comes with 3 test points as well as a raw BNC output. To locate this problem, using an oscilloscope can be very helpful.

- **BNC signal:** We noticed that sometimes the raw BNC output is very noisy when connected to an oscilloscope. This happens when the BNC connector is loosely soldered to the board. Two of the BNC pins require a large amount of tin to solder them steadily, which may sound counter intuitive after working with many of the SMD components. Nevertheless, applying more tin to these pins steadies the BNC connector and fixes the issue.

- **TP1, TP2 & TP3 signals:** The main PCB holds three testing points which help locate the problem. Any of the testing points can be connected to an oscilloscope in order to look at the signal. The first testing point (TP1) is the raw signal after travelling through a  $1k\Omega$  resistor, namely R4. This signal should have roughly the same shape as the raw output, usually a bit more smooth. The second test point (TP2) is the signal after travelling through the amplifying circuit. This circuit boosts the signal by roughly a factor of 25. The shape should still resemble the TP1 signal, but with a much greater amplitude. The third test point (TP3) is the signal after travelling through the peak detector. This should hold the amplified signal and decay very slowly ( $\sim 1ms$ ) compared to the other test point signals ( $\sim 500ns$ ). If any of these signals do not resemble the expectations as in figure 3, then most likely a component within that circuit does not make proper connection. Using a multimeter the signal can be traced through the circuit and the disconnected component can be found.
- **High minimum threshold:** When the minimum threshold is very high, or even at its maximum, no count is registered because the Arduino doesn't receive the input for starting to detect another signal. In this case the problem might lie in the main PCB and/or in the SiPM PCB. However, no matter where it lies, it is very often because of a connection that has not been properly established. Start by checking the voltage difference between the VH and GND of the 6-pin header. If the readout is roughly 29.4V move on by checking the BNC signal and the TP1, TP2 and TP3 signals. If any of these are not working as expected, please refer to the other points of the present list. If everything works properly, check all the connections on the SiPM board and subsequently make sure that the SiPM is not broken (because either of heat or pressure) by using the multimeter in diode mode. Finally, make sure that the scintillator is steadily plugged in the 6-pin header before providing the Arduino with power (this was found to be the most common cause of the above problem). Very often these steps solve the issue, if not, the reset threshold can be manually adjusted in the Arduino code to a higher value. Be aware that this last process would result in a lower count of muons when performing the experiment.
- **Malfunctioning Arduino:** Sometimes no signal output can indicate a malfunctioning Arduino. This can be clear if the Arduino does not turn on after providing power to it, but can also happen without a direct visual indication. In a CosmicWatch, the Arduino acts as a power source for the board through the 5V Arduino pin. We found a few boards on which the 5V pin gave off a too low voltage (below 4.5V). This most likely indicates a malfunctioning surface mount on the Arduino. Theoretically, the component can be replaced by removing the Arduino and fixing the non functioning component. At first we had a lot of trouble trying to remove the Arduino so that we instead desoldered the surface mounts on top of the Arduino, scratched the Arduino pin circuitry (to make sure the latter is completely ineffective and doesn't interfere with the other part of the circuit), and placed a second Arduino on top of the old one, as seen in figure 72. Later we were introduced to a new tool that allows the removal of tin from pins

Figure 72: *Broken Arduino: problem and solution*

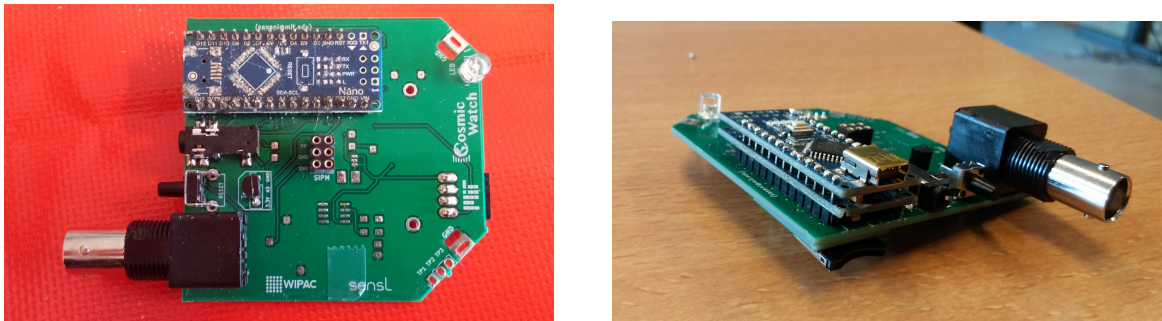
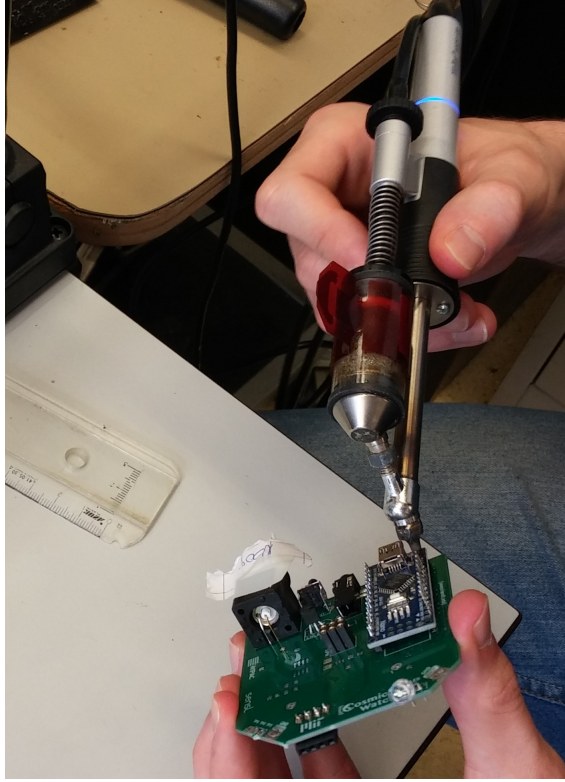


Figure on the left shows an Arduino from which all surface mount components were removed. The circuitry has been scratched to make sure no power can run through it. The figure on the right shows a new Arduino that has been soldered on top of the old one.

with much more ease. This tool consists of a small metal tube, with an adjustable temperature, that is placed over the soldered pin (see figure 73). The heat will melt the tin around the pin and with the press of a button it will vacuum clean all the liquid tin. Using the tool to apply light pressure on the pin will allow the user to remove everything, even the tin stuck inside the hole between the board and the pin.

Figure 73: *Desoldering pump*



*Figure of the desoldering pump, while cleaning the pins on an Arduino. The nozzle of the desoldering pump heats up the tin around the pin, so that it melts and can be subsequently vacuumed into the red chamber with the press of a button.*

### 8.3 Original detector idea

During the project it was envisioned to build a final detector consisting of two scintillator layers above each other to perform tracking. The readout would be provided by the Cosmic Watch electronics, so the SiPM PCBS and the main PCBs. In the end the idea did not materialize, however, in this section, some considerations and computations made for the original final detector plan are presented.

#### 8.3.1 Detector geometry

In the original plan for the final detector there would be two scintillator layers above each other. A sketch of the geometry is shown in Fig. 74, with the length of the scintillators in the horizontal direction indicated. The separation distance the two scintillator layers should be such that we have an optimal combination of angular resolution and the number of events registered in the combination of the two layers. The number of events  $N$  is obtained by integrating the cosine square law over the angle  $\theta$  as defined in Fig. 74, and multiplying this by a factor 2 to take into account positive and negative values of  $\theta$ :

$$N = 2 \int_0^\theta \cos^2 \theta d\theta. \quad (18)$$

The angle  $\theta$  as a function of  $h$ , the distance between the scintillators is:

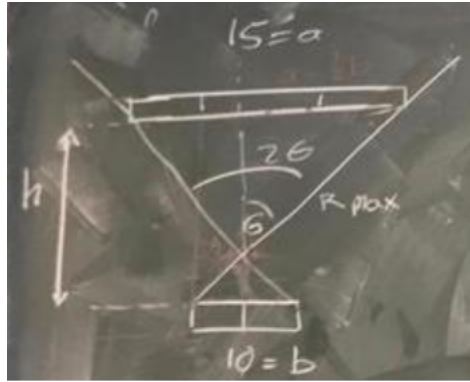
$$\theta = \arctan \left( \frac{10 \text{ cm}}{h} \right). \quad (19)$$

The angular resolution was then defined as:

$$\theta_{resolution} = \frac{1}{\Delta\theta}. \quad (20)$$

Where  $\Delta\theta$  is the change in the angle when changing the distance between the two scintillator layers. To determine the optimal distance between the detectors, both 18 and 20 were plotted in the same figure. Before doing this both the number of events and the angular resolution were normalized by dividing by the maximum value of the respective quantities. The resulting figure is shown in Fig. 75. It should be noted that the angular resolution resembles a straight line except for when very small distances are being considered. The optimal distance is chosen at the intersection of the plots, which is at about 40 cm. This means that in the original final detector plan the vertical distance between the two scintillator layers should be 40 cm.

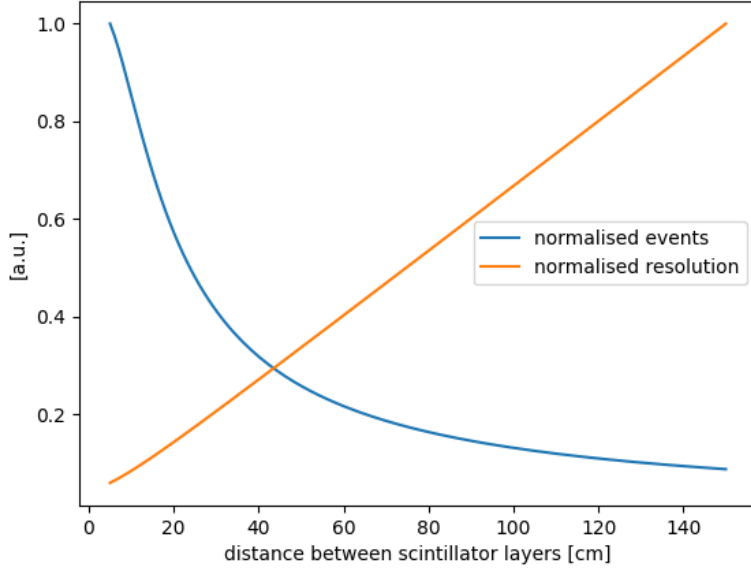
Figure 74: Sketch of the detector geometry.



### 8.3.2 Geometry uncertainties

The first plan was to build a detector with one or multiple detectors in master mode in the top layer and a grid of 3 by 3 detectors in slave mode in the bottom layer. The scintillators of the master detector are 5 cm by 5 cm and the slave detectors are 15 cm by 5 cm, making each individual scintillator block 5 cm by 5 cm. The height was chosen to be 40 cm as motivated in section 8.3.1. In this case  $h$  is not small enough to use the Taylor approximation. Therefore, substituting these parameters into equations 3 to 10, we get the uncertainty in the angles  $\phi$  and  $\psi$  which happen to be the same due to square scintillators. This yields an uncertainty in  $\phi$  and  $\psi$  given in Table 15.

Figure 75: Normalized angular resolution and number of events as function of distance between the scintillator layers



The plots are obtained using 18 and 20, normalization is performed by dividing by the maximum values of the resolution and the number of events respectively.

Table 15: Angular uncertainties

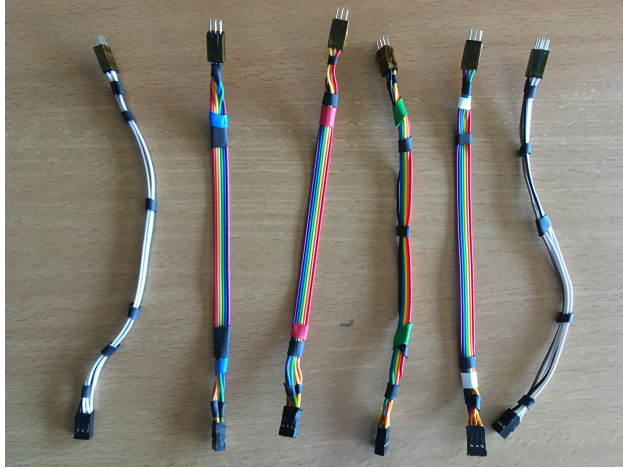
Scintillator	$\Delta\phi$	$\Delta\psi$
I	0.249	0.249
II	0.249	0.245
III	0.245	0.249
IV	0.245	0.245

Uncertainties in  $\phi$  and  $\psi$  for the four different scintillator blocks

### 8.3.3 Cabling

In the original plan for the final detector the main PCBs belonging to the individual scintillators would be placed outside of the active detector area. There were a number of different reasons for this choice. Firstly, placing the main PCBs outside of the track means there are no scattering interactions taking place in the metal components of the main PCB. Also, the data obtained from the detector would be easier to compare with simulations, since the main PCBs do not have to be modelled. Finally, in the case of a possible test beam measurement, the main PCBs are not in the way of the test beam, providing more reliable data.

Figure 76: *Manufactured cables*



*Manufactured cables to connect the SiPM PCB with the main PCB, in order to place the latter outside of the active area of the detectors.*

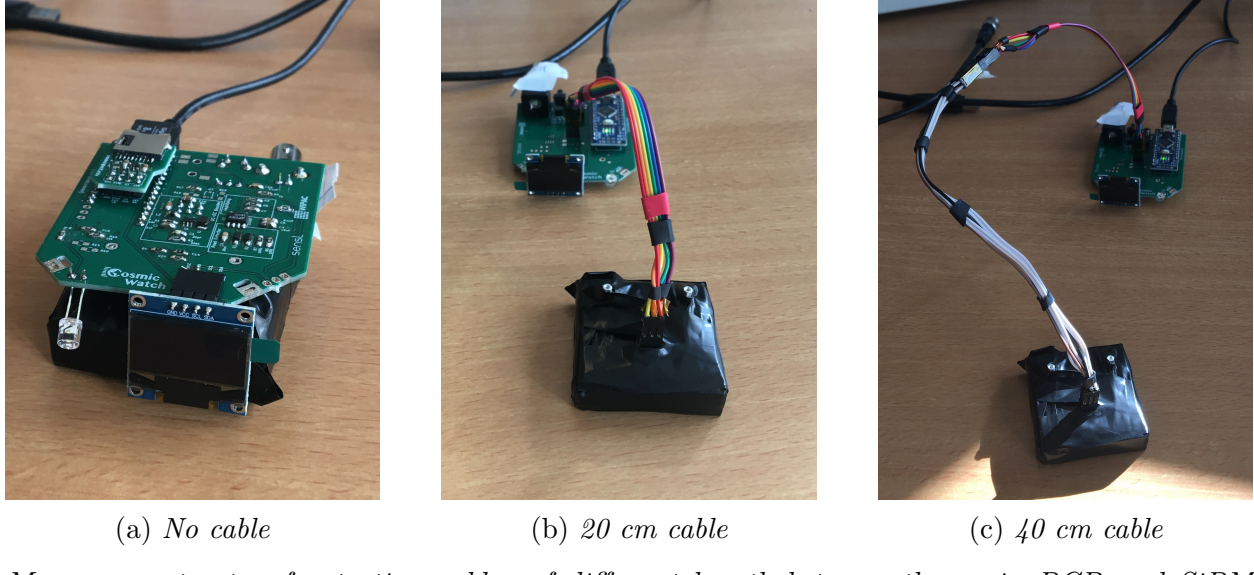
To achieve a working detector with the main PCBs outside of the detector area, each main PCB needs to be connected to a SiPM PCB. Specifically, the 6-pin header on the main PCB must be connected by cable to the 6-pin on the SiPM PCB. Steps in this direction were made during the project using jumper wires, grouped in cables consisting of 6 wires and kept together by cable sleeves. The wire ends were joined by a 6-pin header on one end and a 6-pin on the other end of the cable. The cables had a length of 20 cm. The cables manufactured during the project are shown in Fig. 76.

In order to keep the detector characteristics the same, the Cosmic Watch detector signal should not change when comparing the same detector with and without cable. In order to verify this, measurements were performed using the same detector with no cable, with a 20 cm cable and with a 40 cm cable. The 40 cm cable consisted of two 20 cm cables plugged together. The measurement setup highlighting the different cable lengths is shown in Fig. 77.

Each time the measurement was run until 300 events were registered. In each measurement two signal characteristics were analyzed: the ADC count and the time difference between two subsequent events. For each of the detection characteristics histograms were made with the normalized counts per ADC or time difference bin. For the time differences it is important to note that a minimum cut is applied of 0.5 seconds. An exponential fit was performed on the resulting histograms according to the fitting formula  $y = ae^{-\lambda x}$ , both for the ADC counts and the time differences. The ADC count and time difference histograms and corresponding fit results for the different cable lengths are shown in Fig. 78. It can be seen that for both ADC counts and time differences, the histograms do not change significantly and the fitting results are similar. From this it can be concluded that adding a cable between the main PCB and SiPM PCB does not significantly alter the measurement characteristics.

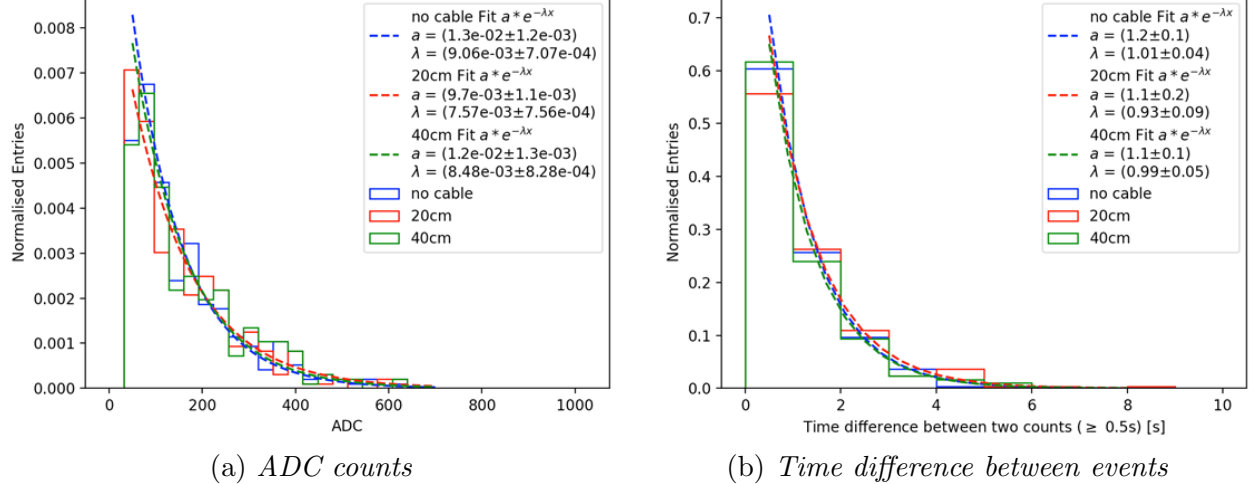
The measurement described above was performed using the standard 5x5x1 cm scintillators. However, in the original plan for the detector the scintillator layers would consist

Figure 77: Setup for the cabling test



Measurement setup for testing cables of different length between the main PCB and SiPM PCB.

Figure 78: Cabling test results

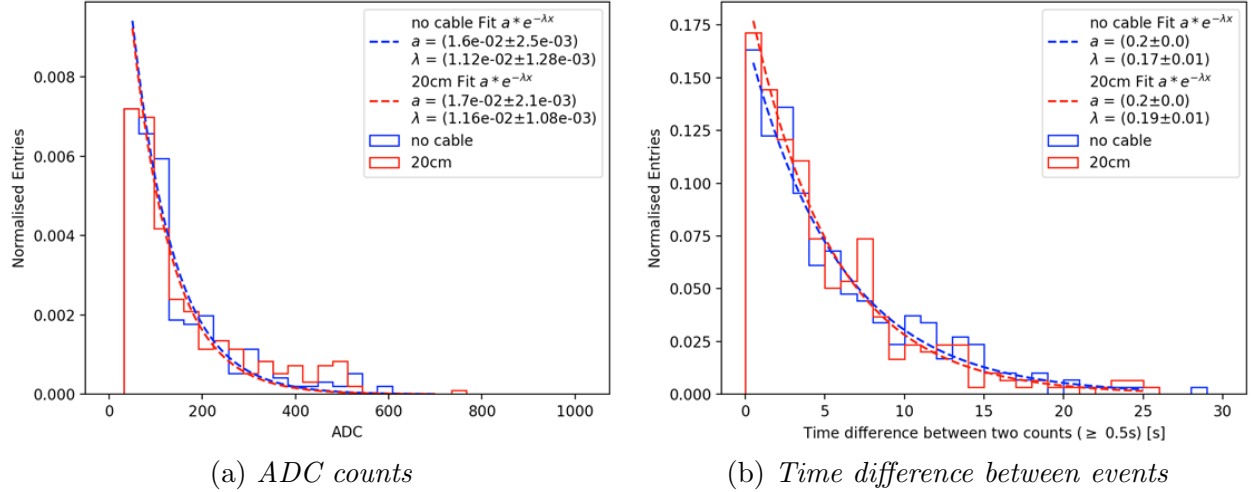


Results of testing different cable lengths. For each different cable length the normalized histogram and the fitting result is shown, for ADC counts and time differences between events.

of a grid of larger scintillators of size 15x5x1 cm. Also with a scintillator of this size some tests were performed, but only using no cable or a single 20 cm cable. Otherwise the testing procedure was the same as described above. The results of the test are shown in Fig. 79. Again it can be seen that there are no significant changes for different cable lengths. However, an interesting difference is observed when comparing the time differences between

events for the standard and big scintillators. For the latter the time difference between events is on average a lot larger than when using the standard scintillator. This is an indication that the big scintillators work less efficient than the standard scintillators, and that signal is lost when using them. This provides an indication that the big scintillators are not working properly when connected to the Cosmic Watch detectors. The scintillators of different sizes will be extensively discussed in section 8.4.

Figure 79: *Cabling test results*



*Results of testing different cable lengths using  $15 \times 5 \times 1$  cm scintillators. For each different cable length the normalized histogram and the fitting result is shown, for ADC counts and time differences between events.*

## 8.4 Scintillators

The scintillator constitutes another fundamental component of the detector. It is the final element that, when connected to the SiPM allows to actually detect the particle, in our case, the muons. This requires a material that is able to absorb energy and re-emit it in the form of light. The detection happens through a Coulomb interaction of the incoming particle with the material of which the scintillator is composed and a subsequent emission of light. The scintillator needs to let the photon propagate to arrive to the photon detector. Another characteristic of the particle that this component allows us to infer is the energy of it when the interaction takes place. In fact the scintillation measured is proportional to the energy deposited in the material with a constant of proportionality highly dependent on the material and the quality of the scintillator. Another quantity dependent on the choice made is the wavelength at which the photon emits after the de-excitation step. Scintillators are also extremely suited for this task because they are responsive and fast in recovering. These qualities allow this material to detect different signals in a time up to a few hundreds of nanoseconds. [4].

#### 8.4.1 The role of the scintillator in our detector

For our detector we started by building cosmic watches where the scintillators used are made by plastic and they go under the category of the organic scintillator (differentiating from the inorganic one grown as crystal), these, are made of fluorescing material in a plastic setup. In particular: the material transparent to visible light is, in this case, polystyrene and the fluorescent agent are POP and POPOP.

Scintillators are wrapped in aluminium in order to facilitate reflection of light and to prevent it from escaping. To avoid a high photon background, they are optically isolated with black tape [4], [21].

#### 8.4.2 Testing different scintillators

##### **Scintillators (5x5x1)cm cosmic watch:**

The first scintillator tested was the classical one of the cosmic watch described above. These pieces arrived polished and highly transparent, therefore, our task was only to wrap them in aluminium foil and isolate them with black tape. Testing the detectors in this first phase of our experiment we encountered one main obstacle: when we used the blue tape instead of the black one the cosmic watch was not possible to use. The signal of the oscilloscope could not be seen because the amount of light coming from the environment was too high and the muons' signal was lost. Only a thick layer of black tape could be the solution to this.

##### **Scintillators (5x5x0.5)cm:**

The main goal of testing scintillators with this shape was learning the procedure to prepare them and starting to have an idea about the characteristic that our final one needed to have. We prepared these scintillators by cleaning them with chemical solvent like wasbenzine, and, since they were already transparent we did not need any polishing. The only step in which paying more attention was fundamental was moving the SiPM from the old setup to the new one. In all these tests, in fact, we needed to use the same SiPM. This was a very delicate step, not always successful. During this process, sometimes, it was necessary to solder it again on the board. This happened in a couple of situations because the SiPM was not soldered solid enough to undergo this process of removal and connection to the new scintillator. In this phase of testing it was becoming clear that the rate at which the signal could be read on the oscilloscope reducing the thickness of the scintillator was lower. Note: the tests on this scintillator shape have been conducted only with the oscilloscope, testing the BNC, test point 1, 2 and 3 but without any calibration process.

##### **Scintillators (5x15x0.5)cm:**

With the aim to reach a final setup building a grid of scintillators stripes able to cover a larger area given a small number of detectors the logical solution appears to be substituting small squared scintillators with long stripes. The only available material had a thickness of 0.5 cm. We proceeded with preparing them towards sawing the shape we wanted (three times longer than the cosmic watch one) and making the holes to screw the SiPM board in the center of the stripe. A first test of these scintillators was successful but the number of muons counted in the same amount of time as the first scintillator was smaller. The test conducted here involved checking the functioning of the detector with the oscilloscope and only later, as will be explained, with the aim of computing the time difference between two counts we

inferred other characteristic of this shape of scintillator. See Figure 78. The decreasing of the count rate has been quantified, for example the count rate computed dividing the number of events for the needed amount of time to obtain them decreased once from 0.8 to 0.6 events per seconds. (This data is obtained after calibrating the board).

### Scintillators (5x15x1)cm:

In order to be able to read a more realistic number of muons the optimal solution seemed to enhance their thickness. This idea started a long process of researching the material we needed and talking with scintillators expert at Nikhef. The two main steps described here are the ones that required the highest amount of time in this phase of testing different scintillators.

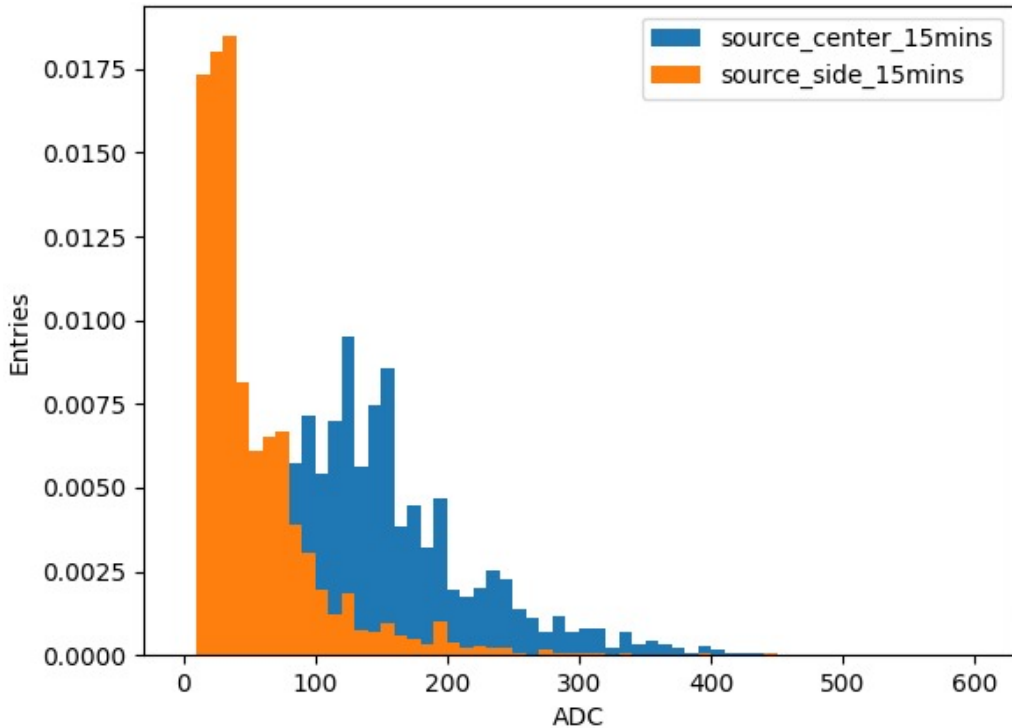
- Glued scintillators: The first proposed solution was gluing two scintillators (15x5x0.5)cm together and obtaining the desired thickness of 1cm. This process required the use of two new experimental solutions of optical cement and optical cement hardener. This procedure should avoid the appearing of a difference in the index of refraction between the two layers and the final product should perform in the same way as a unique piece of scintillator. The waiting time can be more than 24 hours, therefore, given the time pressure we found it necessary to think of a second possibility.
- One component scintillators: We found big solid scintillators that we could cut and drill in order to obtain the same result as in the point above but in only one piece. The main problem of this material was obtaining it as transparent as possible. It was, in fact, not smooth enough to reflect the light in its interior. We experimented a technique that turned out to be successful. This involved using different wet sand papers with increasing P-number and wet ordinary paper to polish the non-smooth sides of the scintillators.

#### 8.4.3 The final choice

Testing the (15x5x1)cm scintillators glued and not glued with the oscilloscope showed that the solid one had a higher counts rate, the first decision taken was, therefore to build the final detector with these scintillators. The troubleshooting started when we took data for the first time with the final detector without success as will be described later in Section 2.5.3. The problem was with the scintillators that, because of the lack of time were tested only with the oscilloscope. Analyzing the Arduino outputs shows a signal 10 times weaker coming from the big scintillator compared to the original one coming from the one of the Cosmic watch. A deeper test conducted with the radioactive source showed that positioning it in the center of the scintillator led to a completely different output if compared to the one obtained positioning the source in the center of it. (See Figures 80, 81). This result brought up an issue that implied that the reflection of the housing of the scintillator did not work as expected. In particular, the further the photons are created from the center the more times they need to collide with the boundaries and so, a higher number of these escape the scintillator and only a fraction of that reaches the center where the sensor (the SiPM), is placed. This was an unexpected and interesting issue that caused a sudden change of plan in the configuration, leading us to a decision that implied going back to the very first scintillators of the cosmic watch for the final configuration. To support this decision, another

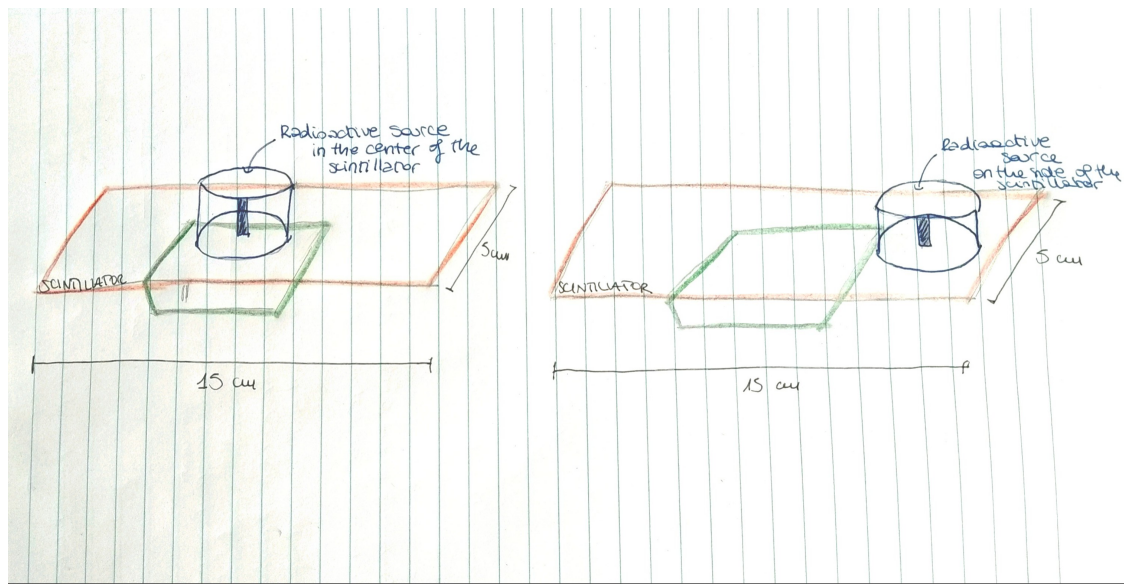
analysis was also made on the cable connection of the scintillators to the board instead of the usual 6-pin component. A result that was very clear looking at the plots printed to check if the detector was still functioning in the same way when connected with the cable showed that the time difference between two counts of the big scintillators compared to the one of the small configuration was much higher as it can be seen in Figures 77a, 78a and 83 . For a further comparison with the final result for this part see Section 3.2.

Figure 80: *Different position of the source on the scintillator*



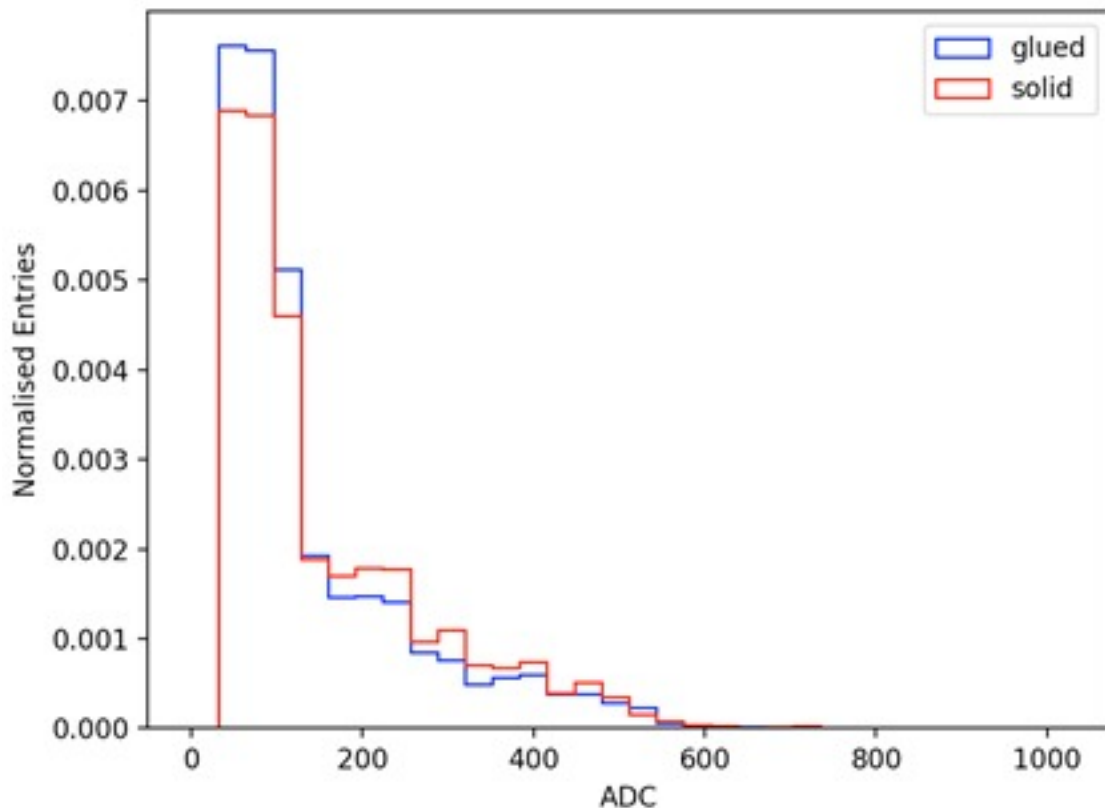
*ADC values in the two different configurations in which the radioactive source it's in the middle or on the side of the scintillators*

Figure 81: *Different position of the source on the scintillator, sketch*



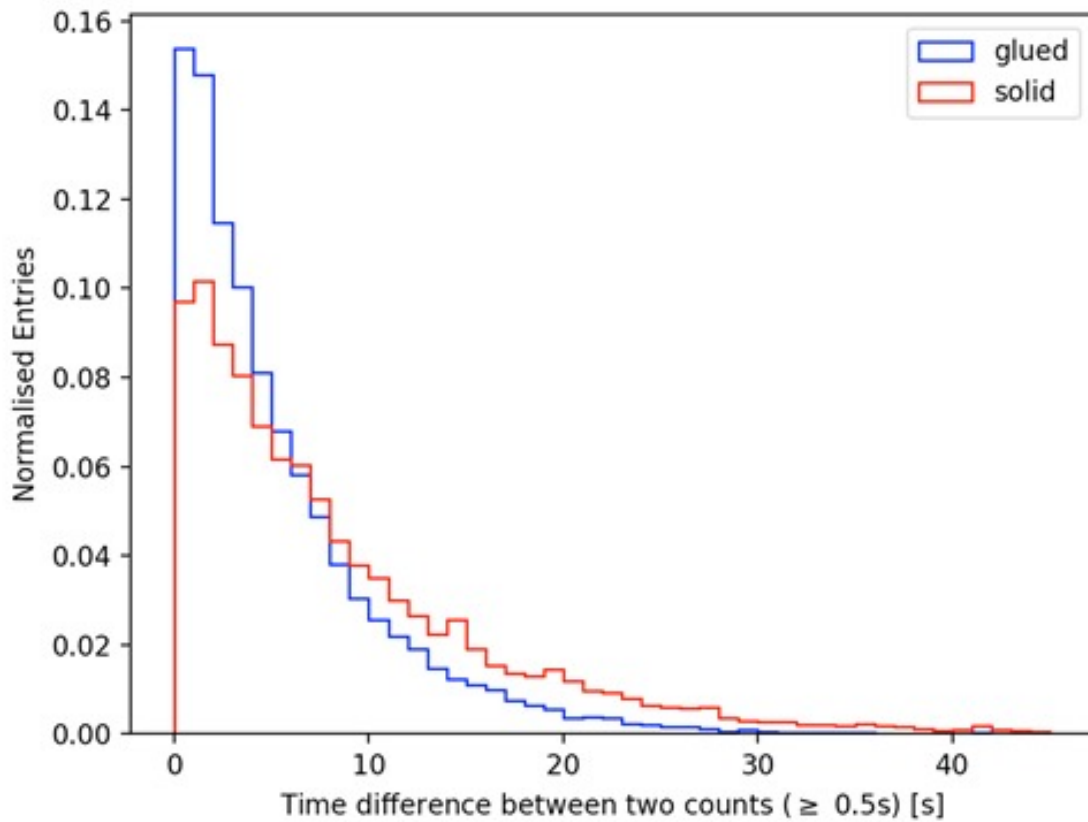
Configuration on the left: radioactive source in the center of the scintillator. Configuration on the right: radioactive source on one side of the scintillator.

Figure 82: *ADC values for glued and one-piece scintillator*



*ADC values for the glued and the solid one piece scintillators of sizes 2(5x15x0.5)cm and (5x15x1)cm.*

Figure 83: Time difference between 2 counts for the solid and glued scintillator



Difference in time between two counts for the scintillators of sizes 2(5x15x0.5)cm and (5x15x1)cm. This figure can be compared with figure 78a in order to see the difference between two counts for the scintillator of size (5x15x1)cm.

## 8.5 Reflections on individual work

- Carlo: Contributed to the project by first working with the Arduino code to make the troubleshooting possible and to solve some key issues that prevented most of the detectors to count any signal in the first weeks of the project. After that, I spent a lot of time in testing and thinking of a setup for the coincidence mode through the jack cables. I did that together with Mattia and Ben: we studied and worked a lot with the Master and Slave mode of the detectors, and tested many different solutions and configurations, and think about a possible use in the final detector using USB hubs and amazing jack cable splitters. Moved to work on the data acquisition part towards the end of the project, where a Python module was written from scratch to read from the Arduinos, deal and manage the serial port connections and the configuration of the detectors, and finally process and save the result in the desired format. I then moved to work on the live plotting script to show the animation of the muons coming into the detector. During the duration of the project, I built and dismantled different configurations with an insane amount of USB and jack cables many many times. Together with Florian I set up and managed the Github repository. I also tried to cheer up the group in the most difficult moments, and tried to be always realistic. Sometimes I also was a bit angry >: (.
- Rens: Contributed to the project by testing scintillators, machining scintillators, calculating uncertainties, calibration, detector design, detector construction. Contributed to the report by writing: sections 2.3.1, 4.2.4.
- Florian: My contributions are split in direct, foreground work, background support and organisation: Foreground
  - Established simpler, more reliable more controllable serial communication to detectors than originally provided
  - Electronics calibration including muon signal analysis, serial control of signal generator, study of board, cable and signal impedance and countermeasures to cable reflections. This spans from coding to the calibration of all detectors, analysis and dedicated Arduino scripts, close collaboration with Noor
  - Design and manufacturing of support structure after numerically evaluating expected muon-like events vs. angular resolution vs. covered zenith angle for initially planned tracking station, help by Noor
  - Muon and background signal studies needed for calibration and how changes to cables and/or scintillator potentially influence ADC conversion by Arduino
  - DAQ framework and analysis framework in python including documentation and instructions, collaboration with Carlo
  - Offline identification and analysis of muon-like events to validate coincidence measurements and allow offline coincidence measurement for setups with more than three detectors for which the jack connection is not reliable, collaboration with Carlo
  - Investigation of significantly differing count rates per scintillator-sipm combination, with Noor

- SMT mounting of one detector, development of debugging strategies for non-working boards and faster SMT soldering technique
- Cable manufacturing, testing and analysis
- Scintillator machining ( $15 \times 5 \times 1[\text{cm}]$ ) and preliminary testing that signals are still readable by SiPm and can be digitised by circuit, with Noor
- DAQ and analysis framework for radioactive calibration
- Performed angle measurement and analysis, initiated energy spectrum measurement and provided analysis framework
- Commissioning of various detector setups in various readout modes for various measurements, built of contingency setup used for angle and lead measurements after it became apparent that neither coincide mode via jack or big scintillator work as expected

## Background

- Maintainer of shared git repository, verified pull requests and merges to ensure latest stable code is on main and available for all, bash scripts to ensure that code developed with different OS and python versions run on all individual and lab machines, documentation and instructions eg serial communication, linux screen command , help with code debugging
- installation of Centos8 and needed libraries e.g. ROOT + pyROOT compatible with python 3.6 on lab machine
- Learned basics of geant4 and allpixsquared to shallowly cross-check simulation
- Selection, request of purchase and/or organization for various laboratory equipment such as machine oscilloscope + probes with the correct impedances, Bosch profiles for the support structure, lead plates, all sorts of cables (in cooperation with the Nikhef Electronics Department), pyserial-compatible USB hub
- Documentation and instructions for different steps (e.g. how to use serial communication, DAQ, analysis scripts . . . )

## Organisation

- Discussed and planned next steps and assigned task, check in with teams and helped with code, analysis, and interpretations
- Tested and reflected on different leadership strategies with Noor e.g. instructions, encouragement to use git and logbook, and meetings, Pandemic was additional obstacle, overall stressful and frustrating experience
- Communication of current status, obstacles and next steps to group and Professor
- Organised and managed first two weekly reports

Regarding the final report, I provided plots with my interpretation of the results but did not write anything. My main learning achievements are how to maintain of a shared coding environment and framework and an advanced usage of git, analog and digital signals in circuits, especially impedance difference and oscilloscope probes, shallow detector simulation with geant4 and allpixsquared, team leadership strategies and how to deal with a lack of sleep and high frustration level.

- Ben: Contributed to the project by first testing and learning about the functionality of coincidence mode together with Carlo and Mattia: By trial and error we tested

the properties of the master and slave roles that detectors could fulfill. At first we tested the properties with two detectors to understand the basics, and later moved to three detectors to understand the more difficult properties. Moved to fixing individual CosmicWatches later in the project working closely with Mattia. With respect to the report, contributed by writing in sections 2.1, 2.2, 2.5, 8.1 and 8.2.

During the troubleshooting of CosmicWatches we learnt a lot about circuits and soldering by experts help and guidance, searching on the internet and a lot of trial and error. The latter led to creative ways of problem solving, such as the Arduino towers, while the former led to learning new problem solving techniques, such as creating a short when a pad was missing, later applied to other troublesome boards. Additionally, we became much better at finding problems regarding dysfunctional CosmicWatches, framing them and finally solving them. Last but not least, we became more acquainted with the working tools and were introduced by experts to new instrumentation, such as the desoldering pump, which we can now use alone.

Lastly, despite some stressful and more difficult moments, I overall had a great time working on this project together with everyone, in particular, Mattia, whom I worked with on a daily basis. I'm very pleased with what we've accomplished (managed to fix 11 detectors when only very few were working at first) while having a great deal of fun in the process.

- Mattia: Contributed to the project first of all by learning about the functionality of coincidence mode together with Ben and Carlo: we started by using only two detectors and subsequently we moved on by using three detectors in coincidence mode. At this point, we thought that jumping to use multiple detectors was straightforward, which instead turned out to be more tricky than what expected. This was because of the large number of cables and splitters in the setup. After this, always working closely to Ben, I moved on by fixing individual CosmicWatches. This work lasted for the vast majority of the last period, since detectors kept breaking until the very last days. Nevertheless, we succeeded in fixing most of them and finally we were able to provide the group with 11 perfectly working detectors! In the last days I also took part to the electronic calibration, working along with Rens. With this regard, in this report I contributed by writing in sections 2.1, 2.2, 2.5, 8.1 and 8.2.

Thanks to this project, I was able first of all to deepen my knowledge in understanding how electronic circuits work. I especially improved my soldering technique by using new advanced tools, such as the soldering pump, under the advice and guidance of the experts here at Nikhef. Along with this, searching on the internet and perform a lot of trial and error was a big part of my daily experience. In particular I had a lot of fun during the last weeks when conceiving new creative ways of fixing non-working detectors, such as building Arduino towers and applying long wires to recreate the circuit on the board. These processes led me to improve my problem finding and problem framing techniques, since Ben and I constantly supported and sought advice in each other. Solving problems in fact was found to be the very last step of this much longer process. In conclusion, I am very satisfied with what Ben and I achieved in this project, since now we have eleven working detectors, which the entire group can enjoy for their measurements.

- Marta: Contributed to the project by working mainly on testing the scintillators and on the measurements with the lead. These were the main two tasks I completed in the past few weeks respectively with Noor and Rens and with Ali and Ben. In both cases the results achieved were very different from what we expected but, because of this reason, we had the possibility to understand more about the component of the detectors we were working with. Especially, the scintillators measurements conducted by other groups helped us in understanding the issues we were encountering like, for example the big scintillator malfunctioning explained in section 8.4 discovered thanks to the work of the radioactive source calibration group and to the work done by Florian with cables 8.3.3. Even if team work was not always successful, in my point of view this was still a satisfying group achievement. For what concerns the lead, it was interesting to learn how to use the code Carlo has written to take data and being able to plot data that we could try to understand. 6.2. The discussion to interpret the result was probably one of the most interesting part in this project even the surprise for almost never reaching what expected made it challenging. During the first weeks, I worked, like every member of the group on the cosmic watch and I was lucky enough to having it not working for 3 weeks in a raw, always for a different reason and this, again made understand the circuit we were dealing more in detail. 5.2. For the report I contributed writing the section about scintillators (See Sections 2.4,8.4). This was my first practical project in physics and, even if sometimes there was the feeling that components were not working for understandable reasons, discussing it in a group to work out a possible explanation was always pleasant and being able to share time with the team in person allowed me to learn practical hardware competencies and how to use GitHub.
- Niels: Contributed to the project by working on the calibration with a radioactive source. This turned out to be a lot more challenging than it seemed at first glance. It turned out that the spectra obtained with the source on the detector were very different from what we expected, which is the typical  $\beta$ -spectrum (we used  $\beta$ -sources). Because of the slow Arduino which is used in the Cosmic Watch detector, it constantly felt like the detector was just not suited for measuring the source spectrum, since the activity of the sources is very high. So we spent a lot of time taking data, analyzing it and concluding it was not as expected. Making various improvements in our measurement technique this continued to be the case. So actually at the end it felt like we (me, Cecile and Ali) did not accomplish a great deal with the radioactive calibration. However, it does feel like we learned a lot in the process. As the cliche says, you learn more from failure than from success. Interpreting the results, thinking about what is not adding up and coming up with improvements for the measurement are a very different learning process compared to your standard course in which you make some exercises and finish with an exam. With regard to the report I wrote section 8.3.1, section 8.3.3, and collaborated on sections 6.2 and 4.1.
- Cecile: Contributed to the project by testing the big scintillators in the first week after we finished building our individual detectors, together with Niels and Rens. The testing was a bit inefficient due to detectors that were not working correctly. Then after a week we divided the group into new subgroups and I worked on radioactive

calibration, together with Niels and Ali. There were a lot of obstacles in this process. Since the detectors are built for muons and they do not have the same energy spectrum as our radioactive source. Besides this, the arduino can only detect particles at a relatively slow rate compared to the decay rate of the source. This caused a lot of problems with comparing the known spectrum with our measurements. We tried to overcome these problems as much as possible by setting the threshold as low as possible and using a blackbox with lead inside to shield out detector from background. These measures had less of an impact than we had hoped, but we tried to work with what we had as much as possible.

It was the first time that I have done a big practical project and learned a lot about the way an experiment is set up and everything that comes along in the process. It was nice that we had a lot of freedom to try out different things and it turned out to be lot more improvising and adjusting than I would have imagined.

For the report I worked on the abstract and section 1, 4.1 and 7.

- Alexandra: Contributed to the project by working on the radioactive calibration with Cecile and Niels, in which we took various measurements with big and small scintillators with the source and analyzed the data. I also worked the lead measurement, taking data along with Ben and Marta, and writing a script to read and plot the data. In both of these sections, the results were somewhat less promising than we hoped. In the case of the radioactive calibration it turned out that the energy spectra of muons and Sr-90 were different and this caused problems, which we tried to mitigate by lowering the threshold and using lead and a blackbox to reduce background. The lead analysis also yielded results that did not fully match our calculations, however it was too late to take more measurements. I enjoyed doing the measurements and getting familiar with procedures of hardware and experiments, however I underestimated how many obstacles there would be to getting good results, and how many things we didn't foresee going wrong. Given the time limitations, I felt that my group and I did our best to work around problems, even if imperfectly. Finally, I wrote the Introduction and Theory sections or the report, as well as parts of the Radioactive Calibration and Muons' passage through lead sections.
- Lefteris: Contributed to the project by completing the simulations part. I completed and organized the set up of each part of simulations, made the comparison of the simulation results and the experimental data, a process that lead to a lot of interesting observations for both the scintillator detector's characteristic and cosmic muons' physics. The general results of my work predicted a lot of limitations of the first configuration for the 7 detectors case and lead to a possible analytical explanation combining experimental data and results from other simulations. Also, all parts of the simulations lead to usefull information for the experimental measurements and at a better the understanding of the experimental data. But the most important point of the process I completed are some of the limitations of the cosmic watch detectors I observed, which can help other future projects based on that detector.
- Noor: Contributed to the project by being one of the first to finish the cosmic watch and uploaded all the Arduino code to every ones detector and helped with soldering.

After the individual soldering and testing I introduced the idea of making a tracking detector and presented the grid of scintillators. Then I helped in forming the groups and took, together with Florian, the task of calibrating all muon detectors. This seemed straight forward, but took a long time since the calibration was dependent on the shape of the signals we wanted to inject in the circuit and needed a lot of analysis. For this purpose I wrote, together with Florian, scripts to analyse the data and create the right waveform. I learned a lot about the equipment (from looking up many manuals and asking questions to professionals) and got a better understanding of the mechanics behind ‘simple’ processes, like matching in- and output impedance. I also took part in the scintillator group with Rens and Marts and looked for the best scintillators that we could use for the final detector. I sawed, drilled and polished the scintillators and packed them in aluminimum foil and tape and attached the SiPMs to them. I also helped building the support structure of the detector and set up some test measurements for the lead analysis. I also tried to schedule most weekly meetings and convince people to keep on track and document what they were doing, however I am not sure this was successful since I was very busy with finishing my own tasks as well. I learned a lot from this course, from working in a big group (which can be very challenging) to coding more sufficient, working with GitHub, understanding hardware and also learnt that you can never assume that something works without testing it properly, even when you think you are 99% sure. Regarding the report, I wrote the electronics calibration section, the section about the mechanical design and wrote the ADC spectra analysis of the lead and angle measurements and something about the time window.

- Oline Contributed to the project by working on the detector simulations alongside Lefteris. This involved implementing a model of the detector in the the allpix and geant4 simulation software with various detector configurations. It required acquiring a comprehension of how to evaluate real systems in simulated environments, and the limitations the latter had in capturing the complexities of the former. She also contributed on the results by producing plots on the number flux as a function of incoming angle, and the fit to the expected functional form. Furthermore, she contributed by organizing and distributing the write up of the various sections of paper. She formulated the main structure/layout of the paper and contributed on writing the simulation section, introduction, acknowledgement and results related to the angular distribution.